

Cell-to-Cell Communication as a Strategy to Regenerate Three-dimensional Tissue

by

Ricardo Antonio Rossello

A dissertation submitted in partial fulfillment
of the requirements for the degree of
Doctor of Philosophy
(Biomedical Engineering)
in The University of Michigan
2007

Doctoral Committee:

Professor David H. Kohn, Chair
Professor Paul H Krebsbach
Professor Martin A. Philbert
Assistant Professor Michael Mayer



3D Rendering of Pluripotent Adult Stem Cells (Bone Marrow Stromal Cells)

© Ricardo Antonio Rossello

All Rights Reserved

2007

Dedication

To my beloved mother and father for never telling me how to live; but living and letting me watch; and to Prof. Jorge W. De Jesus

Acknowledgements

As I conclude my current academic pursuits, I would like to acknowledge all the people who have helped me along the way, and in more ways than one, to complete this work.

I am grateful for all of the friends I have made while in Michigan; you know who you are. All of you played a vital role in the successful completion of my work and will always hold a special place in my heart. In particular, I would like to thank my surrogate family in Michigan, the Cervi's. Without their care, love and attention I would have never been able to weather the storm. To my lab mates, Kyungsup Shim, Sharon Segvich, Lihn Luoung, Nadder Sahar, Joseph Wallace, Erin Gatenby, Shan Lee, Lisa Winkle, I deeply appreciate your help, advice and, most of all, your friendship.

To my committee members, all of whom are highly dedicated and extremely busy, thank you for taking the time to converse and discuss my research, and other aspects of life – I shall always cherish those conversations. To my advisor, David H. Kohn, my gratitude for allowing me to learn under his tutelage; I know I have become a better critical thinker for it. I also appreciate the help of Dr. Eddy Kizana and Jeff Maganck, both of whom contributed to my research. My very special thanks go to Joe (Zhuo) Wang, who spent countless hours teaching me the intricacies of surgeries and who contributed greatly to the advancement of this thesis.

Finally, I'd like to thank my family for their support and encouragement, and last, but not least, I'd like to thank my better half, Natasha Cervi, for her unconditional love.

Table of Contents

Dedication	ii
Acknowledgements.....	iii
List of Figures	ix
List of Tables	xii
List of Appendices	xiii
Chapter 1 Introduction	1
1.1 Problem Statement and Thesis Aim.....	1
1.2 Cell-based Constructs	2
1.3 Seeding Strategies and Template Chemistry for 3D tissue engineered constructs	4
1.4 Gap Junctions.....	5
1.5 Outline of Thesis Content	7
1.6 References.....	10

Chapter 2 Establishing Micro CT Thresholds for Tissue Engineered Bone and Comparison of Bone Regenerated from Bone Marrow Stromal Cells and BMP-7 Transduced Cells.....	21
2.1 Introduction.....	21
2.2 Materials and Methods.....	24
2.2.1 Bone marrow stromal cell isolation and culture	24
2.2.2 Generation of recombinant adenovirus and cell transduction.....	25
2.2.3 Gelatin sponge preparation	26
2.2.4 Preparation of bioceramic (Mineralized PLGA) scaffold.....	26
2.2.5 Transplantation into host mice.....	26
2.2.6 Micro-CT image acquisition and analysis	27
2.2.7 Mineral ashing	28
2.2.8 Histology.....	28
2.2.9 Analysis of bone ingrowth.....	30
2.2.10 Statistical analyses	30
2.3 Results.....	31
2.3.1 Threshold analysis	31
2.3.2 Comparison of bone regenerated with different cell types.....	33
2.4 Discussion.....	35
2.5 CONCLUSIONS.....	41
2.6 References.....	53

Chapter 3 Effects of Cell Seeding and Self-Mineralizing Template on Differentiation and	
Volume of Regenerated Bone.....	59
3.1 Introduction.....	59
3.2 Materials and Methods.....	62
3.2.1 Bone marrow stromal cell (BMSCs) isolation and culture.....	62
3.2.2 Scaffold Preparation.....	63
3.2.3 Mineralization of Scaffolds.....	63
3.2.4 Pre-Wetting Scaffolds.....	64
3.2.5 Cell Seeding.....	64
3.2.6 Cell Counting and Histology	65
3.2.7 Dye transfer studies.....	66
3.2.8 RTPCR Analysis of differentiation markers.....	67
3.2.9 Transplantation of cell-scaffold constructs.....	69
3.2.10 Micro-CT 3D image acquisition and analysis	69
3.2.11 Histological analyses	70
3.2.12 Analysis of bone ingrowth.....	71
3.3 Results.....	71
3.3.1 Filtration seeding achieves a higher number of attached cells	71
3.3.2 Micromass seeded cultures enhance gap junction dependent cell-cell communication.....	72
3.3.3 Seeding and template conditions alter bone marker expression	73
3.3.4 Different seeding techniques led to distinct patterns of osteogenesis.....	75
3.4 Discussion.....	75

3.5	References.....	87
Chapter 4 Connexin 43 as a signaling platform for increasing the volume and spatial		
distribution of regenerated tissue.....		
93		
4.1	Introduction.....	93
4.2	Materials and Methods.....	96
4.2.1	Viral Vector Production.....	96
4.2.2	Culture and Transduction of BMSCs.....	96
4.2.3	Western Blot.....	97
4.2.4	2D and 3D Cell Culturing.....	98
4.2.5	Dye transfer studies of Cx43.....	99
4.2.6	Real-time PCR Analysis.....	100
4.2.7	In-vivo transplantation.....	101
4.2.8	Micro-CT 3D image acquisition and analysis.....	101
4.2.9	Histology and Morphological Analyses.....	103
4.3	Results.....	103
4.3.1	Characterization of Cx43-GFP modified BMSCs.....	103
4.3.2	Overexpression of Cx43 increases GJIC.....	104
4.3.3	Cx43 overexpression enhances overall and spatial distribution of differentiation markers.....	105
4.3.4	Cx43 Gene-Modified Cells Regenerated More Bone In-Vivo.....	107
4.4	Discussion.....	108
4.5	References.....	119

Chapter 5 Conclusions	127
5.1 General Conclusions	127
5.2 Future work.....	133
Appendices.....	137

List of Figures

CHAPTER 1

Figure 1-1: Generalized mechanism for the role of gap junction intercellular communication in bone cells.	9
----------------------------------------------------------------------------------------------------------------	---

CHAPTER 2

Figure 2-1 Autothresholding mechanisms use a bimodal to find a threshold value by finding the midpoint of the intermodal zone.....	44
Figure 2-2 Correlation between volume fraction of regenerated bone determined by micro CT and ash fraction at different thresholds.	45
Figure 2-3 Correlation between area fraction of regenerated bone determined by micro CT and area fraction determined on same section by H&E staining.....	46
Figure 2-4 Comparison of von Kossa images that have been stitched together (left) and the analogous μ CT planes (right) at (a) 4 weeks, (b) 8 weeks and (c) 12 weeks for sections of ossicles regenerated from BMSCs.....	47

Figure 2-5	Correlation between area fraction of regenerated bone determined by micro CT and area fraction of mineral determined by von Kossa staining on the same section.	48
Figure 2-6	Bone regeneration as a function of cell type and time.....	49
Figure 2-7	Overall volume and total mineral (ash) content of ossicles regenerated from transplanted BMSCs and BMP-7 transduced cells.	50
Figure 2-8	Quantification of mineral distribution on von Kossa stained slides for the 4 week samples.	51
Figure 2-9	Correlation between volume fraction of regenerated bone determined by μ CT at different thresholds and mineral fraction determined by ashing when BMSCs are in a ceramic scaffold for 6 weeks.	52

CHAPTER 3

Figure 3-1	Percent of cells adhering to PLGA (A) and mineralized (B) scaffolds at different time points following seeding via different techniques.	81
Figure 3-2	Cell count and distribution varies in seeded scaffolds, 6 hours after seeding.....	82
Figure 3-3	Seeding alters gap junction intercellular communication.	83
Figure 3-4	Expression of differentiation markers is increased with alternative seeding techniques and a mineralized template.	84
Figure 3-5	Volume fractions and patterns of osteogenesis vary as a function of scaffold surface and seeding techniques.....	85
Figure 3-6	Topographic analysis of mineral distribution within bone ossicles.....	86

CHAPTER 4

Figure 4-1	BMSCs are highly transduced with Cx43-GFP	113
Figure 4-2	GJIC in BMSCs, as measured by Calcein-AM transfer is enhanced with Cx43 overexpression:.....	114
Figure 4-3	Cx43 overexpression is associated with higher levels of OCN mRNA expression at all times.....	115
Figure 4-4	Micro CT renderings and histological sections of ossicles regenerated following subcutaneous transplantation of BMSCs.....	116
Figure 4-5	Cortical-like thickness and trabecular-like bone volume fraction of tissue engineered bone.	118

List of Tables

Table 1	Comparison between optimal thresholds determined from regressions against ash fraction and auto thresholds determined using histograms and threshold calculating algorithm.	42
Table 2	Linear transformations of threshold in Hounsfield units (HU) to physical mineral density threshold (mg/cc)	43

List of Appendices

A1. FlowCulture Perfusion System Design and Specifications.....	138
A2. ALP activity assay (24 well plate)	161
A3. Cell Counting with Hemocytometer	163
A4. Cell Proliferation by Flow Cytometry (BrdU and PI).....	167
A5. Designing a Filtration Device for Scaffolds	168
A6. Protocol for Extracting Bone Marrow Stromal Cells from Rat Femur and Tibiae	176
A7. Filtration Seeding of Scaffolds	178
A8. Subcutaneous Transplantation of Gelform-BMSCs into Mice.....	181
A9. Cell Seeding by Micromass	183
A10. Protocol for Flow Cytometry Activated Cell Separation (FACS).....	185
A11. Immunohistochemistry stain on Connexin43-treated cranial defect sections....	186
A12. Westernblot Protocol and Precedures	187
A13. Infection Protocol for Adherent Cell Types.....	188

A14. Repair of craniotomy defects with genetically modified cells.....	191
A15. Transduction of BMSCs with LV-Cx43-GFP	193
A16. LVCx43GFP Plot.....	195
A17. Calvarial Defect Model: Enhanced GJIC regenerates more bone in a critical sized defect.....	196

Chapter 1

Introduction

1.1 Problem Statement and Thesis Aim

Skeletal defects present a major clinical challenge with over 5.5 million fractures and 1 million bone grafting procedures done each year ¹. Present clinical skeletal defect therapies, such as allogenic bone transplantation and non-bioactive material implantation, have limitations ²⁻⁶. This reality points to the need of novel cell-based strategies that can be tested in 3D in-vitro models and validated in-vivo.

Employing strategies that increase the rate of bone formation and enhance distribution of osteogenesis may help overcome these limitations ⁷⁻⁹. Factors that may enhance bone formation include enhanced nutrient flux, stress, cell-cell adhesion, cell-cell communication, growth factors, and cell motility¹⁰⁻²². Designing initial seeding strategies that can exploit these factors may enable higher cell differentiation and bone formation ²³⁻²⁷. Alternatively, cells can be altered endogenously to express higher levels of a particular protein or transcription factor that enable higher differentiation and bone formation.

The aims of this thesis and underlying studies are therefore (1) to employ exogenous strategies that can alter bone regeneration and differentiation by virtue of the

biomimetic nature of the scaffold and initial seeding conditions that enhance nutrient flux, stress, cell-adhesion, cell-cell communication, with an emphasis on gap junction intercellular communication (GJIC) and (2) To endogenously overexpress the gap junction forming protein Cx43 in bone marrow stromal cells and measure the impact in GJIC, cell differentiation, and bone regeneration in 3D, along with the impact of higher GJIC when cells are stimulated with the bone osteogenic factor BMP7.

The following sections present the background relevant to this thesis, finalizing with the outline of the content presented in the same.

1.2 Cell-based Constructs

A cell-based approach^{28, 29} in which a porous, 3-dimensional synthetic construct provides a substrate for cells can enhance cellular growth, proliferation, and provide a temporary template for the formation of extracellular matrix and new tissue³⁰⁻³³. Poly(a-hydroxy acids) such as poly(lactic acid) and poly(glycolic acid) are considered biocompatible and degrade over controllable time scales into natural metabolites, which makes them attractive materials for scaffolds³⁴. PLGA (polylactic glycolic acid) supports osteoblast attachment and growth, in vivo and in vitro³⁵.

A suitable cell type can be found in the bone marrow stroma, which consists of a heterogeneous population of cells that provide the structural and physiological support for hematopoietic cells³⁶. The stroma contains cells with stem-cell like characteristics called Bone Marrow Stromal Cells (BMSC). These cells have the potential to differentiate into osteoblasts, chondrocytes, adipocytes, fibroblasts, and hematopoietic cells³⁶. BMSCs are a heterogeneous mixture of cells isolated from bone marrow aspirate

which adhere to tissue culture plastic. They contain a subpopulation of mesenchymal stem cells capable of differentiating into specific tissue, given the proper biological cues.

However, in-vivo transplants of BMSCs and other cells used to regenerate tissue engineered bone, exhibit deficiencies in formation as the inner core of the ossicles lacks the nutrient transport necessary to thrive^{7, 37, 38}. Several important considerations must be taken into account to improve the initial conditions of the cell-scaffold construct. Cell seeding and cell-substrate adhesion properties are of paramount concern. Cell seeding conditions control the initial number of cells seeded and the localization of these cells. Cyclic seeding conditions, such as filtration, may enhance adhesion because cells have the opportunity to adhere several times. Cell-substrate interactions are important because they determine the adhesion affinity, and may promote important signaling cascades.

In order to form tissue equivalents, cells must be properly seeded into porous scaffolds. These seeding conditions may dictate the ultimate properties and direction of the new tissue. Static or gravitational seeding is the most commonly employed means of entrapping the cells in the scaffold^{27, 39}. However, this method has inherent limitations in cell retention and localization. In rigid scaffolds, cells usually attach at very low percentages and show dispersed localization, producing large variability in the resulting engineered tissue^{24, 40}. Furthermore, the ability for cells to adhere into the substrate is of pivotal importance. When cells attach to the substrate in high numbers, higher cellular coverage inside the scaffold is possible. Also, as cells attach expeditiously, they can start the biological processes and signaling that will lead to proliferation, migration and differentiation^{9, 26}.

1.3 Seeding Strategies and Template Chemistry for 3D tissue engineered constructs

To address the seeding density and localization problem, an alternative method of seeding can be done by filtering the cells into the scaffold in a cyclic manner. This method circulates the cell suspension through the scaffolds, with a small pressure gradient applied by a peristaltic pump. The homogeneous cell suspension that filters through the scaffold is cycled through and may produce higher cell density and even cellular distribution. The increased cell density, nutrient flux and sheer stress point to the potential of producing higher cellular adhesion and lower variability among samples 21-23. As an added benefit, the oscillatory flow gradient increase proliferation and differentiation in BMSCs^{41,42}.

A higher density of cells is desired to increase the cell-cell contacts that enable cellular communication and signaling. However, such high densities may produce an adverse microenvironment due to a supersaturation of cells inhibiting transport³⁹. Passive nutrient diffusion is one of the biggest obstacles in 3D cell-scaffold composite systems⁴³. Particularly for bone, the outer layer of cells and tissue prohibits proper exchange of nutrients and byproducts inside the ossicle's core. One way to bypass this is by seeding cells in dense micromasses. These micromasses are placed in a particular location in the scaffold (center), leaving less crowded areas where nutrients can flow through. Micro masses could provide the benefits of higher density cell-cell communication, while allowing for transport of nutrients and cellular byproducts, as well as migration of cells that would enable a differentiation gradient from the core to the periphery.

To create a favorable biomimetic environment, a mineralized layer on a PLGA scaffold can be a dominant factor for the enhancement of cell adhesion and osteoconductivity^{44,45}. The increased adhesion will lead to a higher density of cells in the construct which is desired for increased cell-cell communication. This bone like apatite can form on the polymer scaffold and mimic physiological conditions by incubating it in simulated body fluid (SBF)³⁴, producing ion concentrations are similar to blood plasma. In this case, the PLGA will function as a bulk material that degrades at a controlled rate while the mineral layer serves as a biological interface. Additionally, the surface mineralization is expected to provide a bioactive surface to moderate Ca⁺⁺ flux into the cells, for enhanced differentiation, signaling and cellular growth^{12, 45-48}. This calcium flux is an important cell-cell messenger in osteoblasts that may be important for proper bone remodeling and regeneration^{13,49}.

These seeding and substrate mineralization approaches exploit the initial exogenous physical conditions of the cells and substrate to overcome the incomplete regeneration of tissue. Alternatively, an endogenous approach to enhance cell-cell communication (gap junction intercellular communication) could be employed to overcome some of these problems.

1.4 Gap Junctions

Gap junctions are present in all types of vertebrates, except very few cases such as red blood cells platelets, and some neurons⁵⁰. This ubiquity makes it reasonable to consider gap junctions a fundamental structure necessary for cell differentiation and signal transfer. Composed of two juxtaposed hemichannels present on the surfaces of

adjacent cells, Gap Junctions form a transcellular channel that permits the rapid and efficient propagation of ions, metabolites, and second messengers between adjoining cells. These hemichannels are called connexins. Each Connexin monomer is a polypeptide consisting of 4 transmembrane domains (two extracellular loops, one intracellular loop, and intracellular carboxylic and amino ends). Throughout different types of tissue, gap junctions play a mayor and extensive role in response to mechanical, electrical and chemical stimuli⁵¹⁻⁵³.

Out of the 20 known connexins, only Cx43, Cx45, and, to a lesser extent, Cx46 have been shown to exist in bone cells^{54,55}. The primary gap junction in bone is Cx43^{54,56,57}. Cx43 produced Gap junctions have been demonstrated between osteoblasts^{8,58-62} as well as communication between osteocytes and osteoblasts^{1311,63}. The extensive network formed by osteocytes is also dictated by their gap junctions.

Gap junctions have been found to exist between bone marrow stromal cells⁶⁴. They have considerable consequences in defining the structural organization of the hematopoietic environment⁶⁵. This opens the possibility that bone marrow stroma can receive developmental cues via gap junctions⁵⁹.

Genetic modifications have been made to elucidate the role of Connexin 43 mediated gap junctions in different bone forming cell types and mouse models. Cx43 knockout mice have shown delayed ossification and osteoblasts dysfunctions⁸. Several studies indicate that the increase of Cx43 expression either by upregulation or transfection increases GJIC⁶⁶⁻⁶⁸, and have elucidated potential mechanisms of cell-cell communications⁶⁹⁻⁷². To understand the role in bone formation, null mice (Gja1jrt/+) carry a point mutation in the Cx43 gene that produces dominant negative properties⁷³. Cx43 null mice exhibit

profound mineralization defects in shape and mineralization of skeletal elements⁷⁴. These mice die pre-natally due to severe defect in the heart leading to swelling and blocking of the right ventricle outflow⁷⁵. Cells obtained from the cranium of these null mice showed delayed differentiation and mineralization⁷⁶. In order to understand the role of communication through gap junctions in bone cells, Rat osteosarcoma cell line UMR has been used as a model to determine the role of Cx43 in cells^{8, 77}. These cells are characterized for not expressing Cx43, but do in fact express Cx45.

Gap junctions have been implicated in many important mechanisms in bone regeneration such as the regulation of Erk, RankL, Tbox expression, responses to growth factors such as BMP-2, and the diffusion of paracrine agents such as PTH^{52, 56, 78-80}. A generalized mechanism for the gap junctional role of Connexin in bone cells can be developed based on the research done on this area (Figure 1). Our experiments investigate the effects of gap junctions when cells are stimulated with a potent osteoinductive agent.

1.5 Outline of Thesis Content

The coming chapters describe the experiments performed to address the aims of this thesis. The second chapter of this thesis contains a preliminary study that was performed to validate the micro CT thresholds for tissue engineered bone. These thresholds were used to analyze all in-vivo data in the subsequent chapters. Chapter number 3 addresses the effects exogenous seeding strategies and mineralized template on gap junction intercellular communication (GJIC), cell differentiation in 3D constructs, and bone regeneration in-vivo.

Chapter 4 examines enhancing endogenous cell-cell communication in bone marrow stromal cells, by transducing these cells with the most prevalent gap junction forming protein in bone, Connexin 43 (Cx43). Transfection efficiencies, Cx43 expression and GJIC were quantified to measure the expression level and function of the gap junctions. GJIC is measured and compared in both 2D and 3D cultures, as well as cell differentiation. Furthermore, the distribution of GJIC and differentiation markers is quantified, to quantify any differences in these parameters between cells on the surface of 3D scaffolds and those seeded at the core. To assess the effect of enhanced GJIC on tissue engineering in-vivo, cells are transplanted subcutaneously in nude mice, and examined for amount and spatial distribution of the regenerated tissue. The bone morphogenetic protein 7 (BMP7) was used to test the effects of higher GJIC along with a tissue forming stimulus. Cells were also transduced with a 7 base pair deletion on the Cx43 gene (Cx43 Δ 7), in order to assess the dominant negative effects of Cx43 in GJIC both in-vitro and in-vivo (Appendix 17).

The final chapter summarizes the important findings and interpretations of this thesis and presents a framework for future works

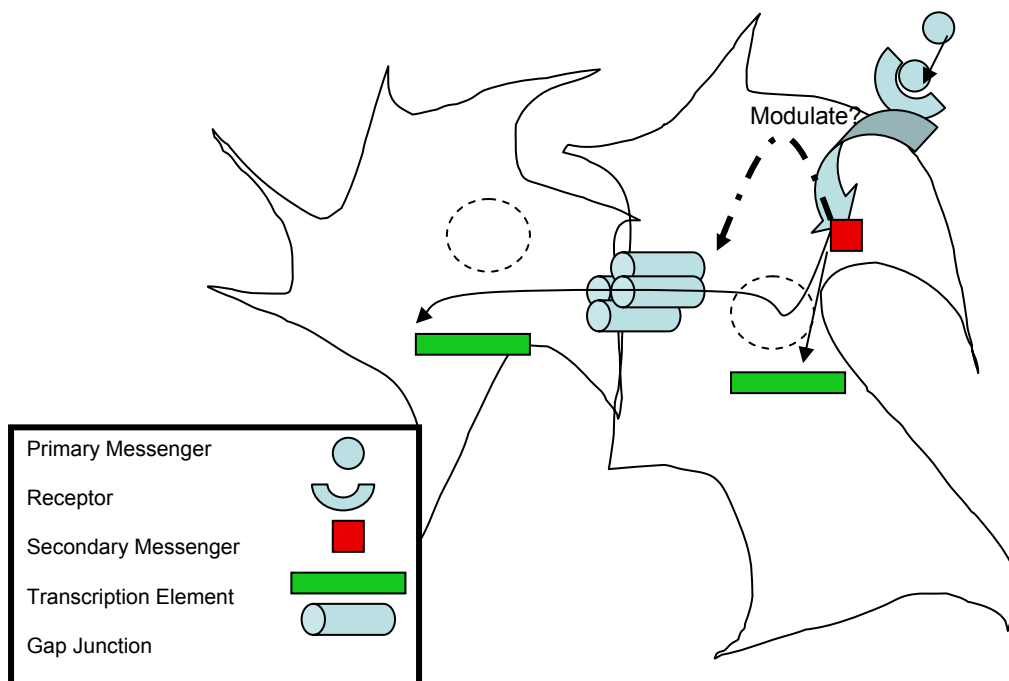


Figure 1-1: Generalized mechanism for the role of gap junction intercellular communication in bone cells.

A primary messenger in the form of a hormone, growth factor, or mechanical stimulation elicits a response from the host cell. This response is the production or influx of secondary messengers (e.g cADP, IP3, Ca²⁺) that enable the activation of a cascade (e.g. ERK). This cascade produces a transcriptional response in the host cell. The secondary messengers produced can modulate the gap junctions to either open or close. If open, these secondary messengers will go through the gap junction channel and elicit the same response (as in the host cell) in adjacent cells, without the need for a primary messenger to stimulate that cell.

1.6 References

1. Cheung C. The future of bone healing. *Clin Podiatr Med Surg.* 2005; 22(4):631-41. viii.
2. Amiel C, Bailly C, Friedlander G. Multiple hormonal control of the thick ascending limb functions. *Adv Nephrol Necker Hosp.* 1987; 16:125-136.
3. Logeart-Avramoglou D, Anagnostou F, Bizios R, Petite H. Engineering bone: Challenges and obstacles. *J Cell Mol Med.* 2005; 9(1):72-84.
4. Janouskova O, Fales I, Kobyłka P, Vonka V. Gene therapy of the graft versus host reaction. *Cas Lek Cesk.* 2003; 142(9):530-533.
5. Valimaki VV, Aro HT. Molecular basis for action of bioactive glasses as bone graft substitute. *Scand J Surg.* 2006; 95(2):95-102.
6. Langer R, Vacanti JP. Tissue engineering. *Science.* 1993; 260(5110):920-926.
7. Laurencin C, Khan Y, El-Amin SF. Bone graft substitutes. *Expert Rev Med Devices.* 2006; 3(1):49-57.
8. Lecanda F, Towler DA, Ziambaras K, et al. Gap junctional communication modulates gene expression in osteoblastic cells. *Mol Biol Cell.* 1998; 9(8):2249-2258.
9. Goldstein AS. Effect of seeding osteoprogenitor cells as dense clusters on cell growth and differentiation. *Tissue Eng.* 2001; 7(6):817-827.

10. Altman GH, Horan RL, Martin I, et al. Cell differentiation by mechanical stress. *FASEB J.* 2002; 16(2):270-272.
11. Cherian PP, Siller-Jackson AJ, Gu S, et al. Mechanical strain opens connexin 43 hemichannels in osteocytes: A novel mechanism for the release of prostaglandin. *Mol Biol Cell.* 2005; 16(7):3100-3106.
12. Romanello M, Veronesi V, D'Andrea P. Mechanosensitivity and intercellular communication in HOBIT osteoblastic cells: A possible role for gap junction hemichannels. *Biorheology.* 2003; 40(1-3):119-121.
13. Romanello M, D'Andrea P. Dual mechanism of intercellular communication in HOBIT osteoblastic cells: A role for gap-junctional hemichannels. *J Bone Miner Res.* 2001; 16(8):1465-1476.
14. Zaman MH, Matsudaira P, Lauffenburger DA. Understanding effects of matrix protease and matrix organization on directional persistence and translational speed in three-dimensional cell migration. *Ann Biomed Eng.* 2006;
15. Zaman MH, Trapani LM, Sieminski AL, et al. Migration of tumor cells in 3D matrices is governed by matrix stiffness along with cell-matrix adhesion and proteolysis. *Proc Natl Acad Sci U S A.* 2006; 103(29):10889-10894.
16. Schwiebert EM. Extracellular ATP-mediated propagation of Ca^{2+} waves. focus on "mechanical strain-induced Ca^{2+} waves are propagated via ATP release and purinergic receptor activation". *Am J Physiol Cell Physiol.* 2000; 279(2):C281-3.

17. Lecanda F, Warlow PM, Sheikh S, Furlan F, Steinberg TH, Civitelli R. Connexin43 deficiency causes delayed ossification, craniofacial abnormalities, and osteoblast dysfunction. *J Cell Biol.* 2000; 151(4):931-944.
18. Stains JP, Civitelli R. Cell-to-cell interactions in bone. *Biochem Biophys Res Commun.* 2005; 328(3):721-727.
19. Leonova EV, Pennington KE, Krebsbach PH, Kohn DH. Substrate mineralization stimulates focal adhesion contact redistribution and cell motility of bone marrow stromal cells. *J Biomed Mater Res A.* 2006; 79(2):263-270.
20. Franceschi RT, Yang S, Rutherford RB, Krebsbach PH, Zhao M, Wang D. Gene therapy approaches for bone regeneration. *Cells Tissues Organs.* 2004; 176(1-3):95-108.
21. Rutherford RB, Nussenbaum B, Krebsbach PH. Bone morphogenetic protein 7 ex vivo gene therapy. *Drug News Perspect.* 2003; 16(1):5-10.
22. Krebsbach PH, Gu K, Franceschi RT, Rutherford RB. Gene therapy-directed osteogenesis: BMP-7-transduced human fibroblasts form bone in vivo. *Hum Gene Ther.* 2000; 11(8):1201-1210.
23. Rossello RA, Krebsbach PH, Kohn DH. Effects of self-mineralizing templates and cell seeding techniques on volume of regenerated bone. *Trans 31st Annual Meeting Soc for Biomat.* 2005;

24. David H. Kohn, Kyungsup Shin, Sun-Ig Hong, Elena V. Leonova, Ricardo A. Rossello, Paul H. Krebsbach. Organic template mediated self assembly of mineral as a model system for biomineralization and bone tissue engineering. *MRS*. 2005;
25. Cartmell SH, Porter BD, Garcia AJ, Guldborg RE. Effects of medium perfusion rate on cell-seeded three-dimensional bone constructs in vitro. *Tissue Eng*. 2003; 9(6):1197-1203.
26. Zhao F, Ma T. Perfusion bioreactor system for human mesenchymal stem cell tissue engineering: Dynamic cell seeding and construct development. *Biotechnol Bioeng*. 2005; 91(4):482-493.
27. Burg KJ, Holder WD, Jr, Culberson CR, et al. Comparative study of seeding methods for three-dimensional polymeric scaffolds. *J Biomed Mater Res*. 2000; 51(4):642-649.
28. Meyer U, Wiesmann HP, Berr K, Kubler NR, Handschel J. Cell-based bone reconstruction therapies-principles of clinical approaches. *Int J Oral Maxillofac Implants*. 2006; 21(6):899-906.
29. Handschel J, Wiesmann HP, Depprich R, Kubler NR, Meyer U. Cell-based bone reconstruction therapies--cell sources. *Int J Oral Maxillofac Implants*. 2006; 21(6):890-898.
30. Hollister SJ, Maddox RD, Taboas JM. Optimal design and fabrication of scaffolds to mimic tissue properties and satisfy biological constraints. *Biomaterials*. 2002; 23(20):4095-4103.

31. Taboas JM, Maddox RD, Krebsbach PH, Hollister SJ. Indirect solid free form fabrication of local and global porous, biomimetic and composite 3D polymer-ceramic scaffolds. *Biomaterials*. 2003; 24(1):181-194.
32. Cima LG, Vacanti JP, Vacanti C, Ingber D, Mooney D, Langer R. Tissue engineering by cell transplantation using degradable polymer substrates. *J Biomech Eng*. 1991; 113(2):143-151.
33. Rezwani K, Chen QZ, Blaker JJ, Boccaccini AR. Biodegradable and bioactive porous polymer/inorganic composite scaffolds for bone tissue engineering. *Biomaterials*. 2006; 27(18):3413-3431.
34. Murphy WL, Kohn DH, Mooney DJ. Growth of continuous bonelike mineral within porous poly(lactide-co-glycolide) scaffolds in vitro. *J Biomed Mater Res*. 2000; 50(1):50-58.
35. Ishaug SL, Crane GM, Miller MJ, Yasko AW, Yaszemski MJ, Mikos AG. Bone formation by three-dimensional stromal osteoblast culture in biodegradable polymer scaffolds. *J Biomed Mater Res*. 1997; 36(1):17-28.
36. Krebsbach PH, Kuznetsov SA, Bianco P, Robey PG. Bone marrow stromal cells: Characterization and clinical application. *Crit Rev Oral Biol Med*. 1999; 10(2):165-181.
37. Kofron MD, Zhang JX, Lieberman JR, Laurencin CT. Genetically modified mesodermal-derived cells for bone tissue engineering. *IEEE Eng Med Biol Mag*. 2003; 22(5):57-64.

38. El-Amin SF, Kofron MD, Attawia MA, Lu HH, Tuan RS, Laurencin CT. Molecular regulation of osteoblasts for tissue engineered bone repair. *Clin Orthop Relat Res.* 2004; (427)(427):220-225.
39. Glicklis R, Shapiro L, Agbaria R, Merchuk JC, Cohen S. Hepatocyte behavior within three-dimensional porous alginate scaffolds. *Biotechnol Bioeng.* 2000; 67(3):344-353.
40. Holy CE, Shoichet MS, Davies JE. Engineering three-dimensional bone tissue in vitro using biodegradable scaffolds: Investigating initial cell-seeding density and culture period. *J Biomed Mater Res.* 2000; 51(3):376-382.
41. Li YJ, Batra NN, You L, et al. Oscillatory fluid flow affects human marrow stromal cell proliferation and differentiation. *J Orthop Res.* 2004; 22(6):1283-1289.
42. Holtorf HL, Sheffield TL, Ambrose CG, Jansen JA, Mikos AG. Flow perfusion culture of marrow stromal cells seeded on porous biphasic calcium phosphate ceramics. *Ann Biomed Eng.* 2005; 33(9):1238-1248.
43. Nair LS, Bhattacharyya S, Laurencin CT. Development of novel tissue engineering scaffolds via electrospinning. *Expert Opin Biol Ther.* 2004; 4(5):659-668.
44. Katz RW, Hollinger JO, Reddi AH. The functional equivalence of demineralized bone and tooth matrices in ectopic bone induction. *J Biomed Mater Res.* 1993; 27(2):239-245.

45. Ducheyne P, Qiu Q. Bioactive ceramics: The effect of surface reactivity on bone formation and bone cell function. *Biomaterials*. 1999; 20(23-24):2287-2303.
46. Jorgensen NR, Henriksen Z, Brot C, et al. Human osteoblastic cells propagate intercellular calcium signals by two different mechanisms. *J Bone Miner Res*. 2000; 15(6):1024-1032.
47. Triggle DJ. L-type calcium channels. *Curr Pharm Des*. 2006; 12(4):443-457.
48. Berridge MJ, Lipp P, Bootman MD. The versatility and universality of calcium signalling. *Nat Rev Mol Cell Biol*. 2000; 1(1):11-21.
49. Rottingen J, Iversen JG. Ruled by waves? intracellular and intercellular calcium signalling. *Acta Physiol Scand*. 2000; 169(3):203-219.
50. Willecke K, Eiberger J, Degen J, et al. Structural and functional diversity of connexin genes in the mouse and human genome. *Biol Chem*. 2002; 383(5):725-737.
51. Pettway GJ, Schneider A, Koh AJ, et al. Anabolic actions of PTH (1-34): Use of a novel tissue engineering model to investigate temporal effects on bone. *Bone*. 2005; 36(6):959-970.
52. Civitelli R, Ziambaras K, Warlow PM, et al. Regulation of connexin43 expression and function by prostaglandin E2 (PGE2) and parathyroid hormone (PTH) in osteoblastic cells. *J Cell Biochem*. 1998; 68(1):8-21.

53. Wyatt LE, Chung CY, Carlsen B, et al. Bone morphogenetic protein-2 (BMP-2) and transforming growth factor-beta1 (TGF-beta1) alter connexin 43 phosphorylation in MC3T3-E1 cells. *BMC Cell Biol.* 2001; 2:14.
54. Stains JP, Civitelli R. Gap junctions in skeletal development and function. *Biochim Biophys Acta.* 2005; 1719(1-2):69-81.
55. Steinberg TH, Civitelli R, Geist ST, et al. Connexin43 and connexin45 form gap junctions with different molecular permeabilities in osteoblastic cells. *EMBO J.* 1994; 13(4):744-750.
56. Stains JP, Civitelli R. Cell-cell interactions in regulating osteogenesis and osteoblast function. *Birth Defects Res C Embryo Today.* 2005; 75(1):72-80.
57. Civitelli R. Cell-cell communication in bone. *Calcif Tissue Int.* 1995; 56 Suppl 1:S29-31.
58. Stanka P. Occurrence of cell junctions and microfilaments in osteoblasts. *Cell Tissue Res.* 1975; 159(3):413-422.
59. Doty SB. Morphological evidence of gap junctions between bone cells. *Calcif Tissue Int.* 1981; 33(5):509-512.
60. Palumbo C, Palazzini S, Marotti G. Morphological study of intercellular junctions during osteocyte differentiation. *Bone.* 1990; 11(6):401-406.
61. Jones SJ, Gray C, Sakamaki H, et al. The incidence and size of gap junctions between the bone cells in rat calvaria. *Anat Embryol (Berl).* 1993; 187(4):343-352.

62. Schiller PC, D'Ippolito G, Balkan W, Roos BA, Howard GA. Gap-junctional communication is required for the maturation process of osteoblastic cells in culture. *Bone*. 2001; 28(4):362-369.
63. Thi MM, Kojima T, Cowin SC, Weinbaum S, Spray DC. Fluid shear stress remodels expression and function of junctional proteins in cultured bone cells. *Am J Physiol Cell Physiol*. 2003; 284(2):C389-403.
64. Dorshkind K, Green L, Godwin A, Fletcher WH. Connexin-43-type gap junctions mediate communication between bone marrow stromal cells. *Blood*. 1993; 82(1):38-45.
65. Montecino-Rodriguez E, Leathers H, Dorshkind K. Expression of connexin 43 (Cx43) is critical for normal hematopoiesis. *Blood*. 2000; 96(3):917-924.
66. Kizana E, Ginn SL, Allen DG, Ross DL, Alexander IE. Fibroblasts can be genetically modified to produce excitable cells capable of electrical coupling. *Circulation*. 2005; 111(4):394-398.
67. Dull T, Zufferey R, Kelly M, et al. A third-generation lentivirus vector with a conditional packaging system. *J Virol*. 1998; 72(11):8463-8471.
68. Zufferey R, Nagy D, Mandel RJ, Naldini L, Trono D. Multiply attenuated lentiviral vector achieves efficient gene delivery in vivo. *Nat Biotechnol*. 1997; 15(9):871-875.
69. Stains JP, Lecanda F, Screen J, Towler DA, Civitelli R. Gap junctional communication modulates gene transcription by altering the recruitment of Sp1 and

- Sp3 to connexin-response elements in osteoblast promoters. *J Biol Chem.* 2003; 278(27):24377-24387.
70. Hagen G, Muller S, Beato M, Suske G. Sp1-mediated transcriptional activation is repressed by Sp3. *EMBO J.* 1994; 13(16):3843-3851.
71. Majello B, De Luca P, Lania L. Sp3 is a bifunctional transcription regulator with modular independent activation and repression domains. *J Biol Chem.* 1997; 272(7):4021-4026.
72. Lania L, Majello B, De Luca P. Transcriptional regulation by the sp family proteins. *Int J Biochem Cell Biol.* 1997; 29(12):1313-1323.
73. Flenniken AM, Osborne LR, Anderson N, et al. A Gja1 missense mutation in a mouse model of oculodentodigital dysplasia. *Development.* 2005; 132(19):4375-4386.
74. Lecanda F, Warlow PM, Sheikh S, Furlan F, Steinberg TH, Civitelli R. Connexin43 deficiency causes delayed ossification, craniofacial abnormalities, and osteoblast dysfunction. *J Cell Biol.* 2000; 151(4):931-944.
75. Reaume AG, de Sousa PA, Kulkarni S, et al. Cardiac malformation in neonatal mice lacking connexin43. *Science.* 1995; 267(5205):1831-1834.
76. Furlan F, Lecanda F, Screen J, Civitelli R. Proliferation, differentiation and apoptosis in connexin43-null osteoblasts. *Cell Commun Adhes.* 2001; 8(4-6):367-371.

77. Jorgensen NR, Geist ST, Civitelli R, Steinberg TH. ATP- and gap junction-dependent intercellular calcium signaling in osteoblastic cells. *J Cell Biol.* 1997; 139(2):497-506.
78. Schiller PC, Roos BA, Howard GA. Parathyroid hormone up-regulation of connexin 43 gene expression in osteoblasts depends on cell phenotype. *J Bone Miner Res.* 1997; 12(12):2005-2013.
79. Zhang W, Green C, Stott NS. Bone morphogenetic protein-2 modulation of chondrogenic differentiation in vitro involves gap junction-mediated intercellular communication. *J Cell Physiol.* 2002; 193(2):233-243.
80. Wyatt LE, Chung CY, Carlsen B, et al. Bone morphogenetic protein-2 (BMP-2) and transforming growth factor-beta1 (TGF-beta1) alter connexin 43 phosphorylation in MC3T3-E1 cells. *BMC Cell Biol.* 2001; 2:14.

Chapter 2

Establishing Micro CT Thresholds for Tissue Engineered Bone and Comparison of Bone Regenerated from Bone Marrow Stromal Cells and BMP-7 Transduced Cells

2.1 Introduction

To regenerate complex tissues such as bone, a variety of cell types, including differentiated cells, progenitor cells and genetically modified cells have been delivered from designed scaffolds¹⁻³. Bone regeneration from transplanted cells has been accomplished in open and closed systems in large and small animals, and human clinical trials are underway^{4,5}. Comparison of the quantity and quality of bone regenerated via different strategies is lacking, however, in part because standardized means of analyzing bone regeneration are lacking. Standard radiographic and histological techniques provide a starting point for analysis of regenerated tissue and efficacy of tissue engineering strategies⁶. These techniques are useful, but they cannot be easily used to measure the amount of new bone tissue nor the mineral content of that bone tissue in three dimensions. The gold standard for accurately measuring the amount of new bone tissue is histomorphometry, where two-dimensional sections of a region with the scaffold are stained and the amount of new bone tissue is quantified. The gold standard for measuring

the bone mineral content is ash weighing. In this procedure, bone is heated to temperatures upwards of 800°C, eliminating organic phases, and the remaining non-organic weight is measured and normalized to starting weight or tissue volume. Although these techniques provide an accurate determination of the amount of mineral and the mineral content, their usefulness in analyzing tissue engineering strategies is limited because specimens are destroyed in the process eliminating the possibility of further molecular and biochemical analyses.

Micro-computed tomography (μ CT) has become an important tool to overcome these limitations. This imaging modality has a wide range of biological applications including vascular and pulmonary trees, adipose tissue, embryonic development, cartilage and hepatic tissue, and it is particularly well suited for bone.⁷⁻¹⁷ For bone, μ CT provides detailed spatial reconstruction of mature^{18, 19} and regenerated bone²⁰⁻²³. These reconstructed μ CT images can be used to determine bone architecture in three orthogonal directions. The bone volume fraction (BVF) and bone mineral density (BMD) can also be calculated using algorithms that are independent of orientation using custom or commercially available software. One concern, however, when performing these calculations is separating the bone tissue from the other tissues within the image. This is particularly crucial for BVF calculations where care must be taken to accurately determine a threshold for the voxel intensity that distinguishes bone from marrow, air, fibrous tissue or surrounding scaffold.

Three thresholding approaches have been employed to solve this problem. One approach employs an autothresholding function that uses the frequency distribution (histogram) of voxel values in the images to determine the threshold between two

populations. This algorithm assumes that the image has a bimodal histogram, a mid-point of the intermodal zone is chosen as the cut-off between bone and soft tissue based on optimization of the variance between the two histogram peaks²⁴. The second approach that has been used for trabecular bone thresholding is local thresholding^{25, 26}. In this approach, the local neighborhood of every voxel within the μ CT image is taken into account when determining if a voxel is bone. This approach is powerful; however it can be complex to implement. Because of this complexity, and because many bone regenerative approaches do not have a bimodal histogram (Figure 1), the vast majority of tissue engineering studies do not employ these methodologies. Instead, they use a simple global threshold where a single grayscale value is selected and voxels with intensities over that number are defined as bone. Using this global thresholding approach is a source of concern because the source of such standardization is unclear and may lead to an inaccurate quantification of the amount of bone and, therefore, an inappropriate comparison of bone regenerated under different conditions.

Because of these limitations, the goal of these experiments was to determine a global threshold for quantification of volume fraction of tissue engineered bone using μ CT. To determine the appropriate threshold, the amount of regenerated bone determined via μ CT was compared to the amount of regenerated bone determined by the more conventional techniques of ashing and quantitative histology. Regressions were performed on three types of data over a range of thresholds to determine the threshold that yielded the best fit between μ CT data and conventional data. First, the BVF determined from μ CT was compared with the ash fraction to compare the amount of new bone three-dimensionally. Second, the 2D area fraction of bone determined from μ CT

and the 2D area fraction determined via H&E staining in a closely aligned histological plane were used for visual and quantitative comparisons. Quantification of bone on H&E stained sections can be subject to variation because measurements are dependent on subtle changes in the matrix architecture, so von Kossa staining, which has high contrast in areas of mineralization, was also employed. The third regression comparison compared the 2D area fraction of bone determined from μ CT with 2D mineral fraction determined by thresholding von Kossa stained histological sections. In order to make this analysis applicable to images obtained using different μ CT scanners, the thresholds were normalized to the Bone HU value from the hydroxyapatite phantom. This hydroxyapatite has a similar radiodensity to mature bone and does not change. Normalizing to this value (reported as % Bone HU) reflects the ratio of the threshold radiodensity in comparison to the radiodensity of mature bone. After an appropriate threshold was determined, a comparative study between the amount and distribution of bone regenerated *in-vivo* from transplanted murine BMSCs and BMP-7 transduced cells was conducted.

2.2 Materials and Methods

2.2.1 Bone marrow stromal cell isolation and culture

Five- to eight-week old male C57BL/6 mice were used to isolate bone marrow cells from the femoral, tibial and humeral cavities (six bones per animal), as previously described²⁷. Briefly, bone marrow cells were isolated by extracting the marrow from the bone cavities. The bone marrow was mixed with complete medium (minimum essential medium (α -MEM; Gibco Laboratories, Grand Island, NY), 10% fetal bovine serum

(FBS; Gibco), 100 µg/ml penicillin G, 100 IU/ml streptomycin). Cells were pelleted by centrifugation at 1000 rpm for 5 min at 4°C and resuspended in 10 ml α -MEM. Cell number was determined with a hemocytometer and cells were plated in 75 cm² flasks at a density of 50,000 nucleated cells/cm² and cultured in complete medium at 37°C in 5% CO₂/95% air. The medium was replaced twice per week and at near confluence (~90%), the adherent cells were washed with phosphate-buffered saline and released by means of a 0.25% trypsin-EDTA solution (Sigma, St. Louis, MO). Cells were replated in 75 cm² flasks at a density of 50,000 cells/cm² and passaged 1-2 more times.

2.2.2 Generation of recombinant adenovirus and cell transduction

AdCMVBMP7 was constructed by Cre-*lox* recombination, as previously described²⁸. Briefly, a full-length mouse BMP-7 cDNA was cloned into pAdlox to produce pAdlox BMP-7. pAdlox and ψ 5 virus were co-transduced into CRE8 cells. A plaque assay was used to purify the virus from the cell lysate and serial dilutions were used to infect 293 cells. Positive plaques were purified by CsCl gradient ultracentrifugation. The purified virus was stored in glycerol phosphate-buffered saline and titered by the method described above.

Mouse C4 cells, a widely used cell strain from C57L/J mice, from American Type Culture Collection (ATCC) were cultured in complete medium at 37°C in 5% CO₂/95% air. Transduction was performed *ex vivo* for 24 hrs. C4 cell infection with AdCMVBMP - 7 was at a multiplicity of infection (MOI) of 200 Plaque-forming units (PFU)/cell. Cells, 80-90% confluent in 75 cm² flasks, were exposed to the appropriate dilution of virus in 8 ml of medium for 24 hrs at 37°C in a humidified atmosphere of 5% CO₂ before trypsinization, counting, and resuspension in complete medium.

2.2.3 Gelatin sponge preparation

Gelatin sponges (Gelfoam®; Pharmacia & Upjohn, Kalamazoo, MI) were cut to have 3×3×2 mm³ dry dimensions. The sponges were pre-wet in complete medium, and air bubbles were removed by applying gentle pressure on the sponge between two pieces of sterile filter paper. Two million BMSCs or transduced C4 cells were collected, suspended in 50 µl complete medium, and loaded onto each sponge by capillary action.

2.2.4 Preparation of bioceramic (Mineralized PLGA) scaffold

Porous, 3D organic templates (85:15 poly(lactide-co-glycolide), diameter = 4mm x height = 1mm, 90% porosity, pore size 250-425µm) were prepared by solvent casting-particulate leaching process. Scaffolds were each be incubated in a 50-mL solution of simulated body fluid (SBF) for 7 days for mineral film formation. The SBF solution will be changed every 24 h to ensure sufficient ion concentrations for mineral growth. The SBF was prepared by dissolving the following reagents in deionized water: 141 mM NaCl, 4.0 mM KCl, 0.5 mM MgSO₄, 1.0 mM MgCl₂, 4.2 mM NaHCO₃, 2.5 mM CaCl₂, and 1.0 mM KH₂PO₄. SBF was buffered to maintain a pH 7.4 with Tris-HCl and washed at 37°C for the duration of the incubation period.

2.2.5 Transplantation into host mice

All procedures involving animals were performed in accordance with protocols approved by the University Committee on Use and Care of Animals (UCUCA) at the University of Michigan. A total of 60 implants (30 BMSC loaded implants and 30 transduced cell loaded implants) were transplanted subcutaneously into 15 nude mice, as previously described¹. Briefly, nude mice (nu/nu) were anesthetized by an intraperitoneal

injection of 100 mg/kg ketamine and 10 mg/kg xylazine. An incision was made on the back of each mouse and implants were inserted into the subcutaneous cavities. Four gelatin/cell constructs (2 BMSC, 2 BMP-7) were placed per mouse and wounds were closed with surgical clips. The location of the constructs within each mouse was randomized.

2.2.6 Micro-CT image acquisition and analysis

Ossicles were scanned on a high resolution cone beam micro-CT system (Enhanced Vision Systems (now GE Healthcare Preclinical Imaging), London, Ontario, Canada) while immersed in distilled H₂O. The x-ray source voltage and current were 80 kVp and 80 μ A, respectively. To reduce the potential for beam hardening artifact, the x-rays were passed through a 0.2mm Al filter immediately upon exiting the source and the specimens were immersed in dH₂O during the scanning process. Projection images were acquired over 198 degrees using 2x2 binning and an exposure time of 1100 ms, and four frames were averaged for each projection to improve the signal to noise ratio. The projection data was then corrected and reconstructed using the Feldkamp cone-beam algorithm to create three-dimensional images with an isotropic voxel size of 18 μ m. The scanner was calibrated once daily using a phantom that contained air, water and hydroxyapatite..

Bone volume fractions were determined by using a MatLab program designed to integrate all grayscale voxels above a particular threshold. To determine the overall volume of the ossicles, the program determined the perimeter of each 2D μ CT slice by tracing the outer edge. The program then integrated all the perimeters to determine the 3D surface area, and the number of voxels inside the surface defined the total volume.

High density voxels outside of the 3D surface and unattached to the ossicle were discarded, while voxels inside were evaluated at the specified thresholds to determine the BVF, which was calculated as the number of voxels above the threshold relative to the total number of voxels. Bone volume fractions were calculated for all samples at a range of thresholds (600-2000, in increments of 100) ,in order to create a library of BVF values for regression against ash fraction and histologically determined bone and mineral fractions. % bone HU (threshold/bone HU) was calculated for all of the thresholds, in order to make the results applicable to any μ CT device. The bone HU (Hounsfield units) was obtained from the calibration scans of actual bone. Auto thresholds, generated using a previously described method that operates on the histogram of all grayscale values within the image,²⁴ were also recorded for comparison.

2.2.7 Mineral ashing

After μ CT scanning, 5 ossicles from each group were weighed, placed in a muffle furnace at 100°C for 36 hrs to remove the soft-tissue in the ossicles, and reweighed. This fraction was heated to 800°C for 48 hrs to obtain the final inorganic weight. The final inorganic weight was normalized to the ossicle weight (without soft tissue) to determine ash fraction.

2.2.8 Histology

To assist in matching histological sections to μ CT slices, a landmark was created in each ossicle by making a small cut with a scalpel before it was scanned in the μ CT system²⁵ The longitudinal and transverse distances to the landmark from a reference point on the surface were recorded to define the approximate location and orientation of

the slices of interest, thus making it easier to locate when viewing the μ CT and histological sections. After μ CT scanning, the remaining ossicles from each group were rinsed in dH_2O , dehydrated in graded ethanol, and processed for histology. Some of the specimens were decalcified in 10% formic acid for 5 days, embedded in paraffin, sectioned in $5\mu\text{m}$ slices, deparaffinized, hydrated, and stained with hematoxylin and eosin (H&E). The remaining specimens remained undecalcified and were embedded in plastic, sectioned to $5\mu\text{m}$ and stained with von Kossa. For both decalcified and undecalcified sections, the first $5\mu\text{m}$ section below the landmark was used for comparison with the first μ CT slice below the landmark. The next 3 serial sections ($\sim 50\mu\text{m}$ apart from each other) were also compared with their corresponding μ CT slices for three regression analyses. Since the histological sections were approximately $50\mu\text{m}$ apart, the maximum distance between the histological and μ CT slices is $< 50\mu\text{m}$. Both H&E and von Kossa stained slides were photographed and processed blindly with respect to treatment group with Image Pro Plus 4.0. A 2D visual alignment followed to subjectively compare the histological sections with the analogous micro CT sections. This approach, although not an exact mathematical registration of the images, allows for both good side by side visual comparison (Figure 3) and quantitative comparison for the von Kossa and μ CT data sets. The amount of mineral present in the von Kossa images was set using a grayscale selection mechanism relative to a standard (Image Pro Plus 4.0). The same approach was used to compare the actual amount of bone fraction in the H&E stained sections with a μ CT slice. Here, bone fraction in the H&E slides was determined by careful visual examination of regions where bone was observed. These selected sections

were quantified and the results were stated as a fraction of the complete area of the ossicle.

2.2.9 Analysis of bone ingrowth

A custom program was developed to determine the distribution of regenerated bone as a function of the distance to the geometric center of each ossicle. Using the von Kossa stained sections, the centroid was calculated using a MatLab script ⁸ and used as a frame of reference to divide the ossicles into 4 regions. Defining the centroid as the 0th percentile and the edge as the 100th percentile, boundaries were calculated by lines that radially pointed into the center from the edges. Using the same selection criterion for defining mineral as above, the program determined the percent of bone present in regions 0-25%, 25-50%, 50-75% and 75-100% of the area away from the centroid.

2.2.10 Statistical analyses

Linear regression analyses were performed to determine the thresholds with highest R^2 values and an optimal threshold range for defining de-novo bone. This optimal threshold is defined as a range where $R^2 > 0.85$. The BVF predicted by μ CT was regressed against ash fraction over a range of thresholds (600-2000 in increments of 100) to determine a volumetric correlation. Two dimensional correlations were also performed over the same threshold range to compare the 2D area fraction of bone determined from μ CT vs. the 2D area fraction determined via H&E and von Kossa. Regressions were performed for each cell type and time independently and by pooling cell types and time (SigmaStat 3.1). Comparisons between mean BVF or area fraction and ashing or histology at each threshold were also carried out via t-tests (paired, two-

tailed). Because this range of thresholds can vary on different scanners, the ratio of these thresholds to the bone HU value was calculated and will be reported in addition to the actual grayscale values used..

Two way analyses of variance (ANOVA) were used to evaluate effects of time and cell type on overall volume, BVF and mineral content. One way ANOVA on bone fraction as a function of cell type and region were also performed. All analyses were performed using SigmaSTAT version 3.1, using Turkey's HSD post hoc test. Statistical significance for all tests was assumed if the $p < 0.05$.

2.3 Results

2.3.1 Threshold analysis

There was no difference in the optimal threshold range (defined as having an $R^2 > 0.85$) between ossicles formed from BMSC and BMP7 transduced cells. Therefore, thresholding results are reported on data pooled from both cell types. Based on the comparison of μ CT BVF calculations with ash fraction data, there was a slight difference in the optimal threshold with time of implantation (Fig. 2). At 4 weeks, a threshold of 1000 yielded the highest coefficient of variation (Fig. 2a), whereas the threshold with the highest R^2 increased to 1100 and 1300 at 8 and 12 weeks, respectively (Fig. 2b and 2c). The highest R^2 for the pooled times occurred at a threshold of 1000 ($R^2 = 0.9431$, Fig. 2d). There was no significant difference in the BVF of ossicles calculated at a threshold of 1000 vs. 1300. P-values for the regressions in the 1000-1300 range are significant ($p = 0.021$, $p = 0.042$, $p = 0.009$, $p = 0.049$, respectively), while those for higher thresholds were not significant.

Regressions on the quantity of bone determined on 2D μ CT slices vs. H&E sections had the highest R^2 values at a threshold of 1200 for all individual timepoints and the data pooled across timepoints (Fig. 3a through 3d). The range of threshold values with high coefficients of correlation (1000-1300) are identical for the 3D comparison of μ CT BVF to ash fraction data that occur for the 2D comparison of H&E stained sections with corresponding planes of the μ CT images.

von Kossa stained sections verified the location of mineral deposition in 2D and suggested that ossicles were less dense at the early stages of regeneration than at later timepoints (Fig. 4, left panel). This increase in mineral content packing is also observed on comparable 2D planes of the μ CT images (Fig. 4, right panel). Regressions on the quantity of bone determined on 2D μ CT images vs. von Kossa stained sections demonstrated the highest R^2 values at a threshold of 1000 after 4 weeks and 12 weeks of implantation and 1100 after 8 weeks of implantation (Fig. 4). When the data were pooled among timepoints, the global threshold value of 1000 had the highest coefficient of variation (Fig. 5d).

To further ensure that the global threshold range of 1000-1300 on a μ CT image accurately represents the amount of bone, the data were pooled across timepoints and μ CT data was statistically compared with the ash fraction and histology data. There were no significant differences between the μ CT data and the corresponding ash fraction or histology data. When taken in conjunction with the regression analyses, this suggests that this threshold range can accurately be used to quantify the amount of bone on a μ CT image. Therefore, an optimal threshold range was defined as 1000-1300.

Autothreshold values show a marked difference (25-48%) from the threshold with highest R^2 value at 4 and 12 weeks, and this difference was even larger at 8 weeks (Table 1). The autothresholds for the 8 week groups were significantly greater ($p = 0.0213$) than those for the 4 and 12 week periods, and had greater variability within each group, even though the regressions indicate that the optimal threshold range for the 8 week timepoint is similar to the optimal threshold range for the 4 week and 12 week timepoints. Autothresholds were greater than the optimal threshold range determined by the regressions, which would lead to an underprediction of BVF if autothresholds were utilized.

2.3.2 Comparison of bone regenerated with different cell types

Both transplanted BMSCs and BMP-7 transduced cells formed self-contained, mineralized bone and bone marrow organs (Fig. 6c). An intact cortical shell of bone defined the external boundaries of the ossicles, and the internal portion of the implants contained amorphous mineralized tissue (Fig. 6b-6c). While both cell types supported active hematopoiesis, bone formed from BMP transduced cells often had small amounts of fibrous tissue localized to the central regions of the implant. Quantifying the amount of bone indicated that there was a statistically significant increase in the volume fraction of bone regenerated throughout the duration of the study (Fig. 6a). However, there was no significant difference in the volume fraction of bone formed between the two cell types.

Variations in the ossicle volume also occurred throughout the study. The ossicles derived from BMP-7 transduced cells were consistently larger than ossicles formed from BMSCs ($p < 0.001$ for all time points) and significantly larger than the original scaffold after 2 weeks ($p = 0.032$). BMSC derived ossicles were small and maintained the size of

the original implanted scaffold (Fig. 7A). Transient differences in the ossicle volume also occurred throughout the study. The volume of the ossicles was significantly greater in the 12 week group compared to the 4 and 8 week groups in both cell types (BMSC: $p=0.021$ for 4 weeks vs. 12 weeks and $p=0.024$ for 8 weeks vs. 12 weeks; BMP-7: $p=0.049$ for 4 weeks vs. 12 weeks and $p=0.044$ 8 weeks vs. 12 weeks). Similar transient differences occurred in the ossicle ash content. The ash content was significantly greater in the ossicles formed from BMP-7 transduced cells in comparison to ossicles formed from BMSCs at all timepoints ($p = 0.002, 0.001, 0.021$ at 4, 8 and 12 weeks, respectively). The ash content increased significantly after 4 weeks in bone formed from both cell types (Fig. 7b; BMSCs: $p=0.20$ for 4? weeks vs. 8 weeks and $p=0.029$ for 8 weeks vs. 12 weeks; BMP-7: $p=0.001$ for 4? weeks vs. 8 weeks).

There was also a significant difference in the distribution of bone regenerated by the two cell types (Fig. 8). As observed in the μ CT renderings, the ossicles show distinct patterns of osteogenesis (Fig. 6b). The bone regenerated by BMSCs showed significantly more bone formation in the periphery (76-100th percentile region) for the BMSCs vs. BMP-7 transduced cells ($p=0.0198$), with light mineral expression in the central part of the ossicle. There was significantly more internal bone regeneration in the BMP-7 constructs than for the BMSC constructs ($p=0.0308$ in the 0-25th percentile region and $p=0.0242$ in the 26-50th percentile region)..

To demonstrate that the thresholds were not specific to the resorbable gelatin scaffolds, bioceramic scaffolds, synthesized by the self assembly of carbonated apatite²⁹,³⁰, were also tested. The volume fraction of bone regenerated from BMSCs transplanted on these scaffolds for 6 weeks was analyzed. Regressions between BVF (calculated as

the percentage of voxels above the threshold in the bone/bioceramic composite minus the mean percentage of voxels above the threshold in a group of ceramic scaffolds implanted without cells) and ash fraction (calculated as the ash fraction of the bone/bioceramic composite minus the mean ash fraction of a group of ceramic scaffolds implanted without cells) showed that the highest correlation was achieved at 1200 and the range 1000-1300 exhibited R^2 values greater than 0.95 (Fig. 9).

2.4 Discussion

Micro CT has been extensively used to characterize mature trabecular bone^{18, 19, 25, 31, 32} and, more recently, to characterize bone regenerated via a variety of tissue engineering approaches²⁰⁻²³, as well as porous scaffolds themselves³³⁻³⁵. The strength of this technique lies in both the ability to nondestructively image the tissue in 3D and, more importantly, quantification of the structures within the three dimensional image. However, before any analyses can be performed the bone tissue must be separated from the marrow, water, air and other soft tissue within the image. The differentiation between bone and nonbone is generally based upon differences in radiodensity. The inherent difficulty in this procedure may cause image thresholding techniques to have a major impact on the characterization of osteogenesis^{19, 25}. Because of this, there has been an extensive effort to rigorously compare bone morphometric measures from μ CT images with histological sections for trabecular bone measurements.^{19, 36-38} Three major thresholding approaches have been used to facilitate these comparisons.

Algorithm based auto-thresholds have been extensively used to delineate bone from the other tissues³². These methods are statistical in nature, do not segment based on

features within the image, and rely on the assumption that the histogram of all grayscale values within the image has a bimodal distribution. This assumption may not be valid when dealing with small, newly formed bone ossicles, (Figure 1) making this approach variable and potentially inaccurate. In fact, when this approach was applied it resulted in threshold values which were at least 25% greater than the optimal thresholds (those with high R^2 values when compared with reference data), leading to an underestimate in BVF if these autothresholds are used, reiterating its inadequacy for tissue engineered ossicles (Table 1). The second thresholding approach, and perhaps the most extensively validated for trabecular bone have required the use of local and/or adaptive thresholding techniques.²⁶ However, these algorithms can be difficult to implement and, as a result, one of the most common thresholding techniques uses a simple global threshold. For tissue engineered constructs, standardized global thresholding can be a problem because the thresholds may have been determined for mature bone of larger volume and, therefore, may underestimate the amount of newly formed bone. This problem can be exacerbated if the heterogeneity within a specimen is large and if used between specimens¹⁸. These techniques are useful for bone tissue engineering,(Hedberg et al.) but the details of their application are seldom discussed.

The underlying concept in this study is that the gelatin scaffold used to deliver transplanted cells will not directly affect bone measurements in a μ CT image. This vehicle causes little to no interference because it has a radiodensity different than mineralized tissue and, furthermore, it degrades completely within 4 weeks eliminating the possibility of artifact from residual scaffold. The lack of peaks in the histogram between the bone and water regions (Fig. 1) prove that degradation of the gelatin was

complete. Therefore, a direct analysis could be made to compare the BVF calculated from the μ CT data to the actual values determined from ashing the ossicles. Ash content was normalized to the original tissue weight, to account for any discrepancies in size between the samples.

The optimal threshold range for determining volume fraction of regenerated bone was in the 1000-1300 grayscale value range. Confidence in this range of thresholds comes from 3 sources: (1) the range of 1000-1300 has a $R^2 > 0.87$ and $p < 0.05$ (Fig. 2,3,5), (2) the correlations and levels of significance quickly diverge as the threshold is set below 900 or above 1400, and (3) there is no significant difference in the BVF of ossicles measured between 1000 and 1300. A slight increase in the threshold value with the highest R^2 with respect to implantation time was observed when the 3D measures were compared (Fig. 2). This time dependence suggests that mineral packs over time, and is therefore detected at a higher intensity at later times. At earlier times, where the mineral is more dispersed, the amount of mineral present in a voxel might not be enough to be recognized at a higher threshold. However, this time dependence was not present when 2D histological data was compared with analogous μ CT sections (Fig. 3, Fig. 5). This may be due to the inherent 2D limitations of the histology, but this seems unlikely because overestimating (or underestimating) effects of a particular μ CT section are corrected because they are being compared to their analogous closely aligned histological slide. Another possible explanation for the difference in temporal sensitivity of the ash fraction and histological data is that the three-dimensional structure of the bone within the ossicle affects the thresholding process. There may be more partial volume artifact in 3D, and this may have an impact when making comparative measurements since the

ashing process will not be affected by partial volume problems. Because of this, in future studies it may be prudent to select a single global threshold within the 1000-1300 range and apply it to constructs across the timepoints of interest.

This study also compared the osteogenic potential of two cell sources *in-vivo*. Both BMSCs and BMP-7 transduced cells formed mineralized ossicles, but showed different patterns of tissue formation *in-vivo*. The overall volumes of the regenerated ossicles were significantly different between the different cells and time (Fig. 7). At 8 weeks, the ossicles were not significantly bigger than their 4 week counterparts (Fig. 7), but had a significantly greater amount of bone within the implant (Fig. 6a, Fig. 7b). This suggests that bone apposition may occur by further mineralization of the bone that is present as well as new bone formation in areas that were previously unmineralized. The 12 week period shows that the ossicles became larger and, although it was not significantly different, tended to have a higher bone volume fraction. These effects may be contributing to the disparity in auto-threshold values (Table 1) observed in the three time periods. The threshold value increases between 4 and 8 weeks, before decreasing.

The overall size and mineral content of ossicles formed by BMP-7 transduced cells were significantly greater compared to the ossicles formed from BMSCs. BMP-7 not only stimulates osteoblastic differentiation of osteoprogenitors but may also differentiate the transduced non-osteogenic mesenchymal cells to osteoblast lineage cells^{2, 3, 39}. Cell-mediated recombinant protein delivery may be superior to direct growth factor implantation, because the continuous secretion of BMP-7 may act as a paracrine agent, diffusing into the surrounding host tissue and stimulating responsive host cells in a manner similar to that proposed for exogenous recombinant BMP-7. Cell mediated BMP

delivery may also act as an autocrine agent to induce the osteoblastic differentiation of implanted cells. Another possible mechanism is that one of the paracrine effects of secreted BMP-7 is to stimulate responsive cells to synthesize and secrete BMP and hence propagate the signal throughout the implant.

The distribution results verify the qualitative observation that most of the mineral formation is on the periphery for the BMSC transplants (Fig. 8). The development of a shell of bone on the periphery suggests that the cells on the outside differentiate more quickly, possibly because they are exposed to more signals and nutrients. If it occurs before internal mineralization, this tissue formation at the periphery of a scaffold creates a border that increases the resistance to nutrients flowing in and byproducts flowing out, potentially leaving the inside cells trapped and undifferentiated⁴⁰. Bone ossicles formed from BMP-7 transduced cells have more dispersed mineral, and are larger. This decrease in mineral reduces the resistance of nutrients into the core of the construct, enhancing cell nutrition and decreasing the possibility of an undesirable micro-environment due to toxic byproducts. BMP release from the transduced cells seems to enhance the rate of differentiation. This is evident by the significantly higher mineral content in the 4 week group. This rapid differentiation leads to tissue formation throughout the construct.

Based on our study, we hypothesize that co-seeding of BMP-7 transduced cells and BMSCs would have therapeutically advantageous results. BMP-7 transduced cells would be used on the epiphysis area to enhance regional bone density, while BMSC would be placed to construct the shaft of long bones due to the matured bone marrow forming property, most mimicking the structural – functional characteristics of native bone. Such approach may be useful in future clinical trial to bone regeneration.

Other types of scaffolds that are non degradable, degrade at slower rates, or have densities closer to that of bone, such as Ca-P ceramics, may show their presence in CT images. Such materials may also have intensities that overlap with or interfere with the detection of new bone, and the intensity will vary based on the amount and density of ceramic. To overcome these potential complications in analyzing tissue engineered bone, scans of empty constructs should be taken at the selected threshold before implantation. Empty constructs should also be used as an *in-vivo* control for degradation. Using these two controls, it is possible to more accurately determine the percent of voxels in a bone/scaffold composite that actually represent new bone. The amount of bone can be determined from the difference between percent of voxels above the threshold in a bone/scaffold composite and the percent of voxels above the threshold in the starting scaffolds (or scaffolds implanted without cells if the scaffold is highly resorbable). Bounds on the contribution to BVF due to interference from a scaffold are therefore represented by the number of voxels in the scaffold at time zero (upper bound) and number of voxels in the remaining scaffold following implantation (lower bound). Using this technique with ceramic scaffolds, we demonstrated that the optimal thresholds for engineered bone remain in the 1000-1300 range (Fig. 9). If sufficient amounts of bone form within the scaffold, this should allow the amount of new bone to be calculated and validated histologically even though it may not be possible to directly visualize the new bone on a μ CT image. In tandem with the consistency in threshold range between different cell types, this threshold range is therefore deemed to be generally valid for cell based tissue engineered bone.

One final note on the transformation of the threshold data in hounsfield units to other systems. Several systems give a threshold value in terms of a physical mineral density (mg/cc). Recent studies have shown a linear relationship between all the gray scale values below the mature bone calibration⁴¹. This relationship is as follows:

$$\frac{\text{Threshold}(HU)}{\text{Calibration}(HU)} * 1073(\text{mg} / \text{cc}) = \text{Bone Mineral Density Threshold} (\text{mg}/\text{cc})$$

This transformation was applied to the thresholds (HU) used in these experiments and are reported in table 2.

2.5 CONCLUSIONS

This study showed that the μ CT is an accurate tool to analyze the bone content of ossicles. Using an autothresholding algorithm might lead to an underestimate of BVF because a fundamental underlying assumption of this algorithm is not satisfied. Based on 2 and 3 dimensional validations, a threshold range of 1000-1300 (24.2-31.5 % of Bone HU) is optimal for the early stages of bone formation. This threshold should provide some standardization and consistency for characterization of tissue engineered bone.

Table 1 Comparison between optimal thresholds determined from regressions against ash fraction and auto thresholds determined using histograms and threshold calculating algorithm.

<i>Time</i>	<i>Optimal Threshold</i>	<i>Auto Threshold (BMSCs)</i>	<i>Auto Threshold (BMP-7)</i>
4 weeks	1000	1432 +/- 124	1481 +/- 120
8 weeks	1100	2184 +/- 225	2072 +/- 202
12 weeks	1200	1588 +/- 149	1498 +/- 132

**Table 2 Linear transformations of threshold in Hounsfield units (HU) to
physical mineral density threshold (mg/cc)**

Threshold (HU)	Threshold (mg/cc)
600	15558.5
700	18241
800	20816.2
900	23391.4
1000	25966.6
1100	28649.1
1200	31224.3
1300	33799.5
1400	36374.7
1500	39057.2
1600	41632.4
1700	44207.6
1800	46782.8
1900	49358
2000	52040.5

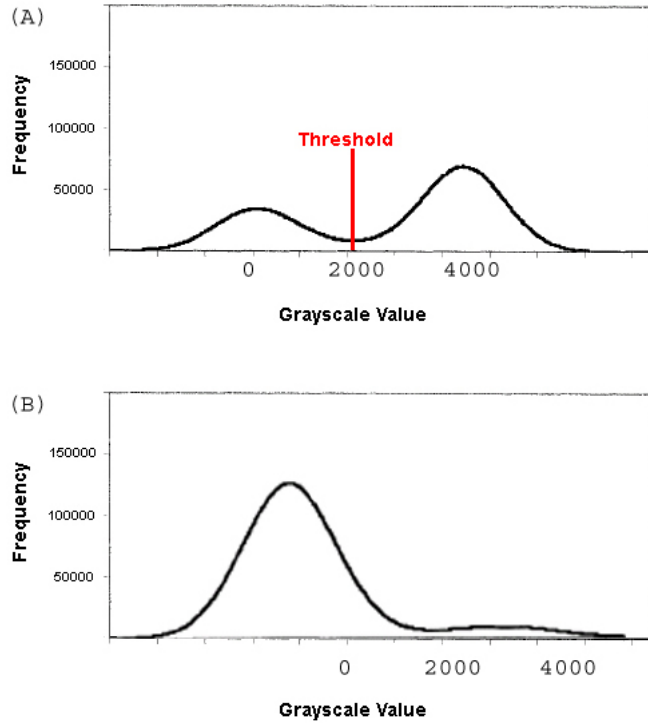


Figure 2-1 Autothresholding mechanisms use a bimodal to find a threshold value by finding the midpoint of the intermodal zone.

When mature bone (a) is analyzed using these autothresholding mechanisms, the typical separation the intensity peaks is even and easy to discriminate and a threshold can then be easily selected. However, when the frequency of mineral is low and tissue is still forming (b), such as in immature ossicles, the skewed unimodal distribution in the histogram violates an underlying assumption of the autothresholding algorithm making this approach difficult to employ. Furthermore, the lack of a bone peak makes it difficult to discriminate between new bone and marrow, fibrous tissue, fat and other soft tissue within the implant.

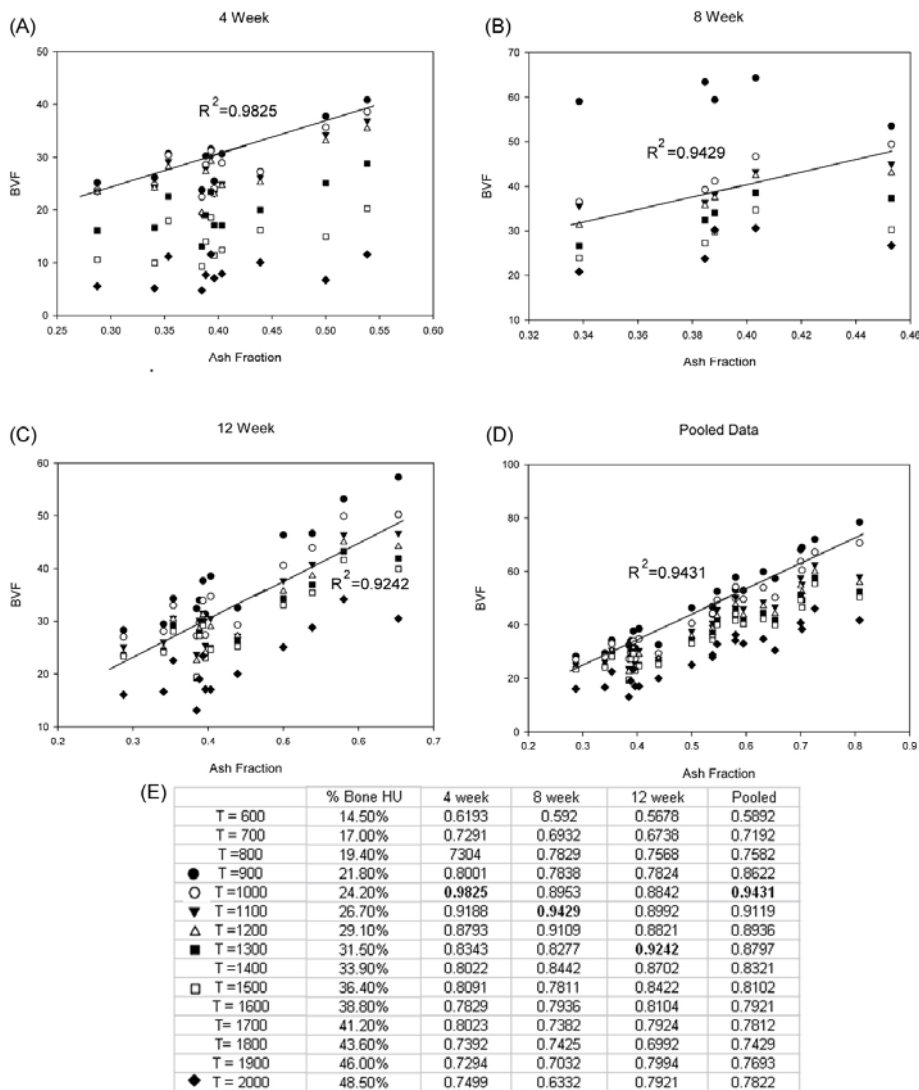


Figure 2-2 Correlation between volume fraction of regenerated bone determined by micro CT and ash fraction at different thresholds.

The optimal regression is depicted by the line on each plot: (A) 4 weeks (B) 8 weeks, (C) 12 weeks, (D) pooled times. The correlation coefficients and % of bone HU for all thresholds are also shown (E). The 1000-1300 range of thresholds yielded a correlation coefficient $R^2 > 0.87$ for all time points and level of significance, $p < 0.049$. Significance ($p < 0.05$) is denoted by *.

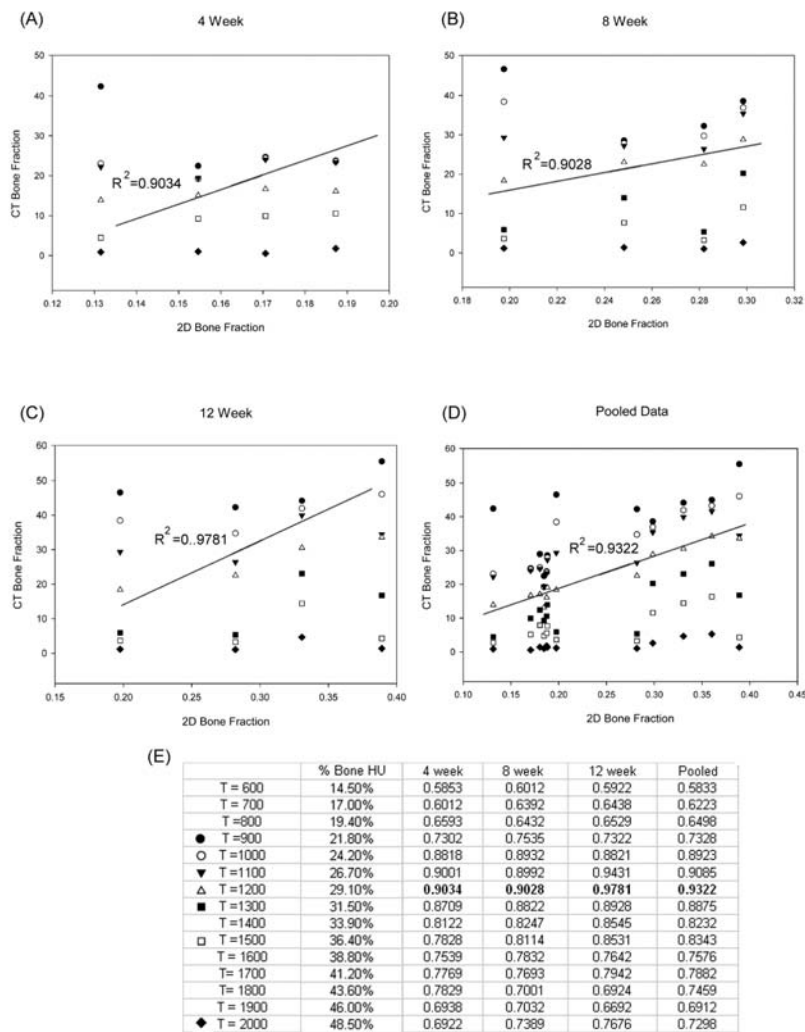


Figure 2-3 Correlation between area fraction of regenerated bone determined by micro CT and area fraction determined on same section by H&E staining.

Regressions were performed for the (A) 4 week, (B) 8 week, (C) 12 week and (D) pooled time groups. The correlation coefficients and % of bone HU for all thresholds are also shown (E). The optimal threshold at each time is 1200, with $R^2 > 0.9$. Significance ($p < 0.05$) is denoted by *.

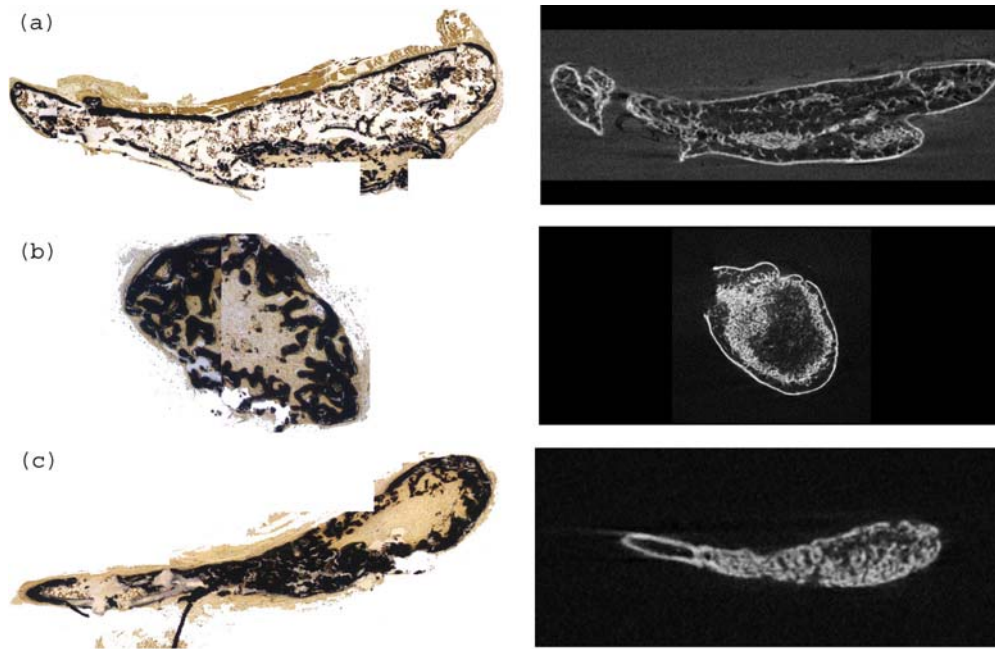


Figure 2-4 Comparison of von Kossa images that have been stitched together (left) and the analogous μ CT planes (right) at (a) 4 weeks, (b) 8 weeks and (c) 12 weeks for sections of ossicles regenerated from BMSCs.

The slides demonstrated that there is increasing mineralization as a function of time, as well as a more dense distribution of mineral.

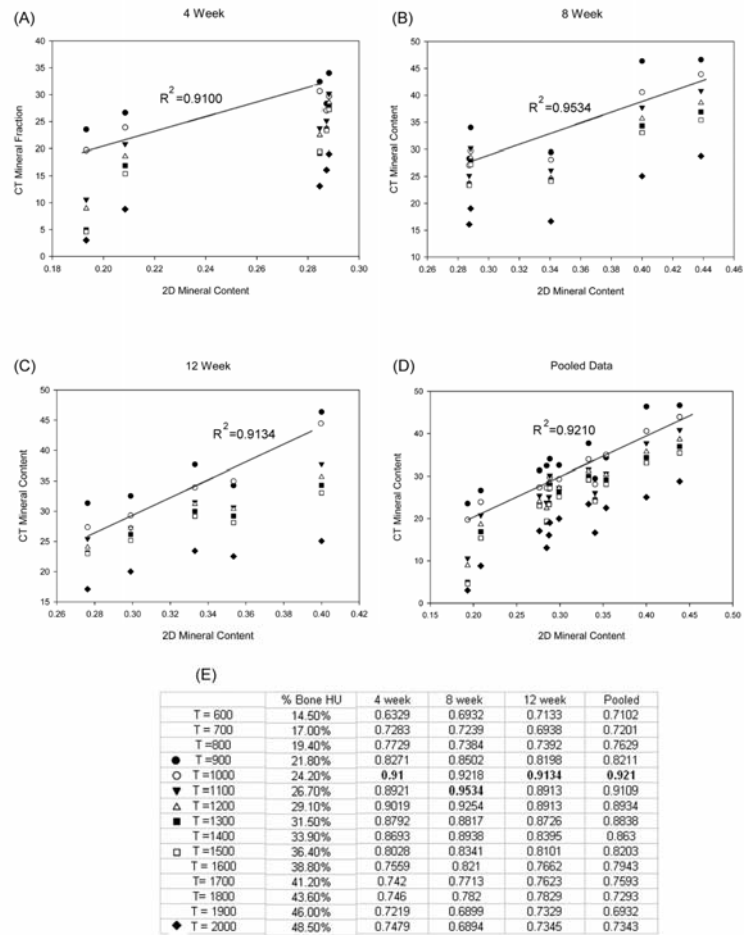


Figure 2-5 Correlation between area fraction of regenerated bone determined by micro CT and area fraction of mineral determined by von Kossa staining on the same section.

Regressions were performed for the (A) 4 week, (B) 8 week, (C) 12 week and (D) pooled time groups. The optimal regression at each time is depicted on the plots. Correlation coefficients and % of bone HU for all thresholds are also shown (E). The optimal thresholds are 1000-1100 for all times. The range of thresholds with the highest correlation coefficients and significance is consistent with the thresholds determined by regressions of the BVF with ash fraction and percent H&E stain. Significance ($p < 0.05$) is denoted by *.

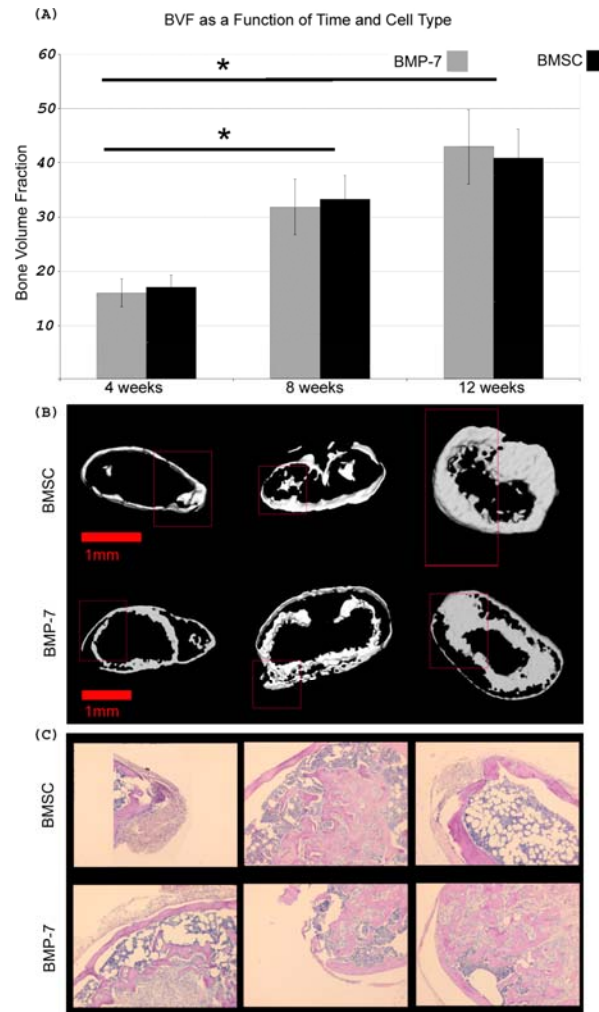


Figure 2-6 Bone regeneration as a function of cell type and time.

(A) volume fraction of regenerated bone determined by micro CT - the volume fraction of bone regenerated with each cell type at each time was calculated at the respective optimal threshold. There was a significant difference (denoted by *) in BVF between the 4 week samples and the 8 and 12 week samples for both cell types. There however was no significant difference between the cell types. (B) μ CT renderings of the regenerated ossicles show increased mineralization as a function of time. (c) H&E slides from both cell types showing normal bone containing fully mature bone marrow.

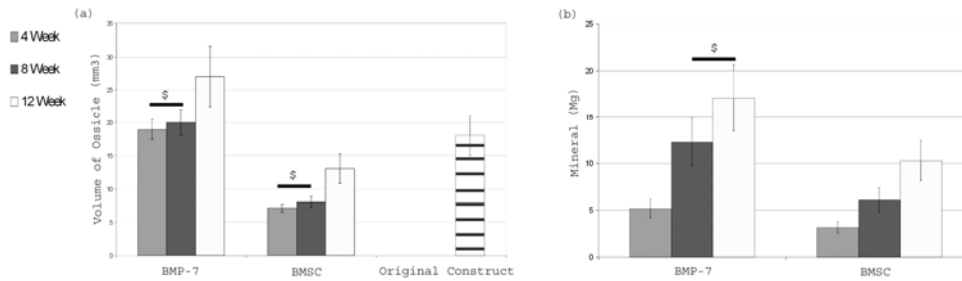


Figure 2-7 Overall volume and total mineral (ash) content of ossicles regenerated from transplanted BMSCs and BMP-7 transduced cells.

The volume of the ossicles was significantly greater in the 12 week group compared to the 4 and 8 week groups in both cell types (a). There was also a significant difference in overall volume between the two cell types ($p < 0.001$ at all time points), with BMP-7 constructs being approximately 2-fold larger. The BMP-7 constructs were also larger than the original size of the gelatin sponge after 12 weeks. (b) the total mineral content was significantly greater in ossicles formed from BMP-7 transduced cells. The total mineral content increased significantly after 4 weeks for both cell types. There was a significant difference between all times in the BMSC group, and between 4 weeks and 8 weeks in the BMP-7 treated constructs. Pairs that are not significantly different are indicated by \$.

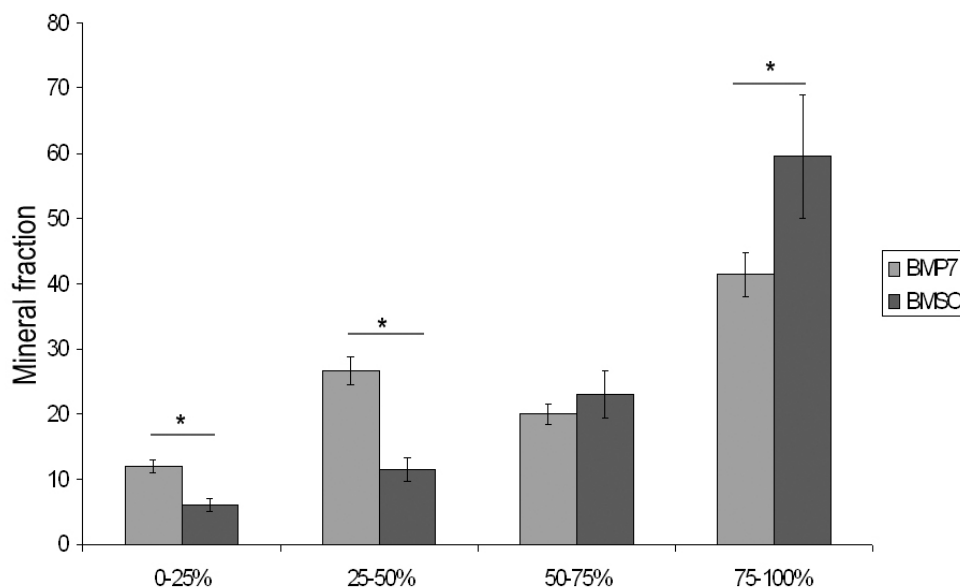


Figure 2-8 Quantification of mineral distribution on von Kossa stained slides for the 4 week samples.

Percent mineral was calculated in 4 regions (0-25%, 25-50%, 50-75%, 75-100% of the area from the centroid to the periphery. There is a significant difference (as denoted by *) in the percent of bone formed at the periphery and central parts of the gelatin foams between the two cell types. Comparing the cell types at different time periods showed no significant difference.

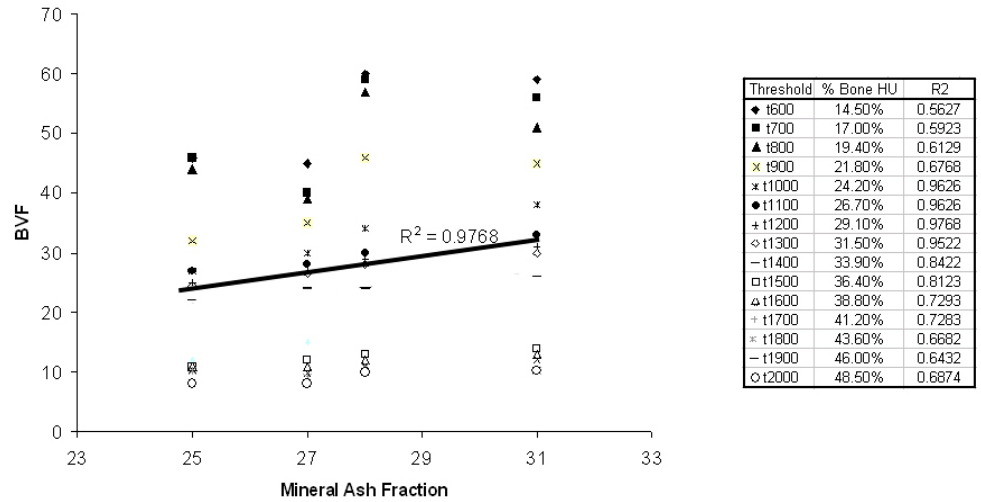


Figure 2-9 Correlation between volume fraction of regenerated bone determined by μ CT at different thresholds and mineral fraction determined by ashing when BMSCs are in a ceramic scaffold for 6 weeks.

The optimal regression is depicted by the line on each plot. The correlation coefficients and levels of significance for all thresholds are shown in the table. The 1000-1300 range of thresholds yielded a correlation coefficient $R^2 > 0.95$, supporting the general use of this threshold for different scaffolds.

2.6 References

1. Krebsbach PH, Kuznetsov SA, Satomura K, Emmons RV, Rowe DW, Robey PG. Bone formation in vivo: Comparison of osteogenesis by transplanted mouse and human marrow stromal fibroblasts. *Transplantation*. 1997; 63(8):1059-1069.
2. Musgrave DS, Bosch P, Lee JY, et al. Ex vivo gene therapy to produce bone using different cell types. *Clin Orthop Relat Res*. 2000; (378)(378):290-305.
3. Franceschi RT, Wang D, Krebsbach PH, Rutherford RB. Gene therapy for bone formation: In vitro and in vivo osteogenic activity of an adenovirus expressing BMP7. *J Cell Biochem*. 2000; 78(3):476-486.
4. Amiel C, Bailly C, Friedlander G. Multiple hormonal control of the thick ascending limb functions. *Adv Nephrol Necker Hosp*. 1987; 16:125-136.
5. Krebsbach PH, Kuznetsov SA, Bianco P, Robey PG. Bone marrow stromal cells: Characterization and clinical application. *Crit Rev Oral Biol Med*. 1999; 10(2):165-181.
6. Pettway GJ, Schneider A, Koh AJ, et al. Anabolic actions of PTH (1-34): Use of a novel tissue engineering model to investigate temporal effects on bone. *Bone*. 2005; 36(6):959-970.
7. Jepsen KJ, Goldstein SA, Kuhn JL, Schaffler MB, Bonadio J. Type-I collagen mutation compromises the post-yield behavior of Mov13 long bone. *J Orthop Res*. 1996; 14(3):493-499.

8. Wallace JM, Rajachar RM, Chen XD, et al. The mechanical phenotype of biglycan-deficient mice is bone- and gender-specific. *Bone*. 2006; 39(1):106-116.
9. Barck KH, Lee WP, Diehl LJ, et al. Quantification of cortical bone loss and repair for therapeutic evaluation in collagen-induced arthritis, by micro-computed tomography and automated image analysis. *Arthritis Rheum*. 2004; 50(10):3377-3386.
10. Ritman EL. Molecular imaging in small animals--roles for micro-CT. *J Cell Biochem Suppl*. 2002; 39:116-124.
11. Fuerst G, Tangl S, Gruber R, Gahleitner A, Sanroman F, Watzek G. Bone formation following sinus grafting with autogenous bone-derived cells and bovine bone mineral in minipigs: Preliminary findings. *Clin Oral Implants Res*. 2004; 15(6):733
12. Peyrin F, Salome M, Cloetens P, Laval-Jeantet AM, Ritman E, Ruegsegger P. Micro-CT examinations of trabecular bone samples at different resolutions: 14, 7 and 2 micron level. *Technol Health Care*. 1998; 6(5-6):391-401.
13. Dedrick DK, Goldstein SA, Brandt KD, O'Connor BL, Goulet RW, Albrecht M. A longitudinal study of subchondral plate and trabecular bone in cruciate-deficient dogs with osteoarthritis followed up for 54 months. *Arthritis Rheum*. 1993; 36(10):1460-1467.
14. Kinney JH, Ryaby JT, Haupt DL, Lane NE. Three-dimensional in vivo morphometry of trabecular bone in the OVX rat model of osteoporosis. *Technol Health Care*. 1998; 6(5-6):339-350.

15. Lill CA, Fluegel AK, Schneider E. Effect of ovariectomy, malnutrition and glucocorticoid application on bone properties in sheep: A pilot study. *Osteoporos Int.* 2002; 13(6):480-486.
16. McLaughlin F, Mackintosh J, Hayes BP, et al. Glucocorticoid-induced osteopenia in the mouse as assessed by histomorphometry, microcomputed tomography, and biochemical markers. *Bone.* 2002; 30(6):924-930.
17. Nishida S, Tsurukami H, Sakai A, et al. Stage-dependent changes in trabecular bone turnover and osteogenic capacity of marrow cells during development of type II collagen-induced arthritis in mice. *Bone.* 2002; 30(6):872-879.
18. Feldkamp LA, Goldstein SA, Parfitt AM, Jesion G, Kleerekoper M. The direct examination of three-dimensional bone architecture in vitro by computed tomography. *J Bone Miner Res.* 1989; 4(1):3-11.
19. Muller R, Van Campenhout H, Van Damme B, et al. Morphometric analysis of human bone biopsies: A quantitative structural comparison of histological sections and micro-computed tomography. *Bone.* 1998; 23(1):59-66.
20. Cartmell S, Huynh K, Lin A, Nagaraja S, Guldberg R. Quantitative microcomputed tomography analysis of mineralization within three-dimensional scaffolds in vitro. *J Biomed Mater Res A.* 2004; 69(1):97-104.
21. Jones AC, Milthorpe B, Averdunk H, et al. Analysis of 3D bone ingrowth into polymer scaffolds via micro-computed tomography imaging. *Biomaterials.* 2004; 25(20):4947-4954.

22. Gauthier O, Muller R, von Stechow D, et al. In vivo bone regeneration with injectable calcium phosphate biomaterial: A three-dimensional micro-computed tomographic, biomechanical and SEM study. *Biomaterials*. 2005; 26(27):5444-5453.
23. Schneider A, Taboas JM, McCauley LK, Krebsbach PH. Skeletal homeostasis in tissue-engineered bone. *J Orthop Res*. 2003; 21(5):859-864.
24. Otsu N. A threshold selection method from gray-level histograms. *IEEE Trans Sys , Man , Cyber*. 1997; 9:62-63-66.
25. Kuhn JL, Goldstein SA, Feldkamp LA, Goulet RW, Jesion G. Evaluation of a microcomputed tomography system to study trabecular bone structure. *J Orthop Res*. 1990; 8(6):833-842.
26. Waarsing JH, Day JS, Weinans H. An improved segmentation method for in vivo microCT imaging. *J Bone Miner Res*. 2004; 19(10):1640-1650.
27. Leonova EV, Pennington KE, Krebsbach PH, Kohn DH. Substrate mineralization stimulates focal adhesion contact redistribution and cell motility of bone marrow stromal cells. *J Biomed Mater Res A*. 2006; 79(2):263-270.
28. Krebsbach PH, Gu K, Franceschi RT, Rutherford RB. Gene therapy-directed osteogenesis: BMP-7-transduced human fibroblasts form bone in vivo. *Hum Gene Ther*. 2000; 11(8):1201-1210.

29. Murphy WL, Kohn DH, Mooney DJ. Growth of continuous bonelike mineral within porous poly(lactide-co-glycolide) scaffolds in vitro. *J Biomed Mater Res.* 2000; 50(1):50-58.
30. David H. Kohn, Kyungsup Shin, Sun-Ig Hong, et al. Self-assembled mineral scaffolds as model systems for biomineralization and tissue engineering . *Proc 8th Int Conf Chem & Biol Min Tissues.* 2005;
31. Ding M, Odgaard A, Linde F, Hvid I. Age-related variations in the microstructure of human tibial cancellous bone. *J Orthop Res.* 2002; 20(3):615-621.
32. Blake GM F. Principles of Bone Densitometry. In: Rodan G (ed). *Principles of Bone Biology.* 1st ed. San Diego: Academic Press, 1996:1313-1332.
33. Ho ST, Hutmacher DW. A comparison of micro CT with other techniques used in the characterization of scaffolds. *Biomaterials.* 2006; 27(8):1362-1376.
34. Moore MJ, Jabbari E, Ritman EL, et al. Quantitative analysis of interconnectivity of porous biodegradable scaffolds with micro-computed tomography. *J Biomed Mater Res A.* 2004; 71(2):258-267.
35. Knackstedt MA, Arns CH, Senden TJ, Gross K. Structure and properties of clinical coralline implants measured via 3D imaging and analysis. *Biomaterials.* 2006; 27(13):2776-2786.

36. Fajardo RJ, Ryan TM, Kappelman J. Assessing the accuracy of high-resolution X-ray computed tomography of primate trabecular bone by comparisons with histological sections. *Am J Phys Anthropol.* 2002; 118(1):1-10.
37. Thomsen JS, Laib A, Koller B, Prohaska S, Mosekilde L, Gowin W. Stereological measures of trabecular bone structure: Comparison of 3D micro computed tomography with 2D histological sections in human proximal tibial bone biopsies. *J Microsc.* 2005; 218(Pt 2):171-179.
38. Chappard D, Retailleau-Gaborit N, Legrand E, Basle MF, Audran M. Comparison insight bone measurements by histomorphometry and microCT. *J Bone Miner Res.* 2005; 20(7):1177-1184.
39. Krebsbach PH, Gu K, Franceschi RT, Rutherford RB. Gene therapy-directed osteogenesis: BMP-7-transduced human fibroblasts form bone in vivo. *Hum Gene Ther.* 2000; 11(8):1201-1210.
40. Laurencin C, Khan Y, El-Amin SF. Bone graft substitutes. *Expert Rev Med Devices.* 2006; 3(1):49-57.
41. Kozloff, K, Thornton, M, Goldstein, S.A. Validation of a Micro-Ct System for Quantitative Densitometry. 5th Combined Meeting of the Orthopaedic Research Societies of Canada, USA, Japan and Europe, 2004

Chapter 3

Effects of Cell Seeding and Self-Mineralizing Template on Differentiation and Volume of Regenerated Bone

3.1 Introduction

Skeletal defects present a major clinical challenge with over 5.5 million fractures and 1 million bone grafting procedures done each year¹. Present surgical therapies for bone defects or bone loss in the skeleton include autografts²⁻⁶, allografts^{4, 5}, and synthetic materials⁷. Each of these reconstructive and/or regenerative strategies, however, has limitations and lacks clinical predictability. Only a minimal amount of tissue can be harvested for autografts, the harvesting procedure may lead to donor site discomfort and morbidity, and it may be difficult to form this tissue into desired shapes. Autografting, the current “gold standard” for bone regeneration, has failure rates as high as 30%. Allografts have the potential of transferring pathogens^{3, 8(3,12)}. Freeze-drying, demineralization, and irradiation, which reduce immunogenic potential, can also reduce structural integrity, leading to graft fracture³⁽³⁾. Other complications with autografts and allografts include unreliable incorporation, resorption, and non-union of the graft/bone interface⁸⁻¹¹.

Induction of new bone by growth factors requires large amounts of recombinant material, which may not be realistic in cases of massive defects¹². Additionally, successful

use of growth factors relies on the presence of a sufficient population of undifferentiated progenitor cells capable of responding to the inductive cues provided by the growth factor¹³. Synthetic materials are primarily designed to be permanently implanted. Long-term complications include stress shielding, leading to loosening, and mechanical or chemical breakdown of the material itself⁷.

A more biological alternative to the permanent implantation of synthetic materials is a cell transplantation approach where a 3-dimensional natural or synthetic construct provides a temporary substrate for cells to organize, grow, differentiate, and form a functional extracellular matrix and new tissue^{6, 14, 15}. Because bone regeneration is a complex process that requires autocrine, paracrine, and endocrine signals, positional cues, cell-matrix interactions, mechanical forces and cell-cell contacts to mediate the formation of a complex 3D architecture and function, an understanding of developmental processes may help identify strategies that can be used in tissue engineering. Altering simple initial conditions may help maximize some of the necessary processes for tissue development, while solving some of the clinical limitations present in current strategies. Two such initial conditions that can be easily manipulated are the substrate chemistry and the initial cell seeding.

Of particular importance with the use of synthetic materials is that most problems manifest themselves at the biomaterial/tissue interface, in part because the tissue has the ability to functionally adapt, whereas the synthetic material does not. Manipulating the surface chemistry to be more biologically-interactive biomaterials could potentially improve the clinical treatment of bone defects. A mineralized layer on the surface of a porous synthetic 3D scaffold can provide a physiologically favorable environment that

enhances cell adhesion and osteoconductivity^{16, 17}. Besides from substrate effects, calcium/phosphate apatites may have a solution mediated effect when the mineral layer starts dissolving, releasing ions that can serve as both extracellular and intracellular messengers. For example, the release of calcium ions (Ca^{2+}) into the solution can enhance osteogenic differentiation, cell growth, and cell-to-cell signaling¹⁷⁻²¹. Furthermore, once up taken by cells, Ca^{2+} ions become an important intracellular messenger in all bone forming cells, enabling remodeling and regeneration^{22, 23}.

Substrates, biologically active or synthetic, are typically seeded with cells via the commonly employed static seeding technique. This technique relies on gravity as a gradient to percolate cells into a porous scaffold, allowing cells to passively attach to the surface of the 3D construct. Although simple in nature, this approach has limitations due to initial cell adhesion, as well as diminished transport of nutrients, signals, and messengers²⁴⁻²⁶. As such, tissue regenerated from cells seeded statically, typically exhibits only partial regeneration. The regenerated tissue is also characterized by regeneration of tissue in the periphery of the 3D ossicle, while only small amounts of bone are generated in the core.

Alternatively, modifying the initial seeding conditions, via novel seeding techniques, may provide a means to enhance nutrient transport, cell adhesion, and cell-cell communication in 3D scaffold. Such initial seeding conditions may alter the eventual fate of the resulting tissue, indicating the potential impact seeding may have on tissue engineered equivalents. Two novel techniques, seeding by filtration and micromass seeding, may enable higher cell-adhesion rates, cell density, and cell-to-cell communication. Seeding by filtration occurs by circulating a dense cell suspension

through the scaffolds, with the aid of a small pressure gradient applied by a peristaltic pump. The homogeneous cell suspension that filters through the scaffold is cycled through and may produce higher cell density and even cellular distribution. Micromass studies have been performed in-vitro, in a 2D monolayer²⁷. This seeding strategy is achieved by placing a super-dense cluster of cells at a particular location in a 3D scaffold; leaving less crowded areas where nutrients can flow through. Micromasses could provide the benefits of higher density, cell-cell communication, and nutrient and byproduct flux thought to be vital to the proper development of tissue.

Our study aims to investigate a critical question in tissue engineering; namely, can altering simple exogenous initial conditions, specifically surface chemistry and seeding conditions, alter the fate tissue engineered bone equivalents? To examine this question, we compare cell adhesion, cell-to-cell communication, osteogenic differentiation and osteogenic patterns of regenerated bone in-vivo, in synthetic and biomimetic mineralized templates, as well as in scaffolds seeded with cells via static, filtration, and micromass seeding. The impact of this study may reach the clinical setting, by providing tissue new simple, in-expensive, and replicable strategies that regenerate larger and more evenly distributed amounts of bone.

3.2 Materials and Methods

3.2.1 Bone marrow stromal cell (BMSCs) isolation and culture

Five-week old C57BL/6 mice were used to isolate bone marrow cells from the femoral, tibial and humeral cavities (six bones per animal) as previously described²⁸. Briefly, the bone marrow was mixed with minimum essential medium (α -MEM; Gibco

Laboratories, Grand Island, NY) containing 10% fetal bovine serum (FBS) (Gibco) and antibiotics (100 µg/ml penicillin G and 100 IU/ml streptomycin at 37°C in 5% CO₂/95% air). Cells were pelleted by centrifugation at 1000 rpm for 5 min at 4°C and resuspended in 10 ml α-MEM. Cells were plated at a density of 30,000 nucleated cells/cm², and cultured under the same conditions. The culture medium was replaced three times per week and at near confluence (90%) the adherent cells were washed with phosphate-buffered saline solution and enzymatically released by means of a 0.25% trypsin-EDTA (Sigma, St. Louis, MO). Cells were re-plated at a density of 30,000 cells/cm² and passaged 7-10 days after, when confluence was achieved. Cells were passaged twice before they were used in the subsequent experiments.

3.2.2 Scaffold Preparation

Porous, 3D organic templates (85:15 poly(lactide-co-glycolide), diameter = 4mm x height = 1mm, 90% porosity, pore size 250-425µm) were prepared by a solvent particulate leaching process explained elsewhere²⁹⁻³¹.

3.2.3 Mineralization of Scaffolds

Scaffolds were each incubated in a 50-mL solution of modified simulated body fluid (SBF) for 7 days for mineral film formation³². The SBF solution was changed every 24 h to ensure sufficient ion concentrations for mineral growth. The SBF was prepared by dissolving the following reagents in deionized water: 141 mM NaCl, 4.0 mM KCl, 0.5 mM MgSO₄, 1.0 mM MgCl₂, 4.2 mM NaHCO₃, 5.0mM CaCl₂, and 2.0 mM KH₂PO₄. SBF was buffered to maintain a pH 6.8 with Tris-HCl at 37°C for the duration of the incubation period.

3.2.4 Pre-Wetting Scaffolds

Scaffolds were pre-wet with 70% ethanol by pressing wet pads around the surface area for 5 minutes. Afterwards, scaffolds were submerged in 50ml falcon tubes filled with α -MEM and agitated 30 minutes to remove the excess ethanol. The scaffolds were removed from the tube and placed into a new one with fresh α -MEM. The process was done 5-6 times until the pH of the α -MEM in the tube matched that of the sterile α -MEM (pH=7.1). The scaffolds were then left to soak in the media overnight before seeding.

3.2.5 Cell Seeding

The experimental design assessed three methods of seeding (static, dynamic, and filtration) at three time points (1hr, 6hrs, and 24hrs), using both mineralized and non-mineralized PLGA scaffolds. 6 scaffolds were used for each procedure, for a given time point and material. **Static seeding** was performed in 24-well plates by pipetting a cell suspension into the scaffold. Each well contained 1 scaffold. A cell suspension of 1ml (α -MEM; containing 10% fetal bovine serum (FBS) and antibiotics (100 μ g/ml penicillin G and 100 IU/ml streptomycin at 37°C in 5% CO₂/95% air), and cell density of 0.8EE6 cells/ml) was used in static, dynamic, and filtration seeding experiments. The scaffolds were placed into the incubator (at 37°C in 5% CO₂/95% for all seeding methods) immediately after. **Dynamic seeding** was performed by trapping two scaffolds in a 15 ml falcon tube, between meshes, with a stir bar outside the meshes in the bottom of the tube. Because the number of cells was desired to be kept constant, about 5mL of media were added to the cell suspension so that both scaffold and stir bar would be completely submerged. The cell suspension was poured into the tubes, and these were placed in a stir plate inside an incubator. The stir intensity was set at 150rpm. In **filtration seeding** 4

scaffolds were placed in 4 glass cylinders of the same radius. The cell suspension was circulated through the scaffolds with a small gradient applied by a peristaltic pump (1.37ml/min) through small non-stick tubes (silicon tubes, Small Parts Inc, ID=3.5mm). A homogeneous cell suspension is kept by adding a stir bar to the suspension reservoir. Scaffolds (D=4mm, t=1mm) were placed in a cylindrical scaffold chamber (ID=4mm, 20mm). The chamber is made of non-stick glass so that the cells won't attach to its surface and only attach to the scaffolds. In order to generate a laminar profile and keep the pH at 7.4, the length of the tubes was set at 0.3m (Appendix A1, A5). The complete system was placed in a CO₂ incubator, to promote gas exchange through the tubes. Cells that are not seeded in the first filtrate are passed through several times until maximum retention is reached. The mean residence time of cells was approximately 30 mins. Therefore, every 30 mins, the direction of the flux was changed to avoid directional bias on the scaffolds. In **Micromass seeding**, the cell suspension was more concentrated and pipetted into the middle of the scaffold (4.0EE6 cells/ml).

3.2.6 Cell Counting and Histology

After seeding, the scaffolds were washed five times with α -MEM to retrieve all the free (unattached) cells. The five wash benchmark was chosen after test studies confirmed that there was a negligible amount of free cells left in the scaffold after the 5th wash. The washed fraction was pooled and saved to count the free cells present in the media. The apparatus and containers were also washed to determine the number of cells that did not adhere. Free cell count was obtained using a hemacytometer. The % of cells that adhered to the scaffold was determined by subtracting the number of washed cells from the number of cells originally seeded. To verify this counting strategy, 4 scaffolds from

each seeding condition were treated with trypsin-EDTA, to remove the attached cells. Trypsinization was performed for two minutes, followed by flushing of cells with α -MEM. This process was repeated 3 times per scaffold, and the 3 resulting cell suspensions were pooled to obtain the number of attached cells. Cell counts from micromass seeded scaffolds obtained via these two methods are not reported because the count was inconsistent and the treatment destroyed some cells. A 3-way ANOVA on time, template, and seeding strategy was performed to determine significant differences in percentage of seeded cells ($p < 0.005$).

As an alternative three scaffolds for each seeding strategy and time were analyzed histologically to quantify cell retention and qualitatively observe the distribution of attached cells. Scaffolds were fixed in 10% buffered formalin and ethanol. 5 μ m sections were made and placed on 10 slides with 3 sections per slide. Sections were standardized for all scaffolds in 200 μ m increments from the surface. The number of cells per section was quantified and the mean number of attached cells per section is reported. Differences in cell counts were assessed using a 1-way ANOVA on 6 hour sections and differences were assessed at $p > 0.005$.

3.2.7 Dye transfer studies

Fluorescent dye transfer studies were performed to assess gap-junctional intercellular communication (GJIC) between BMSCs seeded in mineralized and non-mineralized scaffolds by static, filtered and micromass seeding strategies. The cell scaffold constructs (4x1mm) were seeded as previously described for 24 hours and placed in 24 well plates. Cells in these circumstances served as recipient cells. Calcein-AM (10 μ M) and Vybrant-DiI were used to label donor cells grown to confluence in a 12-well

plate. As a negative control, 50uM of the gap junction uncoupler alpha-glycyrrhetic acid (AGA) was used (n=5). Donor cells were added to potential recipient cells at 1:8 ratio. Cells were harvested by trypsinisation for quantitative assessment of GJIC by flow cytometry after 5 hours. . The transfer regions for recipient cells ($> 2 \times 10^1 \text{ FI}^{-1}$ and $< 5 \times 10^3 \text{ FI}^{-1}$) and non-labeled, non-recipient cells ($< 2 \times 10^1 \text{ FI}^{-1}$) were defined as the transfer regions based on the initial fluorescence range quantified for non recipient cells, and cells containing both dyes. Florescence above $5 \times 10^3 \text{ FI}^{-1}$ was indicative of cells containing both membrane tracker and calcein-AM. The transfer fraction of cells was determined normalizing the value of the transfer region to the total number of recipient cell counts. This experiment was performed with n=6 groups. Statistical differences in percent of dye recipient cells were measured using a 2-way ANOVA on template and seeding strategy ($p < 0.05$).

3.2.8 RTPCR Analysis of differentiation markers

BMSCs were seeded in Mineralized and non-mineralized scaffolds by static, filtration and micromass strategies. The seeded constructs were placed in 24 well plates supplemented with osteogenic media (α -MEM media, 10% Fetal Bovine Serum, 1% Pen/Strep, 1% 100x β -Glycerophosphate, 1% L-ascorbic acid-phosphate, $\sim 0.05\%$, $\sim 0.05\%$ Dexamethasone). An additional group in which 1.5mM of Ca^{2+} was added to osteogenic media was tested to assess the effects of soluble calcium. Media was replenished every 24 hours, to ensure optimal nutrient contents in the surface of the scaffolds. At 2, 8, and 16 days for analysis real-time PCR was used to detect the expression of two bone differentiation markers (Alkaline Phosphatase (ALP) and Osteocalcin (OCN)). Primers and TaqMan probes were purchased (ABI). The primer

sequences utilized were as follows: OCN, 5'-CCAGCGACTCTGAGTCTGACAA-3', and 5'-CCGGAGTCTATTCACCACCTTACT-3'; ALP; 5'-GCCCTCTCCAAGACATATA-3' and 5'-CCATGATCACGTCGATATCC-3'

Cells seeded scaffolds or in 12 well plates were trypsinized after 2, 8, and 16 days, to remove cells and the total RNA was extracted (Trizol; invitrogen Corp). The RNA was purified (RNeasy, Quigen) and treated with DNase I. Cycling conditions were as follows: 50C for 2 minutes and 95C for ten minutes, followed by 50 cycles of 95C for 15 seconds and 60C for 1 minute. No-template control analyses were run for each primer set and 18s rRNA (ABI) endogenous control was run for each sample. Analysis was performed by first setting an appropriate standard threshold level in the linear part of the reaction for each primer. The crossing value of this threshold was determined (C_t) for each sample. Using the manufacturer's protocols (ABI Prism 7700 Sequence Detection System, User Bulletin #2), mRNA expression levels for each sample/primer were normalized to endogenous rRNA 18S levels and the results were reported as a fold change relative to the OCN expression of BMSCs (filtration seeding, day 2). Filtration seeding was chosen as the normalizing seeding condition because the variation between samples was relatively low compared to static and micromass seeding techniques. All reactions were performed in quintuplets. Three 1-way ANOVAs were used to determine significant differences as a function of seeding condition, scaffold, and time.

Cell seeded constructs were trypsinized after 2, 8, and 16 days, to remove cells and the total RNA was extracted (Trizol; Invitrogen Corp). The RNA was purified (RNeasy, Quigen) and treated with DNase I. Cycling conditions were as follows: 48C

for 10 minutes and 95C for ten minutes, followed by 4 cycles of 95C for 15 seconds and 60C for 1 minute. No-template control analyses were run for each primer set and 18s rRNA endogenous control was run for each sample. The $2\Delta\Delta CT$ relative quantization method was utilized to evaluate gene expression. All reactions were performed in quintuplet and n=4. The results were normalized to the endogenous 18s expression (ABI). A 3-way ANOVA was used to determine significant differences as a function of seeding condition, scaffold, and time.

3.2.9 Transplantation of cell-scaffold constructs

Cells were seeded by static, filtration and micromass seeding as previously described. All cell-scaffold constructs were placed in an incubator for 1 hour (at 37°C in 5% CO₂/95%) until surgery began, to ensure sterility until the moment of implantation. 24 Mineralized and 24 PLGA constructs were transplanted subcutaneously into nude mice (nu/nu). Each of the construct groups contained 6 filtered, 6 micromasses, 6 static, 6 empty scaffolds. Briefly, nude mice (nu/nu) were anaesthetized by an intraperitoneal injection of 1 mg/10 g ketamine and 0.1mg/10 g xylazine. An incision was made on the back of each mouse and the implants were inserted within the subcutaneous cavities. The cell-scaffold specimens were assigned randomly to each pocket. The wounds were closed with surgical clips aseptically. The mice were euthanized after 6 weeks and the regenerated bone ossicles were harvested.

3.2.10 Micro-CT 3D image acquisition and analysis

Ossicles, clear of soft tissue, were scanned on a high resolution cone beam micro-CT system (Enhanced Vision Systems (now GE Healthcare Preclinical Imaging), London,

Ontario, Canada) while immersed in distilled H₂O. The x-ray source voltage and current were 80 kVp and 80μA, respectively. To reduce the potential for beam hardening artifact, the x-rays were passed through a 0.2mm Al filter immediately upon exiting the source and the specimens were immersed in dH₂O during the scanning process. Projection images were acquired over 198 degrees using 2x2 binning and an exposure time of 1100 ms, and four frames were averaged for each projection to improve the signal to noise ratio. The projection data was then corrected and reconstructed using the Feldkamp cone-beam algorithm to create three-dimensional images with an isotropic voxel size of 18μm. The scanner was calibrated once daily using a phantom that contained air, water and hydroxyapatite.

Bone volume fractions were determined by using a MatLab program designed to integrate all grayscale voxels above a particular threshold. To determine the overall volume of the ossicles, the program determined the perimeter of each 2D μCT slice by tracing the outer edge. The program then integrated all the perimeters to determine the 3D surface area, and the number of voxels inside the surface defined the total volume. High density voxels outside of the 3D surface and unattached to the ossicle were discarded, while voxels inside were evaluated at the specified thresholds to determine the BVF, which was calculated as the number of voxels above the threshold relative to the total number of voxels. Using this method, a threshold of 1100 was used to re-construct a rendered image of the ossicles and determine their distribution³³.

3.2.11 Histological analyses

The ossicles were rinsed in water and then decalcified in 10% formic acid for 5 days. After decalcification, the tissues were embedded in paraffin. 5 μm sections were

made and placed on 10 slides with 3 sections per slide. The tissue was deparaffinized hydrated, and the first, fifth, and tenth slides were stained with H & E, and von Kossa. Image Pro Plus 4.0 was used to take pictures of the histological sections.

3.2.12 Analysis of bone ingrowth

A program was developed to determine the distribution of regenerated bone as a function of the distance from the geometric center of each ossicle. Using von Kossa stained sections of bone ossicles regenerated in PLGA scaffolds, the centroid was calculated using a MatLab script³⁴ and used as a frame of reference to divide the ossicles into 4 regions. Defining the centroid as the 0th percentile and the edge as the 100th percentile, boundaries were calculated by lines that radially pointed into the center from the edges. Using this criterion, the program determined the percent of bone present in regions 0-25%, 25-50%, 50-75% and 75-100% of the area away from the centroid. A 2-way ANOVA was performed to differentiate between (1) sections in filtered and micromass generated ossicles and (2) topographical regions within each ossicle; significance was measured at $p < 0.05$.

3.3 Results

3.3.1 Filtration seeding achieves a higher number of attached cells

Filtration seeding led to significantly higher percentage of cells adhered than dynamic or static seeding (figure 1). Scaffolds filtered with cells had high cell retention after 1 hour (82.4±4.1%) and approached carrying capacity by the 6th hour (92.32±6.12). Both dynamic and static seeding increased as a function of time but had

significantly less cell adhesion than filtration at all times ($p < 0.001$, for all times). Dynamic also achieved significantly higher number of attached cells than static seeding ($p(1hr) = 0.003$, $p(6hrs) < 0.001$, $p(24hrs) = 0.021$). The effect of template was only significant in the static seeded scaffolds, where the mineralized layer enhanced adhesion ($p(1hr) = 0.031$, $p(6hr) = 0.028$). There was no significant difference in cell adhesion between mineralized and non-mineralized scaffolds seeded by filtration and dynamic seeding. Histology verifies the adhesion results. The slides qualitatively show that filtration (figure 2C) has an increase in cell number and spatial distribution when compared to static (figure 2A), dynamic (figure 2B), and micromass seeding (figure 2D). Micromass seeding exhibited significantly higher cell counts than static seeding after 6 hours in both mineralized and non-mineralized templates ($p > 0.001$). Histology showed that micromass seeded scaffolds exhibited highly dense centralized localization of cells. Quantitatively (figure 2E), 6 fold increase in the number of cells attached in filtration over static seeding, and validated dynamic seeding and micro mass seeding as suitable seeding techniques that show significantly greater cell adhesion than static seeding ($p < 0.001$, for both over static seeding). The standard deviation in cell cluster number is significantly less in filtered seeding than the other methods (138.7 ± 10.2 cells counts). Micro mass seeding had the highest deviation (68.0 ± 23.4 cells counts).

3.3.2 Micromass seeded cultures enhance gap junction dependent cell-cell communication

A significant increase in calcein-AM transfer between donor and recipient cells in the micromass seeded cells after 5 hours (figure 3) over filtered and static seeded cells ($p = 0.034$, $p < 0.001$, respectively). The presence of a mineralized scaffold had no effect

in calcenin transfer. However, in mineralized scaffolds, transfer in filtered seeded cells and micromass seeded cells is only moderately significant ($p=0.92$). Furthermore, cells containing the gap junction inhibitor AGA, showed little transfer compared to both experimental groups without AGA ($p<0.001$) in both mineralized and PLGA scaffolds, indicating GJIC dependent transfer.

3.3.3 Seeding and template conditions alter bone marker expression

Expression of bone differentiation markers ALP and OCN was significantly altered when different scaffolds and seeding techniques were implemented (figure 6). At day 2, ALP expression was significantly higher in micromass seeded than both filtration and static seeded scaffolds ($p<0.001$ for both), which exhibited no difference in the differentiation marker (fig 6a). At day 8, micromass seeded scaffolds still exhibited significantly higher expression when compared to filtration and static seeded scaffolds ($p<0.001$ for both), however, filtration also significantly expressed more ALP than static ($p<0.001$). At day 16, there was no significant difference in ALP expression between seeding methods.

Expression of osteocalcin (fig 6 b) was different starting at day 8, where micromass seeding exhibited significantly higher expression ($p<0.001$ for both) compared to filtration and static seeded scaffolds. At day 16, OCN expression in micromass seeded scaffolds was significantly greater than filtration and static seeded scaffolds ($p=0.0211$). Cells seeded through filtration expressed significantly higher OCN than statically seeded cells ($p<0.001$).

Template mineralization and the presence of soluble calcium increased ALP and OCN expression over cells seeded in PLGA scaffolds (figs 4C-F). Cells seeded in

mineralized templates by all seeding conditions expressed significantly larger amounts of ALP than cells seeded in PLGA scaffolds (fig 4 C,D; $p=0.021$). Increasing the concentration of soluble calcium to cells seeded in PLGA exhibited a significant increase when compared to cells seeded in PLGA. Filtered and static seeded scaffolds exhibited significant increases in expression ($p=0.032$, $p=0.042$), while only moderately significant in micromass seeded cells ($p=0.099$).

Mineralized scaffolds enhance bone formation: H&E slides showed normal bone containing marrow that included fat, entrapped cells and hematopoietic cells for all groups seeded in mineralized scaffolds (figure 5 A-E). Static seeded scaffolds exhibit small bone formation with, but no marrow. In general, when a mineralized template is used, cells regenerate more bone (Figures 5A-G). Bone formation is observed in the periphery of ossicles produced by filtered seeded cells, with increasing shell thickness in the mineralized scaffolds (figure 5 B,E). Bone generated by micromass seeded scaffolds showed bone growth in the core of the ossicles (Figure 5A,D) and entrapped cells morphology indicative of bone tissue. Statically seeded produced marginal bone formation in PLGA scaffolds and was clearly aided by the presence of a mineral layer in the scaffold (figure 5 C,F,E).

Micromass and filtration seeding led to a higher BVF than static seeding (figure 5G). There was no significant difference in BVF between the filtered (27.3 ± 2.5) and micromass ($31.2 \pm 6.2\%$). However the percentage of variability was higher on the micromass seeded construct than the filtration. Filtered, micromass and statically seeded mineralized scaffolds showed significantly higher BVF (p values = 0.013, 0.037, 0.009, respectively) than the PLGA seeded counterparts.

3.3.4 Different seeding techniques led to distinct patterns of osteogenesis

Distribution analysis performed on Von Kossa sections verified the qualitative observation in the H&E sections, showing a quantitative difference in the distribution of mineral location in micromass and filtered ossicles (figure 9a). The filtered ossicles showed most of the mineral in the periphery while the micromass ones had a more even distribution (figure 6B). The ossicles generated by filtration seeding showed significantly higher BVF in the periphery (75-100%) than in the core (0-25%; $p < 0.001$). The micromass seeded ossicles have significantly more mineral in the core ($p=0.0213$), and significantly less ($p=0.0311$) in the periphery than the filtered ones (figure 9b). There was no significant difference in BVF between topographical regions in the ossicles generated by micromass seeding.

3.4 Discussion

Our data suggests that altering the initial cell seeding conditions and/or using a biomimetic mineral template, can have a profound impact on both the amount and spatial distribution of regenerated tissue. Explicitly, we showed that the initial conditions of mineralizing a polymer scaffold (PLGA) and seeding cells through the novel filtration and micromass techniques, as opposed to the conventionally used static seeding^{26, 35}, enhanced osteogenic differentiation in-vitro and regeneration of bone in-vivo in the longer term. Furthermore, we showed that the filtration and micromass seeding enabled higher gap junction intercellular communication between cells in 3D, an important component for tissue development and homeostasis³⁶⁻³⁹. Coupled together, we speculate

that our results provide simple alternatives that can have a profound impact on the regeneration of 3D tissue equivalents.

Mineralized templates had a significant effect both in cell differentiation in a 3D scaffold (figure 4), and in the amount of regenerated bone in-vivo (figure 5). The examination of differentiation under 3D conditions was important; recently, our group and others have demonstrated differences in cell differentiation between a 2D monolayer and 3D cultures (Chapter 5,). The differentiation data contained a group that only contained soluble calcium. In these cases, there was moderate or significant increase in differentiation, relative to cells seeded in PLGA scaffolds. However, cells in mineralized templates, in general, had significantly higher differentiation marker expression than the soluble calcium group. This suggests that both soluble and insoluble calcium in these biomimetic scaffolds play an important role in differentiation. When cells were seeded in mineralized templates, the ossicles regenerated had a significantly higher BVF, relative to ossicles regenerated by cells seeded in PLGA. Perhaps the most significant effect is observed in the static seeded scaffolds, whereby the presence of a mineral layer, enables bone formation to occur, with entrapped cells in a peripheral shell formation, and marrow cavities forming, compared to partial sections of hard tissue with some entrapped cells observed in the polymer group. These results suggest that a mineralized layer provides a favorable physiological environment for cells to thrive, differentiate and regenerate tissue.

In our studies the effects of adhesion due to a biomimetic surface was also investigated. Other studies have shown that such a calcium/phosphate coating can enhance cell adhesion⁴⁰⁻⁴². However, our results show that, only when statically seeded did cells adhere at higher rates in mineralized scaffolds over PLGA (figure 2). Scaffolds

seeded through dynamic and filtration seeding exhibited similar rates of adhesion. The results for the statically seeded scaffolds are therefore consistent with results of others, yet, coupled with our dynamic and filtration data, suggest that the effect of surface mineralization is less important than cell seeding strategy. Also, mineralized scaffolds did not have an effect on GJIC (figure 3). This may be due the short term nature of the experiments, as other groups have shown that external influences by calcium can increase the GJIC in cells ¹⁸.

Altering seeding conditions had a significant impact in the number of adhered cells in culture, cell density, cell-to-cell communication, differentiation and patterns of osteogenesis. Filtration, dynamic, and micromass seeding showed significant increases in cell adhesion over static seeding. This result is promising, by enabling higher cell retention in constructs that may have other biologically favorable benefits, but are hard to seed due to their rigid nature. Filtration provides a mechanism for uniform and complete capacity seeding of a 3D structure (figure 1, 2), while micromass enables the targeted location of a dense cluster of cells. Cells seeded by filtration and micromass were analyzed for their capacity to engage in cell-to-cell communication, and compared to cells seeded statically. We chose to investigate this factor as intracellular communication through gap junctions is essential for proper development of tissues and homeostasis, specifically in bone ^{43, 44}. The data clearly shows significant increases in GJIC, in both micromass and filtration seeded cells when compared to static seeded cells. This suggests that the higher cell density increases the formation of gap junctions between cells, enabling a higher grade of communication. Whether it is the increased proximity of

cells or the increased stress experienced by the cells the predominant factor enhancing GJIC remains to be elucidated.

Differentiation of cells in a 3D constructs provide insights into the actual processes occurring within these scaffolds. The data showed enhanced differentiation due to the initial alteration in cell seeding. Specifically, cells seeded in micromasses exhibited early signs of differentiation, expressing high levels of ALP in the 2nd day after culture. Coupled with the early expression of the late differentiation marker, osteocalcin (fig 4B), the results imply that micromass seeded cells prompts differentiation onset faster than the other methods. It is also evident that differentiation in filtered seeded cells was greater than in static seeded scaffolds (Fig 4A, B), although different than cells seeded in micromasses. One explanation may be that cells in micromasses experience more nutrient and byproduct transport²⁷ than the supersaturated cells in filtered scaffolds. Although both have the benefits of high density, transport and cell migration may play a role in differentiation.

Bone regeneration was also altered significantly as a function of seeding. Ossicles regenerated from filtered and micromass seeded cells, produced larger volumes of bone compared to static seeded cells (fig 5). This result was particularly important when cells were seeded in PLGA scaffolds, as bone regenerated from statically seeded cells was characterized by sporadic bone formation, without marrow cavity or entrapped cells (fig 5F). Not only did ossicles form from filtered and micromass seeded scaffolds with higher volumes of bone, but the distribution of tissue was significantly different in these two strategies. When seeded by filtration, cells produced a peripheral shell of bone, with diminished bone formation in the core of the ossicle. This may be due to cells

thriving and differentiating in the periphery of the construct, while transport is increasingly impaired, thereby compromising tissue regeneration in the core of the scaffold. This contrasts the spatially distributed formation of bone that characterizes ossicles regenerated by micromass seeded cells. This increased presence of bone formation in micromass seeded ossicles may be due to both cell migration, nutrient transport and, a gradient of differentiation. Because cells are seeded in the core of the scaffold at high densities, and differentiation starts promptly, it enables formation of bone in the center. Cells may also migrate outward or inward from the body, and start differentiating at a later time, causing a differentiation gradient. The end result is a more spatially distributed and uniform tissue equivalent. Future studies may look at the potential effects of migration in micromass seeded scaffolds. The distribution studies in tandem with the overall analysis of the ossicles, strengthens the claim that altering the initial seeding conditions of cells can modify the amount and distribution of bone, and with future studies, such regeneration patterns may be achieved by design.

In conclusion, we showed that both a biomimetic mineral template and the manipulation of initial seeding conditions can have profound effects on the resulting differentiation and in-vivo regeneration of bone. Biomimetic templates provided a physiologically favorable environment for BMSCs for tissue formation, while altering the seeding conditions in these rigid 3D scaffolds enabled higher cell adhesion, cell-to-cell communication, and larger volumes of bone with distinct patterns of regeneration. Altogether, our study addresses and provides a mechanism to solving the critical question of full tissue equivalent regeneration by showing that, with simple manipulations of the initial cell and template conditions, one can significantly enhance the regeneration and

spatial distribution of tissue in-vivo; which has a major impact on bone regeneration and 3D tissue engineering as a whole.

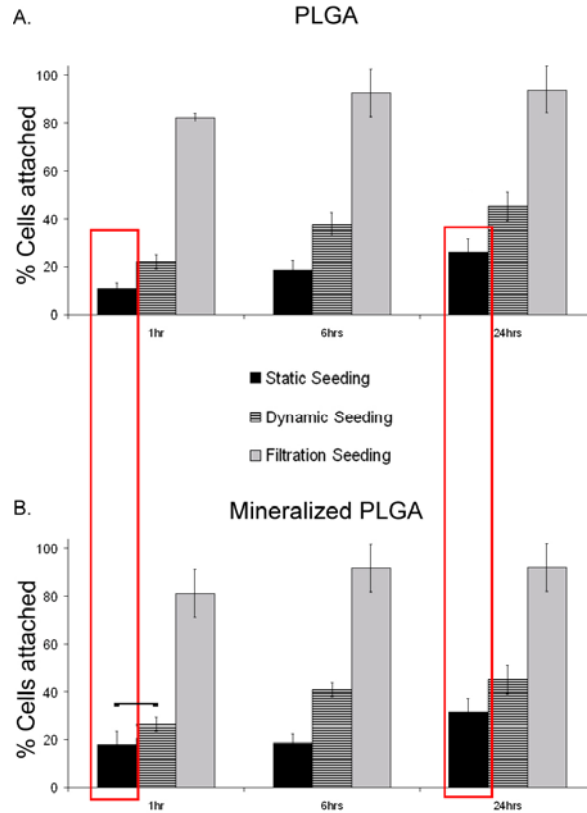


Figure 3-1 Percent of cells adhering to PLGA (A) and mineralized (B) scaffolds at different time points following seeding via different techniques.

Using a filtration approach produces significantly more adhesion and cell retention than both dynamic and static seeding ($p < 0.001$). Filtration reaches a plateau after 6 hours. Both static and dynamic techniques increase the number of adhered cells as a function of time. There were no differences in adhesion between mineralized and PLGA scaffolds, with the exception of static seeding at 1 and 24 hours. Bars indicate pairs that were not significantly different. Boxes denote groups that showed significant difference in adhesion due to scaffold.

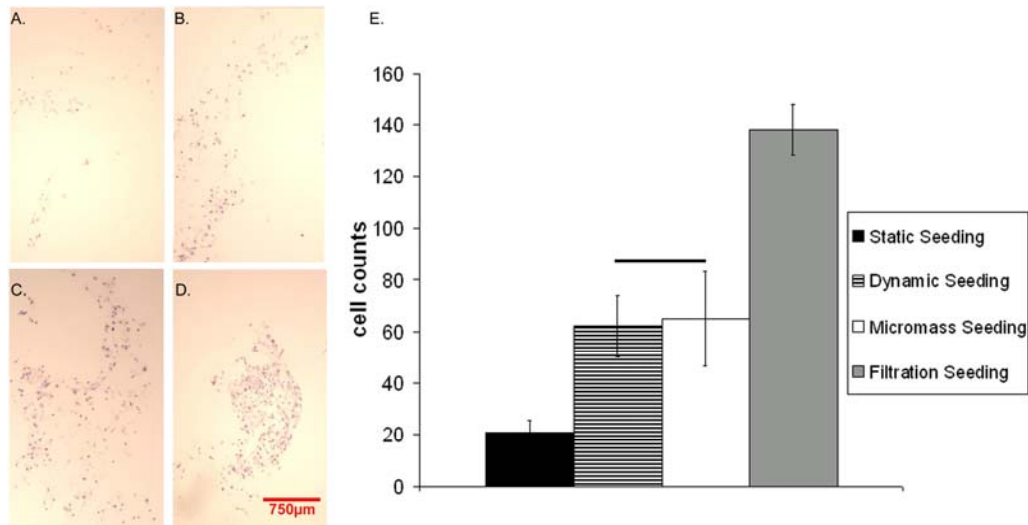


Figure 3-2 Cell count and distribution varies in seeded scaffolds, 6 hours after seeding.

Histological slides demonstrate the even distribution and high cell adhesion produced in scaffolds that were seeded through filtration (A). Static seeding (B) is characterized by a lower yield of cells that are un-evenly allocated throughout the sections. Dynamic seeding showed sections with densely packed cells but also a large variation in cell location (C). Micromass seeding technique was validated showing a densely packed group of cells in the core of the scaffold. Quantification of the mean cell count (E) in histological demonstrates that filtration, dynamic, and micromass seeding techniques enable more cell adhesion ($p < 0.001$). There was no significant difference between micromass and dynamic seeding ($p = 0.672$). Bars indicate groups that are not significantly different.

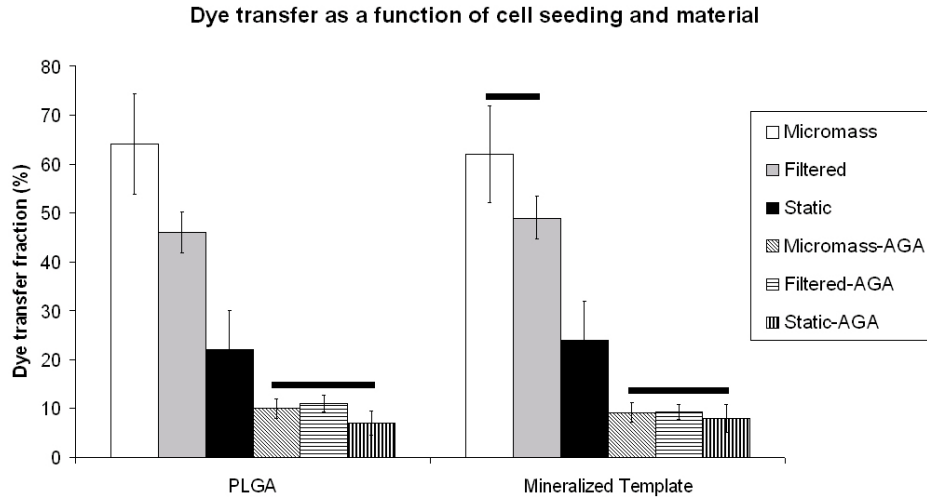


Figure 3-3 Seeding alters gap junction intercellular communication.

Cells seeded in PLGA scaffolds by micromass transferred calcenin at a higher fraction (63.2±/10.6%) than both filtered (46.2±/5.4%) and static seeded cells (23.6±/6.9%). Although there was no significant differences in transfer between cells in mineralized and PLGA scaffolds (for all seeding strategies), micromass and filtered seeded cells exhibit no significant difference in transfer when seeded in a mineralized scaffold (p=9.2). Cells treated with AGA show significantly less transfer than those that were not, as well as showing no difference between seeding conditions exposed to the gap junction uncoupler. This indicates a gap junction dependent transfer of calcenin. Horizontal bars indicate groups that are not significantly different.

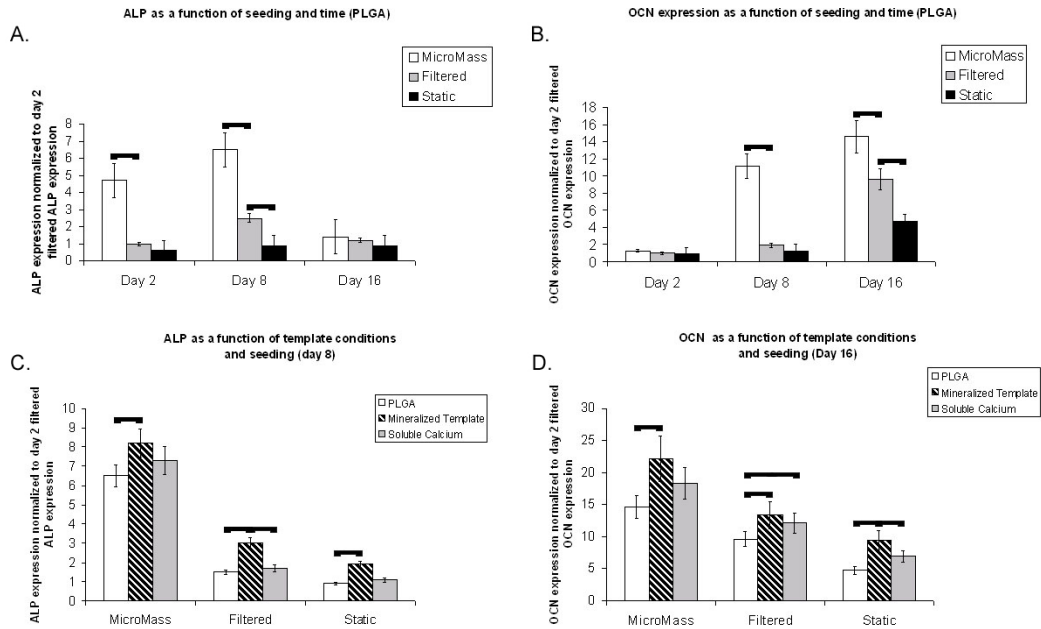


Figure 3-4 Expression of differentiation markers is increased with alternative seeding techniques and a mineralized template.

Alkaline phosphatase (A) and Osteocalcin (B) expression increased significantly in cells seeded by micromass over filtration (ALP: $p(\text{day}2) < 0.001$, $p(\text{day}8) < 0.001$; OCN: $p(\text{day}8) < 0.001$, $p(\text{day}16) = 0.0211$) and static seeding ALP: $p(\text{day}2, \text{day}8) < 0.001$; OCN: $p(\text{day}8, \text{day}16) < 0.001$). Cells seeded in a mineralized template and calcium rich environment also expressed higher levels of ALP (C) and OCN (D) over cells seeded in PLGA. Cells seeded in mineralized templates expressed significantly more ALP and OCN in all seeding techniques over cells seeded in PLGA-only (ALP: $p(\text{day}2) = 0.031$, $p(\text{day}8) < 0.001$, $p(\text{day}16) < 0.001$; $p(\text{day}2) < 0.001$ OCN: $p(\text{day}8) = 0.033$, $p(\text{day}16) < 0.001$). Although cells seeded with increased extracellular calcium did not exhibit a significant difference in ALP relative to those seeded in PLGA, it did exhibit significant differences in expression in OCN expression for filtered and static seeded cells ($p = 0.032$, $p = 0.042$ respectively).

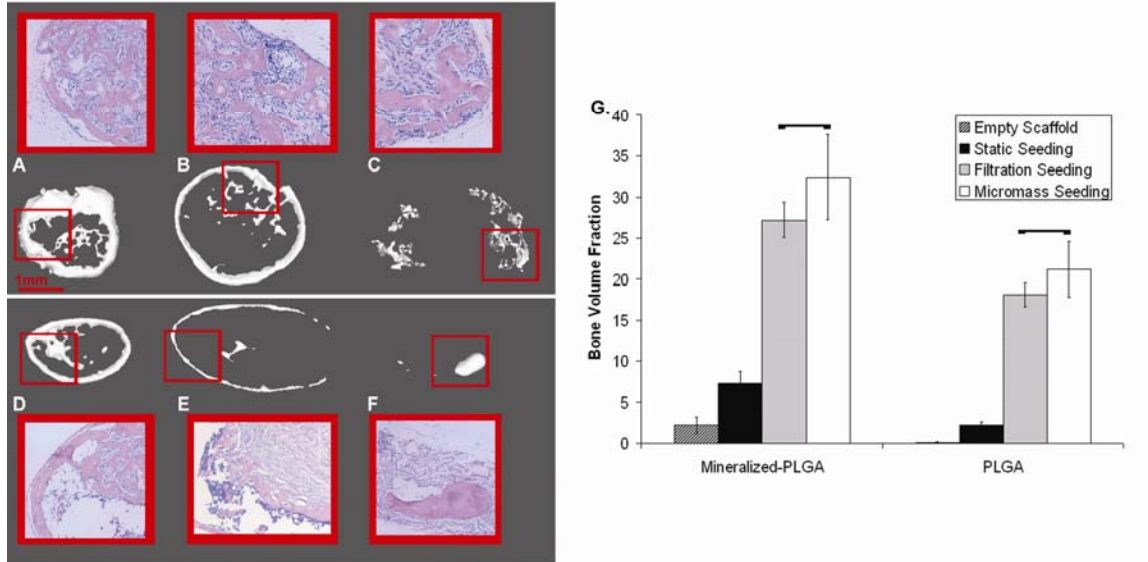


Figure 3-5 Volume fractions and patterns of osteogenesis vary as a function of scaffold surface and seeding techniques.

Macromass seeded scaffolds produce smaller ossicles, with a more abundant mineralization in the core of the scaffold (A, D). Filtered scaffolds (B, E) show a larger shell of bone formation with little or no mineralization in the core of the scaffold in both CT renderings and H&E histological sections. Static seeded scaffolds produce scant mineralization and bone formation (C, F). Mineralization enhances mineral coverage and BVF in all groups. These significant differences as a function of surface material and initial seeding were quantified (G). Both the micromass and filtration seeding yielded significantly larger BVF than static seeding ($p < 0.001$). Although there was no significant difference between the filtration and macromass seeding, the variability is 2-fold greater in the macromass implants. Mineralized scaffolds showed a significantly higher BVF with all seeding techniques than did their PLGA counterpart ($p(\text{micromass})=0.037$, $p(\text{filtration})=0.013$, $p(\text{static})=0.009$). Bars indicate groups that are not significantly different.

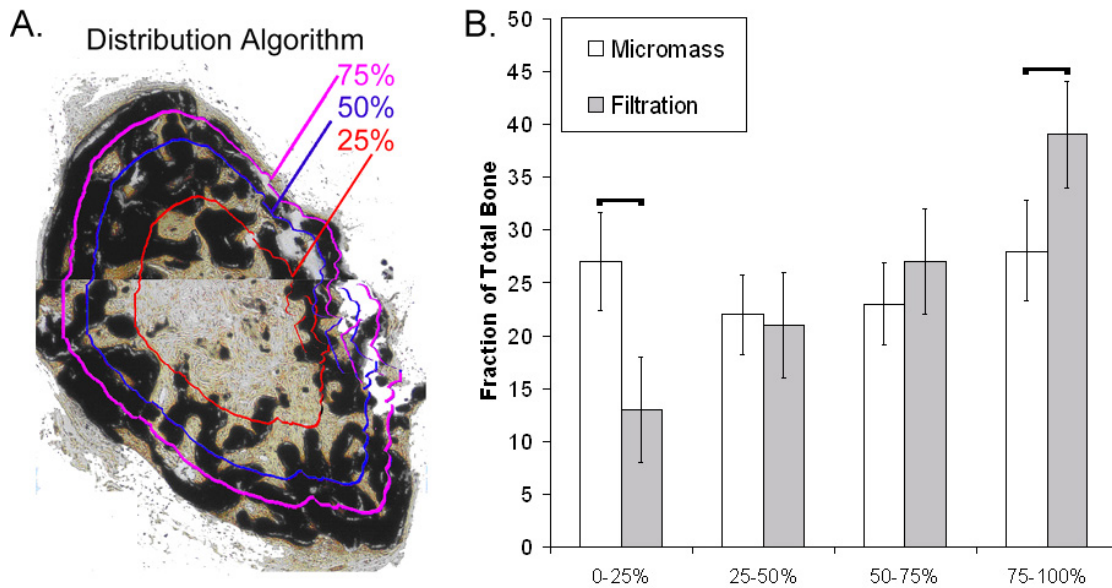


Figure 3-6 Topographic analysis of mineral distribution within bone ossicles.

In order to quantify the observed differences in mineral distribution through out the ossicles, cross sectional slides were analyzed with a program designed to calculate the topographical distribution of the mineral. The program was set to analyze sections in 25% increments from centroid (a). Even distribution of bone in ossicles produced by micromass seeding showed no significant differences in bone % between regions (b). Ossicles generated by scaffolds seeded through filtration showed a significant difference in mineral from the periphery (75-100%) to the core (0-25%); $p < 0.001$. The amount of mineral content in 0-25th% of the micromass ossicles was significantly greater than the filtered ossicles ($p = 0.0213$), while the opposite is true for the periphery ($p = 0.0311$). Horizontal bars indicate groups that are significantly different.

3.5 References

1. Cheung C. The future of bone healing. Clin Podiatr Med Surg. 2005; 22(4):631-41. viii.
2. Friedlaender GE. Immune responses to osteochondral allografts. current knowledge and future directions. Clin Orthop Relat Res. 1983; (174)(174):58-68.
3. Friedlaender GE. Bone grafts. the basic science rationale for clinical applications. J Bone Joint Surg Am. 1987; 69(5):786-790.
4. Goldberg VM, Stevenson S. Natural history of autografts and allografts. Clin Orthop Relat Res. 1987; (225)(225):7-16.
5. Damien CJ, Parsons JR. Bone graft and bone graft substitutes: A review of current technology and applications. J Appl Biomater. 1991; 2(3):187-208.
6. David H. Kohn, Kyungsup Shin, Sun-Ig Hong, et al. **Self-assembled mineral scaffolds as model systems for biomineralization and tissue engineering** . Proc 8th Int Conf Chem & Biol Min Tissues. 2005; .
7. Yaszemski MJ, Payne RG, Hayes WC, Langer R, Mikos AG. Evolution of bone transplantation: Molecular, cellular and tissue strategies to engineer human bone. Biomaterials. 1996; 17(2):175-185.
8. Burchardt H, Glowczewskie F, Miller G. Freeze-dried segmental fibular allografts in azathioprine-treated dogs. Clin Orthop Relat Res. 1987; (218)(218):259-267.

9. Beaman FD, Bancroft LW, Peterson JJ, Kransdorf MJ. Bone graft materials and synthetic substitutes. *Radiol Clin North Am.* 2006; 44(3):451-461.
10. Oklund SA, Prolo DJ, Gutierrez RV, King SE. Quantitative comparisons of healing in cranial fresh autografts, frozen autografts and processed autografts, and allografts in canine skull defects. *Clin Orthop Relat Res.* 1986; (205)(205):269-291.
11. Shaffer JW, Field GA, Goldberg VM, Davy DT. Fate of vascularized and nonvascularized autografts. *Clin Orthop Relat Res.* 1985; (197)(197):32-43.
12. Yoshikawa H, Myoui A. Bone tissue engineering with porous hydroxyapatite ceramics. *J Artif Organs.* 2005; 8(3):131-136.
13. Takagi K, Urist MR. The role of bone marrow in bone morphogenetic protein-induced repair of femoral massive diaphyseal defects. *Clin Orthop Relat Res.* 1982; (171)(171):224-231.
14. Hollinger JO, Winn SR. Tissue engineering of bone in the craniofacial complex. *Ann N Y Acad Sci.* 1999; 875:379-385.
15. Ishaug SL, Crane GM, Miller MJ, Yasko AW, Yaszemski MJ, Mikos AG. Bone formation by three-dimensional stromal osteoblast culture in biodegradable polymer scaffolds. *J Biomed Mater Res.* 1997; 36(1):17-28.
16. Katz RW, Hollinger JO, Reddi AH. The functional equivalence of demineralized bone and tooth matrices in ectopic bone induction. *J Biomed Mater Res.* 1993; 27(2):239-245.

17. Ducheyne P, Qiu Q. Bioactive ceramics: The effect of surface reactivity on bone formation and bone cell function. *Biomaterials*. 1999; 20(23-24):2287-2303.
18. Jorgensen NR, Henriksen Z, Brot C, et al. Human osteoblastic cells propagate intercellular calcium signals by two different mechanisms. *J Bone Miner Res*. 2000; 15(6):1024-1032.
19. Triggle DJ. L-type calcium channels. *Curr Pharm Des*. 2006; 12(4):443-457.
20. Romanello M, Veronesi V, D'Andrea P. Mechanosensitivity and intercellular communication in HOBIT osteoblastic cells: A possible role for gap junction hemichannels. *Biorheology*. 2003; 40(1-3):119-121.
21. Berridge MJ, Lipp P, Bootman MD. The versatility and universality of calcium signalling. *Nat Rev Mol Cell Biol*. 2000; 1(1):11-21.
22. Romanello M, D'Andrea P. Dual mechanism of intercellular communication in HOBIT osteoblastic cells: A role for gap-junctional hemichannels. *J Bone Miner Res*. 2001; 16(8):1465-1476.
23. Rottingen J, Iversen JG. Ruled by waves? intracellular and intercellular calcium signalling. *Acta Physiol Scand*. 2000; 169(3):203-219.
24. Cartmell SH, Porter BD, Garcia AJ, Guldberg RE. Effects of medium perfusion rate on cell-seeded three-dimensional bone constructs in vitro. *Tissue Eng*. 2003; 9(6):1197-1203.

25. Zhao F, Ma T. Perfusion bioreactor system for human mesenchymal stem cell tissue engineering: Dynamic cell seeding and construct development. *Biotechnol Bioeng.* 2005; 91(4):482-493.
26. Burg KJ, Holder WD, Jr, Culberson CR, et al. Comparative study of seeding methods for three-dimensional polymeric scaffolds. *J Biomed Mater Res.* 2000; 51(4):642-649.
27. Goldstein AS. Effect of seeding osteoprogenitor cells as dense clusters on cell growth and differentiation. *Tissue Eng.* 2001; 7(6):817-827.
28. Leonova EV, Pennington KE, Krebsbach PH, Kohn DH. Substrate mineralization stimulates focal adhesion contact redistribution and cell motility of bone marrow stromal cells. *J Biomed Mater Res A.* 2006; 79(2):263-270.
29. Murphy WL, Kohn DH, Mooney DJ. Growth of continuous bonelike mineral within porous poly(lactide-co-glycolide) scaffolds in vitro. *J Biomed Mater Res.* 2000; 50(1):50-58.
30. Liao CJ, Chen CF, Chen JH, Chiang SF, Lin YJ, Chang KY. Fabrication of porous biodegradable polymer scaffolds using a solvent merging/particulate leaching method. *J Biomed Mater Res.* 2002; 59(4):676-681.
31. Mikos AG, Thorsen AJ, Czerwonka LA, Bao Y, Langer R, Winslow DN, Vacanti JP. Preparation and characterization of poly(L-lactic acid) foams. *Polymer.* 1994; 35:1068-1077.

32. Luong LN, Hong SI, Patel RJ, Outslay ME, Kohn DH. Spatial control of protein within biomimetically nucleated mineral. *Biomaterials*. 2006; 27(7):1175-1186.
33. Rossello RA, Wang Z, Krebsbach PH, and Kohn DH. Establishing micro CT thresholds for tissue engineered bone and comparison of bone regenerated from BMSC and transduced C-4 cells. *Trans 31st Annual Meeting Soc for Biomat*. 2005; .
34. Wallace JM, Rajachar RM, Chen XD, et al. The mechanical phenotype of biglycan-deficient mice is bone- and gender-specific. *Bone*. 2006; 39(1):106-116.
35. Holy CE, Shoichet MS, Davies JE. Engineering three-dimensional bone tissue in vitro using biodegradable scaffolds: Investigating initial cell-seeding density and culture period. *J Biomed Mater Res*. 2000; 51(3):376-382.
36. Zhang S, Wu XY, Li YH, Xie LQ. Mechanotransduction in bone. *Space Med Med Eng (Beijing)*. 2001; 14(6):465-468.
37. Goldmann WH. Mechanical aspects of cell shape regulation and signaling. *Cell Biol Int*. 2002; 26(4):313-317.
38. Jorgensen NR, Teilmann SC, Henriksen Z, Civitelli R, Sorensen OH, Steinberg TH. Activation of L-type calcium channels is required for gap junction-mediated intercellular calcium signaling in osteoblastic cells. *J Biol Chem*. 2003; 278(6):4082-4086.
39. Cotrina ML, Lin JH, Alves-Rodrigues A, et al. Connexins regulate calcium signaling by controlling ATP release. *Proc Natl Acad Sci U S A*. 1998; 95(26):15735-15740.

40. Yang Y, Bumgardner JD, Cavin R, Carnes DL, Ong JL. Osteoblast precursor cell attachment on heat-treated calcium phosphate coatings. *J Dent Res.* 2003; 82(6):449-453.
41. Shu R, McMullen R, Baumann MJ, McCabe LR. Hydroxyapatite accelerates differentiation and suppresses growth of MC3T3-E1 osteoblasts. *J Biomed Mater Res A.* 2003; 67(4):1196-1204.
42. Suzuki T, Yamamoto T, Toriyama M, et al. Surface instability of calcium phosphate ceramics in tissue culture medium and the effect on adhesion and growth of anchorage-dependent animal cells. *J Biomed Mater Res.* 1997; 34(4):507-517.
43. Lecanda F, Warlow PM, Sheikh S, Furlan F, Steinberg TH, Civitelli R. Connexin43 deficiency causes delayed ossification, craniofacial abnormalities, and osteoblast dysfunction. *J Cell Biol.* 2000; 151(4):931-944.
44. Stains JP, Civitelli R. Cell-to-cell interactions in bone. *Biochem Biophys Res Commun.* 2005; 328(3):721-727.

Chapter 4

Connexin 43 as a signaling platform for increasing the volume and spatial distribution of regenerated tissue

4.1 Introduction

Cell-to-cell communication, via intracellular chemical and mechanical signals, is critical to maintain tissue homeostasis ^{1, 2}. Gap junction intercellular communication (GJIC) is the most direct way of achieving such signaling ³ and is particularly important to maintain synchronized and cooperative behavior of cells in three-dimensional tissue ⁴. As consequence, the absence of gap junctions has been linked with several debilitating diseases and tissue malformations, such as oculodentaldigital dysplasia, impaired heart function and certain types of cancerous tumors ⁵⁻¹⁰. Of the 19 known gap junction subunits (connexins), connexin43 (Cx43) is the most prevalent ¹¹. The ubiquitous nature of this protein throughout most vertebrate cell types makes it a potent signaling platform that enables cells to communicate directly and also distribute secondary messengers initiated by other biological cues and stimuli ¹²⁻²¹ that play a role in cell differentiation and tissue formation²²⁻²⁶, such as Bone Morphogenetic Proteins (BMPs) and PHT. However, characterization of these stimuli has been limited to in-vitro assessment of cells in a two-dimensional monolayer, and may misconstrue the real impact of these factors in

three-dimensional settings²⁷. Limitations in cell-to-cell communication in 3D may hinder the coordinated behavior of cells, and inhibit proper passage of secondary messengers and eventual tissue formation. Overexpressing Cx43 as a conduit to improve GJIC can be a platform to enhance the distribution of signals among cells in a 3D setting and, therefore, be a powerful strategy in both cell-based strategies and targeted delivery as treatments to boost cell-to-cell communication. Our research, therefore, may have a significant impact in the regeneration of tissue de-novo and in-vivo as well as therapies for diseases in 3D tissues characterized by compromised cell-to-cell communication, such as some forms of cancer and heart disease^{28,29}.

In this study, we focus on the specific effects of Cx43 as a platform to enhance gap junction intercellular communication in 3D. Because of its inherent limitation in producing spatially uniform 3D mineralized tissue equivalents, bone is used as a model tissue. Such limitation is in large part prompted by the early formation of hard tissue in the periphery of tissue engineered bone ossicles which prevents tissue regeneration in the core^{30,31}. In order to examine the role of enhanced GJIC in tissue engineering, we investigated the effects of stable Cx43 overexpression in bone marrow stromal cells (BMSCs), a pluripotent somatic stem cell, by transducing them with a lentiviral vector encoding the Cx43 gene (LVCx43GFP) and seeding them in 2D and 3D cultures. Enhancing gap junction function in BMSCs is attractive because these cells express a low level of Cx43^{32,33} relative to osteoblasts, and have the ability to differentiate into bone, given the proper biological cues^{32,34}.

Both the effects of increased GJIC alone and in combination with an osteogenic stimulus on BMSC differentiation, in 2D and 3D cultures, into an osteogenic phenotype

in-vitro and bone formation in-vivo, were examined. Toward this end, we chose to induce bone formation by both transducing BMSCs with Cx43, and co-transducing Cx43 gene-modified BMSCs with an adenovirus encoding the gene for BMP7³⁵⁻³⁷. BMP7, is a powerful osteoinductive agent that enables differentiation³⁶⁻³⁹ and does not modulate the expression of Cx43⁴⁰. Cell-to-cell communication and osteogenic differentiation were assessed in both a 2D monolayer and 3D cultures. In 3D cultures, differentiation and GJIC were further assessed the surface and the inner core of 3D scaffolds. Because of the differences in cell numbers between 2D and 3D cultures, intracellular communication and mRNA obtained from the cells was normalized. In-vivo regeneration of tissue by cells overexpressing Cx43 was quantified and compared to tissue regenerated by BMSCs. The differences were assessed as a function of total bone volume fraction of bone regenerated after 4, 8, 12 weeks of transplantation as well as quantitatively assessing for differences in the spatial uniformity of the tissue. The same in-vivo studies were performed in BMSCs overexpressing BMP7 and co-transduced with Cx43 and BMP7.

Our experiments aim to answer two critical questions in applied biology. First, can overexpression of Cx43 enhance cell communication throughout three-dimensional structures? Secondly, can such enhanced communication lead to higher and more spatially distributed amounts of engineered tissue? Based on our data, we propose that enhanced GJIC, via genetically engineering cells to overexpress Cx43, as a novel platform to produce spatially distributed communication in 3D, and achieve larger volumes of evenly distributed tissue equivalents. These results have a major impact in the strategic design of cell-based tissue engineering, and may be significant to directed therapies that aim to enhance cell communication in 3D tissue.

4.2 Materials and Methods

4.2.1 Viral Vector Production

Vectors encoding Cx43 and BMP-7 were produced by the University of Michigan Vector Core employing standard transient transfection methods to produce replication incompetent viral vectors. The development and production of the lentiviral vector encoding Cx43GFP has been previously described⁴¹. The vector system was based on the human immunodeficiency virus Type 1 (HIV-1) and the four plasmids required for vector production were kindly supplied by Professor Inder Verma from the Salk Institute, San Diego USA. The development and production of the adenovector encoding BMP7 under the transcriptional control the human CMV promoter has been previously described³⁷. Empty vectors devoid of a transgene and vectors encoding GFP were also produced for lentivirus (LVMT, LVGFP) and adenovirus (ADCMVMT), and employed as controls. A seven base pair deletion mutant (LV Cx43 Δ 7) that produces connexin structures but is disabled from engaging in GJIC was used as a dominant negative control group.

4.2.2 Culture and Transduction of BMSCs

Five-week old C57BL/6 mice were used to isolate bone marrow cells from the femoral, tibial and humeral cavities (six bones per animal), as previously described⁴². BMSCs mixed with enriched minimum essential medium (α -MEM; Gibco Laboratories, Grand Island, NY) containing 10% fetal bovine serum (FBS) (Gibco) and antibiotics (100 μ g/ml penicillin G and 100 IU/ml streptomycin) at 37°C in 5% CO₂/95% air) were plated

at a density of 2.25 million cells per T75 flask. Cells were passaged twice before transduction. For LVCx43GFP, LVGFP, and LVMT transductions, lentiviral vector with a titer of 10^6 transducing units/ml was used on day 3-4 of sub-culture. Transduction was carried out in the presence of 8 μ g/ml of protamine sulfate to enhance the transduction efficiency. Five ml of filtered vector-containing enriched α -MEM was added to the cell cultures for approximately 16 h (transduction phase), followed by replacement of media with fresh media for 6-8 h (recovery phase). The cells were exposed to three cycles of transduction. After 12 days of incubation, transduced BMSCs were examined under fluorescent microscopy to determine transduction efficiency through GFP fluorescence. Ten random fields per well were photographed and transduction was measured as the average fraction of fluorescent cells relative to total cells in the field. Transductions with ADCMVBMP7 and ADCMVMT were performed as previously stated³⁸. Briefly, for in-vitro transduction of BMSCs, adenovirus at the desired titer to achieve a multiplicity of infection of 200 plaque forming units (PFU) was added to cells in serum-free α -MEM. After 4 h, FBS was added to a final concentration of 2% and medium was kept on cells for an additional 24 h.

4.2.3 Western Blot

Western blot analysis was performed using mouse anti-Cx43 with GAPDH as a sample loading control. Cells were lysed in lysis buffer (66 mM Tris-HCl, 5 mM EDTA, 5mM EGTA, 10 mM Na-phosphate, 5 mM NaF, 5 mM Na₃VO₄, 2.5mM PMSF, 10 mM NEM, 2% SDS, 0.5% Triton X-100, pH 8.0). Loading protocols were followed from the western blot kit (Zymed). Blots were incubated in 1% nonfat dry milk solution in PBS overnight with gentle shaking. The following morning, blots were washed 3 times with

PBS, incubated with primary antibodies for 2.5 hours. The resulting bands were quantified by densitometry (ImageQuant, GE), and were normalized to endogenous GAPDH expression. In order to quantify the total Cx43 expression in Cx43-GFP transduced cells, the 74kDa band (sum of Cx43 and GFP fusion protein) was analysed. The results are reported as a ratio, with the denominator being the endogenous Cx43 expression in non-transduced BMSCs. Experiments were performed in triplicate (n=3) and were done 1 week after the end of transduction. One-way ANOVA was performed on the ImageQuant data for band intensity to determine whether the levels of Cx43 expression were significantly different ($p=0.05$) between cell groups. The average of the total Cx43 or Cx43-GFP fusion gene was normalized against GAPDH, for BMSCs, BMSCs transduced to overexpress Cx43-GFP, and BMSCs transduced to overexpress GFP. All values were later normalized to the expression of BMSC Cx43 content.

4.2.4 2D and 3D Cell Culturing

For 2D cultures, 1 million cells were cultured in 6-well plates (Sarstead) and grown to 90% confluence. 3D culture experiments were performed by seeding cells in gelatin sponges (Gelform; Pharmacia & Upjohn, Kalamazoo, MI). Two experiments were done: (1) overall assessment of cell to cell communication and differentiation in 3D construct relative to 2D cultures, (2) assessing the differences in these parameters between the surface and core regions of cell seeded 3D scaffolds. In the 3D studies, the gelatin sponges were designed to have $3 \times 3 \times 3 \text{mm}^3$ dimensions. Studies that examined peripheral vs. core communication and differentiation were performed by entrapping two sponges in 96 well plates (corning), one on top of the other. The thickness of the top

sponge was set at 0.5mm, compared to 2.5mm for the bottom sponge. Cell-gelatin constructs completely covered the side of the plates. The bottom sponge is taken to be the core section of the scaffolds as the walls of the well plate serve to block any flux or communication from the bottom or sides. All sponges were pre-wet in α -MEM, and air bubbles removed by applying gentle pressure on the sponge between two pieces of sterile filter paper. 2.5 million cells were collected, suspended in 50 μ l medium, and loaded onto each sponge by capillary action. Both 2D and 3D cultures were induced to differentiate with osteogenic media (88% MEM- α media, 9% Fetal Bovine Serum, 1% Pen/Strep, 1% 100x β -Glycerophosphate, 1% L-ascorbic acid-phosphate, \sim 0.05% Dexamethasone) one day after culturing. After culture time, the gelfoam-cell constructs are removed from the well-plate and separated for analysis of both surface and core cells.

4.2.5 Dye transfer studies of Cx43

Fluorescent dye transfer studies were performed to assess gap-junctional intercellular communication (GJIC). Calcein-AM (10 μ m, gap junction permeable, molecular probes) and Vybrant-DiI (membrane tracker, molecular probes) were used to label donor cells grown to confluence in a 12-well plate. As a negative control, 50 μ M of the gap junction uncoupler alpha-glycyrrhethinic acid (AGA) was used (Sigma). Donor cells were added to potential recipient cells, cultured to confluence in monolayer (12-well plates) or in 3D constructs (Gelfoam®, 8 days), at a ratio of 1:8. After 5 hours, cells were harvested by trypsinisation for quantitative assessment of GJIC by flow cytometry (BD Biosciences FaCSCalibur), of homogeneous samples. Dye studies were performed on all cell types in the experimental groups, at a sample size equal to six (n=6) wells or

gelfoam constructs. A 2-way ANOVA was used to determine significant differences between 3D and 2D realms and cell type. Two tailed student t-test was applied to determine significant differences between cells in surface of the 3D scaffold (outer 0.5mm) and core (inner 2.5mm) of the 3D constructs ($p=0.05$).

4.2.6 Real-time PCR Analysis

Real-Time PCR was used to detect the expression of two bone differentiation markers, alkaline phosphatase (ALP) and osteocalcin (OCN) on BMSC control groups and cells modified with Cx43 and/or BMP7. PCR was performed using ABI Prism 7700 sequence detection system. Primers and TaqMan probes were designed using Primer Express design software (ABI). The primer sequences utilized was as follows: OCN, forward 5'-CCAGCGACTCTGAGTCTGACAA-3', and reverse 5' - CCGGAGTCTATTCAACCACCTTACT-3'. Cells seeded scaffolds or in 12 well plates were trypsinized after 2, 8, and 16 days, to remove cells and the total RNA was extracted (Trizol; invitrogen Corp). The RNA was purified (RNeasy, Qiagen) and treated with DNase I. Cycling conditions were as follows: 50C for 2 minutes and 95C for ten minutes, followed by 50 cycles of 95C for 15 seconds and 60C for 1 minute. No-template control analyses were run for each primer set and 18s rRNA (ABI) endogenous control was run for each sample. Analysis was performed by first setting an appropriate standard threshold level in the linear part of the reaction for each primer. The crossing value of this threshold was determined (C_T) for each sample. Using the manufacturer's protocols (ABI Prism 7700 Sequence Detection System, User Bulletin #2), mRNA expression levels for each sample/primer were normalized to endogenous rRNA 18S levels and the results were reported as a fold change relative to the OCN expression of

BMSCs (day 2). All reactions were performed in quintuplets. Two 1-way ANOVAs were used to determine significant differences as a function of dimension (3D vs. 2D) and cell types. Differences between surface (peripheral) segments and core (bottom) segments were assessed with a two-tailed student t-test using SigmaSTAT version 3.1.

4.2.7 In-vivo transplantation

Surgery was performed in nude mice (nu/nu) by transplanting gelatin scaffolds ($3 \times 3 \times 2 \text{ mm}^3$) seeded with 2×10^6 cells. The mice were anaesthetized by an intraperitoneal injection of 1 mg/10 g ketamine and 0.1mg/10 g xylazine. A 3 cm longitudinal incision was made overlying the spine. Four subcutaneous pockets were made using blunt dissection through the minimal subcutaneous tissue of the mice. In each pocket, one of the prepared cell-gelfoam specimens (BMSC, BMSC-Cx43, BMSC-BMP7, BMSC-Cx43-BMP7, BMSC-LVMT, BMSC-ADCMVMT) or acellular gelfoam specimen was implanted. The cell-gelfoam specimens were assigned randomly to each pocket. The incision site was closed with wound clips or sutures. The mice were allowed to recover on a recirculated heated water pad. Recovery from anesthesia was monitored closely. Four, 8, and 12 weeks after transplantation, mice were euthanized by cervical dislocation. Ossicles were extracted and stored in 70% ethanol until analysis.

4.2.8 Micro-CT 3D image acquisition and analysis

Ossicles were scanned on a high resolution cone beam micro-CT system (Enhanced Vision Systems (now GE Healthcare Preclinical Imaging), London, Ontario, Canada). The x-ray source voltage and current were 80 kVp and 80 μ A, respectively. To reduce the potential for beam hardening artifact, the x-rays were passed through a 0.2mm

Al filter immediately upon exiting the source and the specimens were immersed in dH₂O during the scanning process. Projection images were acquired over 198 degrees using 2x2 binning and an exposure time of 1100 ms, and four frames were averaged for each projection to improve the signal to noise ratio. The projection data was then corrected and reconstructed using the Feldkamp cone-beam algorithm to create three-dimensional images with an isotropic voxel size of 18 μ m⁴³. The scanner was calibrated once daily using a phantom that contained air, water and hydroxyapatite. Bone volume fractions (BVF) were determined by using a MatLab program designed to integrate all grayscale voxels above a particular threshold. To determine the overall volume of the ossicles, the program determined the perimeter of each 2D μ CT slice by tracing the outer edge. The program then integrated all the perimeters to determine the 3D surface area, and the number of voxels inside the surface defined the total volume. High density voxels outside of the 3D surface and unattached to the ossicle were discarded, while voxels inside were evaluated at the specified thresholds to determine the BVF, which was calculated as the number of voxels above the threshold relative to the total number of voxels. Using this method, a threshold of 1100 was used to re-construct a rendered image of the ossicles and determine their distribution.

A custom program was developed to determine the distribution of regenerated bone as a function of the distance to the geometric center of each ossicle. Using the 2D Micro CT sections, the centroid was calculated with a MatLab script⁴⁴ and used as a frame of reference to divide the ossicles into regions. Defining the centroid as the 0th percentile and the edge as the 100th percentile, boundaries were calculated by lines that radially pointed into the center from the edges. Cortical bone was determined to be the

continuous bone formation in the periphery of the ossicle. The program calculated this thickness by averaging the thickness at 10 degree increments from the geometric center of the ossicle (total 36 data points per ossicle). Trabecular bone volume fraction was determined to be the remaining bone fraction normalized to the potential trabecular space (total bone volume - cortical bone volume).

4.2.9 Histology and Morphological Analyses

The ossicles were rinsed in water and then decalcified in 10% formic acid for 5 days. After decalcification, the tissues were embedded in paraffin. 5 μm sections were made and placed on 10 slides with 3 sections per slide. The tissue was deparaffinized hydrated, and the first, fifth, and tenth slides were stained with H & E. Image Pro Plus 4.0 was used to take pictures of the histological sections in order to observe the overall bone formation, cortical thickness, and trabecular-like bone formation.

4.3 Results

4.3.1 Characterization of Cx43-GFP modified BMSCs

Transfer efficiency of the GFP-Cx43 fusion gene was measured at 83% +/- 4% by assessing the number of GFP positive cells (Fig 1 B) relative to the total number of nuclei per given field two weeks after transduction. Similar efficiency was attained when cells were co-transduced with AD-BMP7 and LVC-Cx43-GFP (85% +/-5%) and control cells with LVGFP (87% +/-7%), indicating that the co-transduction did not alter the transduction efficiency of cells with Cx43 and that no differences in transduction occurred between Cx43-GFP and GFP containing lentivirus. A significant increase in

expression of Cx43 occurred when cells were transduced with LVCx43GFP (Fig. 1C). The total expression Cx43 in BMSCs transduced with Cx43-GFP was significantly higher (3.74 +/-0.49, $p < 0.001$ against both groups) compared to the non-transduced BMSC group (1.0 +/-0.29) and the control LVGFP transduced group (0.89 +/-0.11).

4.3.2 Overexpression of Cx43 increases GJIC

BMSCs transduced with Cx43 exhibited significantly higher transfer of Calcein-AM than BMSCs, both in cells cultured in 6-well plates (2D) and gelfoam scaffolds (3D), relative to non transduced groups ($p < 0.001$ for all, figure 2). There was no significant difference between Cx43 and Cx43-BMP7 or between BMSCs and BMSC-BMP7 transduced cells, suggesting that BMP7 does not modulate gap junction function. Cells transduced with a seven base pair deletion Cx43 gene mutant (Cx43 Δ 7) which enables proper docking of connexin hemichannels but inhibits GJIC, exhibited significantly less transfer than both BMSCs and BMSCs transduced to overexpress Cx43 ($p < 0.001$). The data suggests that Cx43 plays a prominent role in cell-to-cell communication, and inhibition or overexpression will lead to hindered or amplified GJIC, respectively.

When cells overexpress Cx43 the percentage of cells that uptake calcein in 3D cultures was significantly greater than the percentage of those that uptook calcein in 2D cultures (figure 2b, $p > 0.001$ in both Cx43 and Cx43-BMP7 vs. all other cells). BMSCs and BMSCs transduced with BMP7 showed no significant difference in transfer fraction. Cells transduced with control vectors (LVMT, LVGFP, ADCMVMT, ADCMVMT/LVMT), showed no significant difference in GJIC from BMSC (data not shown). The results support the hypothesis that overexpression of Cx43 enhances GJIC in 3D.

BMSCs, BMSCs transduced with BMP7, and BMSC-Cx43 Δ 7, exhibited significantly less calcenin transfer in the core of the scaffold, relative to the periphery (Fig 2b; p (BMSCs) <0.002, p (BMP7) <0.001, p (Cx43 Δ 7) <0.013). However, cells overexpressing Cx43 exhibited similar GJIC transfer in the surface and core sections of the scaffold. Our results imply that cell-cell communication is compromised in cells entrapped in the core of 3D tissue engineered equivalent and that overexpressing Cx43 is one potential solution to overcome this problem. Our data therefore suggests that overexpressing Cx43 provides a platform that enables a more amplified level of cell-to-cell communication.

4.3.3 Cx43 overexpression enhances overall and spatial distribution of differentiation markers

Increased Cx43 expression in BMSCs was associated with significantly higher levels of osteocalcin (OCN) mRNA, relative to control groups (Fig 3a). Two days after differentiation was induced cells overexpressing Cx43 and Cx43-BMP7 exhibited significantly higher levels of OCN mRNA (p<0.001 against all groups) and no significant difference between them (p=0.692). Cells overexpressing BMP7 only expressed higher levels of OCN than BMSCs (p<0.023), although significantly less than cells overexpressing Cx43 (p<0.001). Similar trends were observed on the 8th day after differentiation was induced, although OCN expression increased 4-5 times compared to day 2, in cells overexpressing Cx43. At day 16, cells overexpressing both Cx43 and BMP7 produced significantly more OCN mRNA (p<0.001, relative to all other cell groups, including cells overexpressing Cx43 only). This data suggests a synergistic relationship between Cx43 and the stimulus provided by BMP7. Cells overexpressing

the mutant Cx43 Δ 7 produced significantly less OCN expression than all other cells. In fact, Cx43 Δ 7 overexpressing cells failed to produce significant levels of OCN mRNA at any time. Control vectors (LVMT, LVGFP, ADCMVMT, ADCMVMT/LVMT, data not shown), showed no significant difference in mRNA production compared to BMSC expression, suggesting that the transduction through lentivirus and/or adenovirus did not alter the expression or viability of the cells.

Important differences were observed between 2D and 3D cultures in osteocalcin expression (Fig. 3b). First, osteogenic differentiation as indicated by OCN expression was significantly greater in 2D cultures compared to 3D cultures in BMSCs ($p < 0.021$), BMSCs overexpressing BMP7 ($p < 0.001$), and all control empty vectors (data not shown). Levels of OCN mRNA in cells overexpressing Cx43 Δ 7 were not significant in both 2D and 3D culture. However, when cells overexpressed Cx43, there were no significant differences in OCN expression between the two and three-dimensional cultures, supporting the premise that 2D and 3D cultures are intrinsically different, and the results in one culture system do not necessarily translate to the other. Furthermore, our results suggest that cell-to-cell communication may be a main reason for such a difference observed in the two culture systems, and that overexpressing Cx43 can mediate apparent differences in GJIC between the two systems.

Both BMSCs and BMSC-BMP7 express significantly higher levels of OCN in the surface relative to the core of the scaffold (Fig 3c, $p < 0.001$ for both). Furthermore, the effect of BMP7 is significantly neutralized in 3D, showing a 4 fold decrease in OCN expression relative to 2D monolayer and only a moderate increase over the BMSC group in 3D ($p < 0.092$). When Cx43 is overexpressed along with BMP7, the differences

between 2D and 3D are not present. Combining this observation with the results showing that cells overexpressing Cx43 produce similar levels of OCN in surface and core sections of the scaffold strengthen the hypothesis that Cx43 is a potent signaling platform for 3D cultures that can create a spatially uniform distribution of differentiated cells.

4.3.4 Cx43 Gene-Modified Cells Regenerated More Bone In-Vivo

A qualitative comparison between bone formed from transplanted BMSCs (Fig 4 a,b,c) and BMSCs overexpressing Cx43 (Fig 4.d,e,f) shows that overexpressing Cx43 led to more bone formation and an increased cortical thickness. Bone regenerated by BMSCs, BMSCs overexpressing BMP7 and BMSCs overexpressing Cx43 exhibited a cortical-like barrier with enclosed marrow cavity. However, bone formed from Cx43 transduced cells exhibits a thicker cortex and a smaller amount of marrow. Ossicles formed from co-transduced cells produced large amounts of cortical and trabecular-like bone (Fig 4 j,k,l). Bone regenerated from control groups transduced with LVGFP and/or ADCMVMT were similar to those of BMSCs, denoting no significant change due to vector transduction.

The BVF of ossicles produced by transplanted BMSC-Cx43 cells was significantly higher at all time points than ossicles formed from BMSCs (p(4 weeks)<0.021, p(8 weeks)<0.001, p(12 weeks) <0.003). Ossicles formed from cells stimulated by BMP7 produced significantly higher BVF when Cx43 was overexpressed relative to the BMP7 only group (p(4 weeks) <0.033, p(8 weeks)<0.001, p(12 weeks)<0.001). Co-transduced cells led to significantly higher BVF's than all other groups at 8 and 12 weeks (p<0.001 against all groups at both times). Control cell groups generated

volume fractions that were not significantly different from volume fractions generated by BMSCs at any time.

Cortical thickness was significantly greater in ossicles formed from transplanted BMSC-Cx43 cells (Fig. 5b) compared to the BMSCs ($p < 0.001$, for 4, 8, 12 week time points). Similarly, bone regenerated by co-transduced BMSCs produced a thicker cortical-like periphery than ossicles generated by BMP7 ($p < 0.001$, at 4 and 12 weeks). The trabecular-like BVF was significantly higher in ossicles formed with cells co-transduced with Cx43 and BMP7 after 8 and 12 weeks of implantation (Fig. 5c). In the 4 week period, the BMSC-Cx43 group had significantly more trabecular-like bone formation than the BMSC group ($p < 0.001$). These differences were not observed at the 8 week period ($p < 0.56$), but were again evident in the 12 week time point ($p < 0.001$). In cells transduced with BMP7, cells overexpressing Cx43 exhibited significantly more trabecular BVF ($p < 0.001$, at all time points). Furthermore, the effect of the co-transduction in bone in-growth was significantly greater when cells were co-transduced ($p < 0.001$, against all other groups), suggesting a synergistic effect in the development and growth of bone.

4.4 Discussion

Our data demonstrates that Cx43 overexpression can be a platform to enhance cell-to-cell communication throughout 3-dimensional tissue and as a tool to regenerate tissue in-vivo. Specifically, we demonstrated that cells expressing higher levels of Cx43 exhibit higher GJIC, more osteogenic differentiation in-vitro and, when transplanted, form tissue of larger volume and more uniform spatial distribution. Using Cx43 as a signaling platform can have profound effects in both cell-based tissue engineering and

targeted gene therapy. Tissue engineering will benefit from the production of higher volumes of more highly distributed tissue equivalents, while targeted delivery therapy can use Cx43 delivery to enhance GJIC in communication incompetent cells within living 3D tissue. Our studies have significant impact in applied biology and will likely promote further investigation in the regeneration of other 3D tissues.

To achieve higher cell to cell communication, we genetically engineered cells to over-express the gap junction protein Cx43 (Fig 1). Disruption of gap junctions formed by Cx43 in bone forming cells results in compromised osteogenic differentiation and deficiencies in matrix mineralization and bone formation.^{13, 45-48}. However, the role of overexpressing Cx43 in progenitor cells as a strategy to enhance 3-dimensional tissue regeneration has not been examined. In this investigation, we have shown that overexpression of Cx43 and increased gap junction function (Fig 2), leads to higher cell differentiation in-vitro (Fig 3) and more in-vivo bone formation (Fig 4). Also, bone regeneration in the core of the scaffolds was achieved (Fig 5), which suggests a role for enhanced GJIC in the homeostatic environment necessary for full tissue regeneration. These findings suggest that enhanced GJIC enables cues to distribute more effectively and, cells when induced by the environment, can differentiate and produce higher quantities of tissue.

Regeneration of large and uniform volumes of 3D tissue equivalents has been elusive. When seeded into a 3D ECM analogue, cells in the periphery thrive and differentiate, while those in the core of the scaffold are less viable and exhibit compromised differentiation^{30, 31}. This limitation produces incomplete regeneration of tissue, making it less clinically relevant⁴⁹⁻⁵². Therefore, there is a need to generate 3D

in-vitro models for bone engineering, in order to create strategies and study mechanisms that will help regenerate clinically viable tissue equivalents.

To gain insight into the ability of increased GJIC to enhance spatial distribution of differentiation we cultured cells in monolayer (2D) and scaffolds (3D), and assessed differences in GJIC and osteogenic differentiation between 2D and 3D cultures and between the surface and inner regions of 3D cell cultures. Cells overexpressing Cx43 exhibited higher GJIC in 3D culture relative to the 2D monolayer, whereas control cells and cells overexpressing only BMP experienced similar levels of GJIC. Cells overexpressing Cx43 exhibited similar levels of OCN expression (relative to BMSCs) in 2D and 3D cultures. These results contrast the decreased levels of OCN mRNA in BMSCs and BMSCs overexpressing BMP in 3D cultures when compared to a monolayer. Our data points out to the greater importance of GJIC in 3D constructs compared to a 2D monolayer (Fig 3b). Overexpression of Cx43 enables greater GJIC in 3D and has a high impact on the differentiation of cells, suggesting that more gap junction channels are formed when cells are in a 3D setting as the cell-cell surface contacts increase, enabling higher cell-cell communication when sufficient channels are formed. Secondly, the results suggest cell-to-cell communication is an essential component in the observed differences between 2D and 3D settings (Figs 2b, 3b). Inhibited cell-to-cell communication may enable cells to act independently and un-synchronized, which may affect tissue development and homeostasis. Further insights into the impact that GJIC has in 3D cultures is derived when the core sections of 3D cell-scaffold constructs are compared to surface sections (Figs 2c and 3c). Cells that do not overexpress Cx43 exhibit significantly less GJIC and differentiation in the core of the 3D cultures,

contrasting cells overexpressing Cx43, in which there is no significant difference in GJIC and differentiation between the core and surface, suggesting that enhanced GJIC enables a more even distribution of cues and differentiation in 3D.

The in-vitro results clearly demonstrate the effects in osteogenic differentiation as a function of enhanced Cx43 expression. In-vivo, tissue regenerated by cells overexpressing Cx43 had a larger quantity of bone in-growth relative to control groups (Fig 4 a-l). The larger production of trabecular-like bone ingrowth, characterized by regeneration of bone in the core of the ossicle, and a thicker cortex suggest that when differentiation and bone formation are occurring, the higher level of cell-to-cell communication enables cells to act in a synchronized manner, thereby allowing full development of tissue throughout the scaffold. The significant increases in total bone volume fraction and distribution of tissue in bone formed from cells overexpressing Cx43 relative to that formed from BMSCs suggest that Cx43 can be a powerful tool to regenerate 3D tissue in-vivo.

GJIC also enables the distribution of signals ignited by a secondary stimulus, whether electrical, mechanical or biological in nature, between neighboring cells¹⁴. To test the effect of higher GJIC in tandem with another stimulus, cells were induced to overexpress bone morphogenetic protein 7 (BMP7). This growth factor was chosen because it has potent osteoinductive effects but does not modulate the expression of Connexin 43⁴⁰. Our results showed that enhanced GJIC increased the effect of BMP7, suggesting that the overexpression of Connexin 43 synergistically enhances the effects of other stimuli, by enhancing the distributed differentiation potential of cells throughout a 3D culture (Fig 3) and volume fraction of regenerated bone (Figs 4,5) over cells

overexpressing BMP7 alone. The experiments with BMP7 are an example of a platform that could potentially be extended to other tissues by using connexin 43 with other growth factors or stimuli that enhance the regeneration of a particular tissue of interest.

Combined, our findings suggest that increasing gap junction intercellular communication via overexpression of connexin 43 can be, on its own, a powerful tool to overcome limitations inherent in cell-to-cell communication and regeneration of tissue in 3D, and can complement the effect of another agent or stimulus; leading to regeneration of larger volumes and more uniform tissue. Our strategy may be broadly applied to a wide range of cells and 3-dimensional tissues with the aim to enhance cell-cell communication enabling normal development and homeostasis. This concept can also be applied in future therapies to combat many types of cancer ⁹. As a preventive measure for malignant cancerous tumors, Cx43 gene delivery can be targeted on cancerous and pre-cancerous cells, which are characterized for becoming GJIC deficient. Ultimately, our approach may be a fundamental component overcoming the longstanding problem of inducing synchronized cell behavior in 3D cultures of cells or tissues and developing clinically meaningful tissue engineered equivalents.

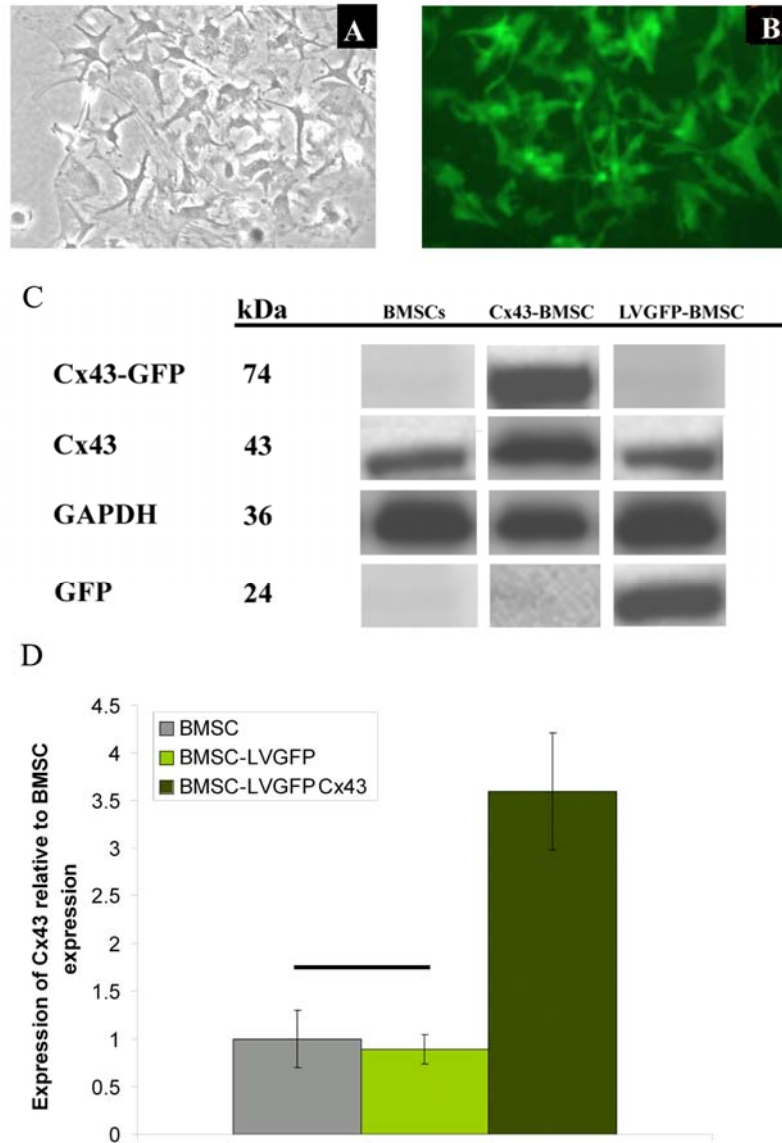


Figure 4-1 BMSCs are highly transduced with Cx43-GFP

Expression of the Cx43-GFP gene in transduced BMSCs was observed under a phase contrast (a) and fluorescent microscope for GFP expression (b). The expression of Cx43-GFP, Cx43, GAPDH and GFP was also measured using western blot analysis (c), Quantification of the band intensities showed a significant increase ($3.74 \pm .49$, $p < 0.001$, d) in overall Cx43 expression in cells that were transduced (d).

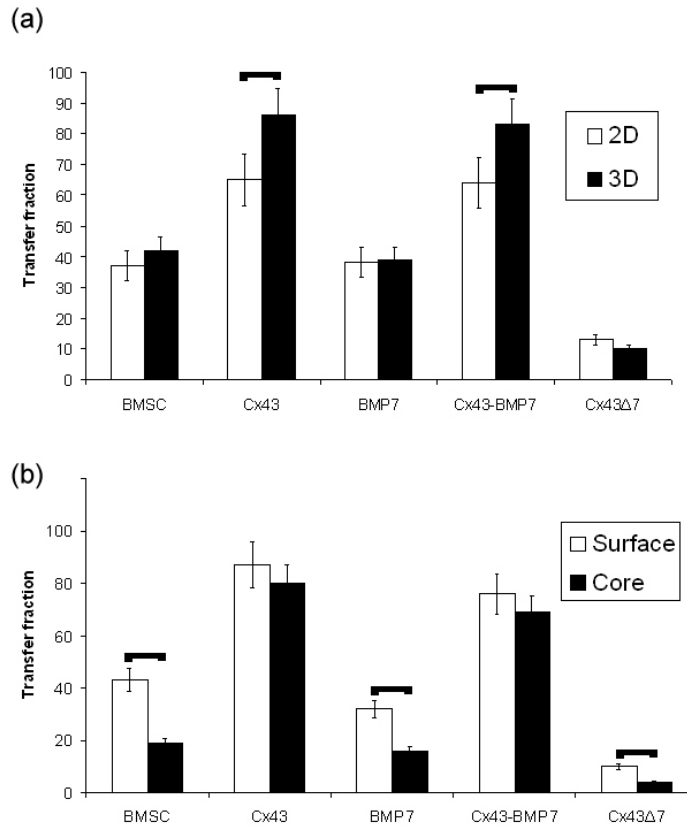


Figure 4-2 GJIC in BMSCs, as measured by Calcein-AM transfer is enhanced with Cx43 overexpression:

The transfer fraction was measured for groups cultured in 2D monolayer and 3D cultures (a). Cells overexpressing Cx43 (Cx43 and Cx43 BMP7) had a significantly higher transfer fraction than the control groups (BMSC, BMP7; $p < 0.001$), and the negative control group (Cx43Δ7; $p < 0.001$). Transfer was enhanced in 3D when cells were overexpressing Cx43, relative to 2D culture. Groups that did not overexpress Cx43 showed significant decreases in dye transfer from the top surface of the construct, to the core section, whereas no significant difference was evident in groups overexpressing Cx43 (b). Horizontal bars represents pairs that are significantly different ($p < 0.005$).

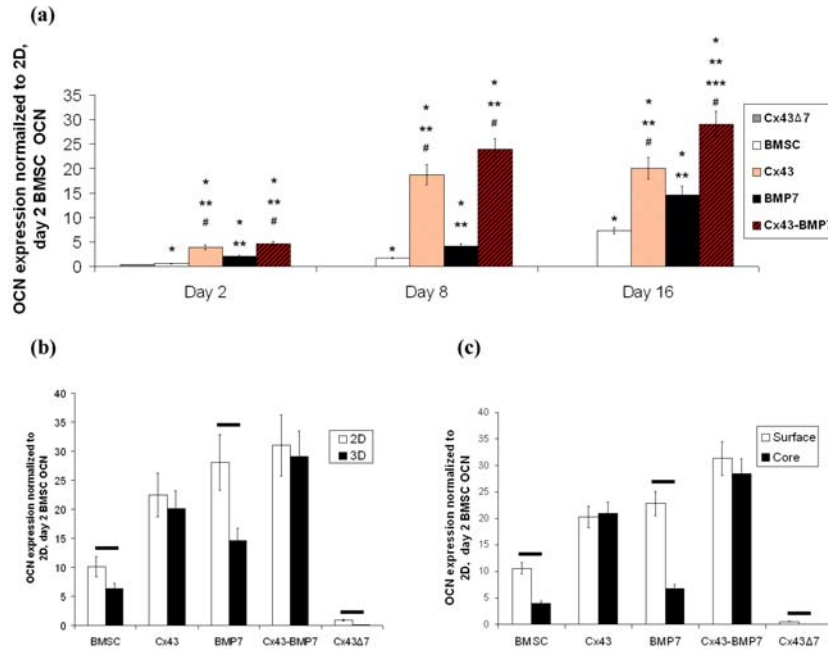


Figure 4-3 Cx43 overexpression is associated with higher levels of OCN mRNA expression at all times

Overexpression of Cx43 had significant effects on OCN expression, when comparing a 2D monolayer to a 3D cell culture (b). The normalized values of OCN mRNA were significantly higher in two dimensions, for cells that did not overexpress Cx43, while cells that overexpressed Cx43 exhibited no significant difference between 2D and 3D cultures. This result suggests that 2D cell culture models may not translate to 3D culture, and that Cx43 overexpression may be a tool to mediate those differences. Surface vs. core studies (c) support this conclusion, suggesting that cell-to-cell communication in the core regions can be enhanced. Cx43 overexpression produces evenly distributed differentiation throughout the 3D culture, providing a tool to regenerate larger and uniformly distributed tissue equivalents. Significant increases are indicated by * = Cx43Δ7, ** = BMSC, *** = Cx43, # = BMP7. Horizontal bars indicate pairs that are significantly different.

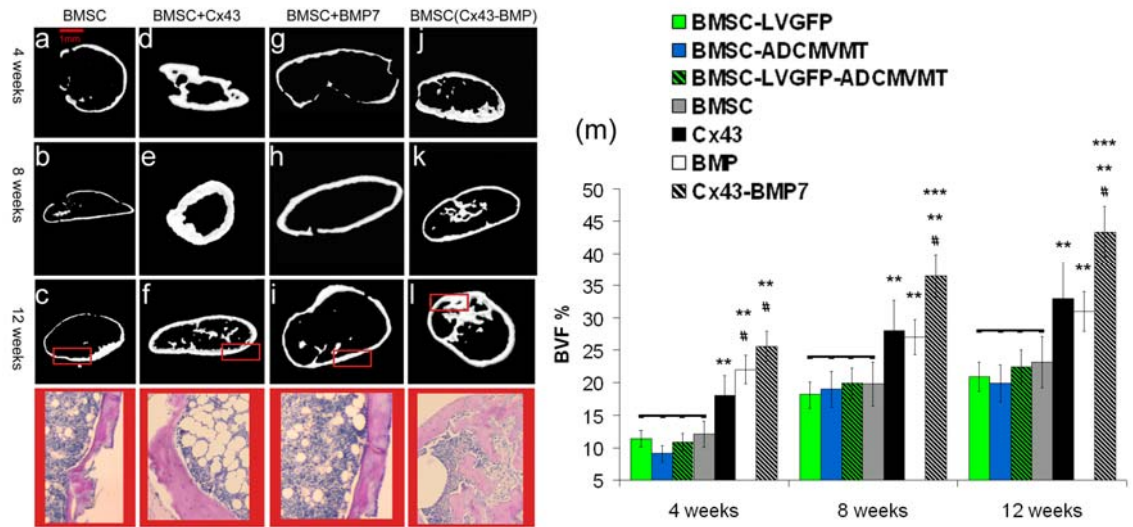


Figure 4-4 Micro CT renderings and histological sections of ossicles regenerated following subcutaneous transplantation of BMSCs.

The micro CT renderings exhibited differences in patterns of bone produced from BMSCs and BMSCs transduced to overexpress Cx43 (a-l). BVF is quantified to assess for these differences (m). Cells overexpressing Cx43 (d-f) regenerate larger volumes of tissue compared to BMSCs. Bone regenerated by BMSCs (a-c) is characterized by a thin periphery of bone tissue. When Cx43 is overexpressed (d-f), ossicles have both thicker peripheral bone formation and more bone regeneration in the core of the 3D construct. Ossicles generated from BMP7 transduced cells (g-i) are characterized by a thin cortex (although larger than BMSCs), while tissue regenerated with co-transduced cells (j-k) exhibits large amounts of bone in-growth and overall bone regeneration. Histological sections validate the CT renderings. The volume fractions (m) reflect a significant increase in bone regeneration in all transduced groups over BMSCs. Tissue regenerated by cells overexpressing Cx43 has significantly higher BVF than the ossicles regenerated from BMSCs at 4, 8 and 12 weeks ($p(4 \text{ weeks}) < 0.032$, $p(8 \text{ weeks}) < 0.001$, $p(12$

weeks) <0.003). When cells were stimulated with BMP7, the co-transduced group produced a significantly higher BVF, relative to the BMP7 transduced group ($p<0.001$ in both 8 and 12 week periods). Finally, co-transduced groups produced significantly higher BVF than any other group in the 8 and 12 week period, suggesting a synergistic relation between Cx43 and BMP7. Significant increases are indicated by ** = BMSC, *** =Cx43, # =BMP7. Horizontal bars represent groups that are not significantly different (control groups and BMSCs).

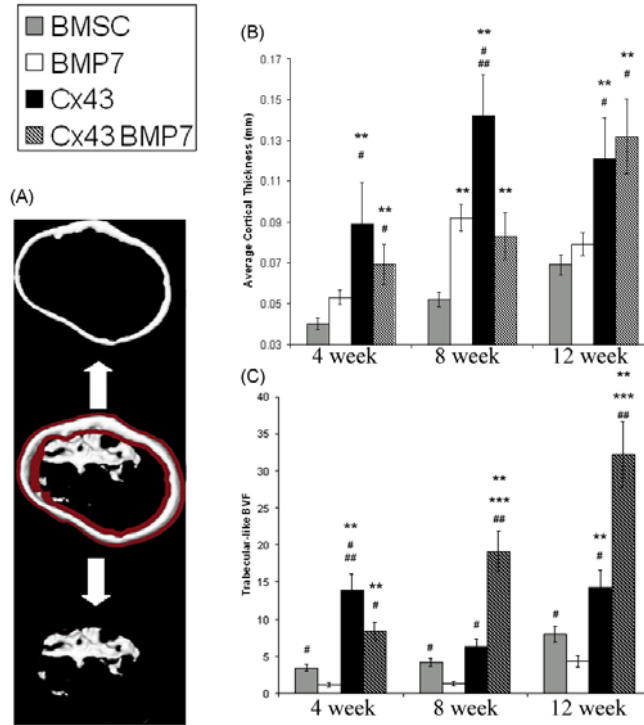


Figure 4-5 Cortical-like thickness and trabecular-like bone volume fraction of tissue engineered bone.

CT data files were analyzed using a custom topological MatLab program that quantifies both the average cortical thickness and trabecular-like BVF (a). Cx43 transduced cells produced an average cortical thickness that was significantly greater ($p < 0.001$, for all time points) than the cortical thickness of bone produced by BMSCs (b). The trabecular-like bone volume fraction (c) was significantly greater in bone regenerated from cells containing Cx43 as well when compared to BMSCs ($p(4 \text{ weeks}) < 0.001$, $p(12 \text{ weeks}) < 0.001$). Co-transduced cells had significantly larger fraction of trabecular-like bone at the 8th ($p < 0.001$) and 12th ($p < 0.001$) week than all groups. Significant increases are indicated by ** = BMSC, *** = Cx43, # = BMP7, ## = Cx43-BMP7.

4.5 References

1. Goldmann WH. Mechanical aspects of cell shape regulation and signaling. *Cell Biol Int.* 2002; 26(4):313-317.
2. Jorgensen NR, Teilmann SC, Henriksen Z, Civitelli R, Sorensen OH, Steinberg TH. Activation of L-type calcium channels is required for gap junction-mediated intercellular calcium signaling in osteoblastic cells. *J Biol Chem.* 2003; 278(6):4082-4086.
3. Cotrina ML, Lin JH, Alves-Rodrigues A, et al. Connexins regulate calcium signaling by controlling ATP release. *Proc Natl Acad Sci U S A.* 1998; 95(26):15735-15740.
4. Jongsma HJ, Wilders R. Gap junctions in cardiovascular disease. *Circ Res.* 2000; 86(12):1193-1197.
5. Flenniken AM, Osborne LR, Anderson N, et al. A *Gja1* missense mutation in a mouse model of oculodentodigital dysplasia. *Development.* 2005; 132(19):4375-4386.
6. Kizana E, Ginn SL, Smyth CM, et al. Fibroblasts modulate cardiomyocyte excitability: Implications for cardiac gene therapy. *Gene Ther.* 2006; 13(22):1611-1615.
7. Boengler K, Heusch G, Schulz R. Connexin 43 and ischemic preconditioning: Effects of age and disease. *Exp Gerontol.* 2006; 41(5):485-488.

8. Paznekas WA, Boyadjiev SA, Shapiro RE, et al. Connexin 43 (GJA1) mutations cause the pleiotropic phenotype of oculodentodigital dysplasia. *Am J Hum Genet.* 2003; 72(2):408-418.
9. King TJ, Bertram JS. Connexins as targets for cancer chemoprevention and chemotherapy. *Biochim Biophys Acta.* 2005; 1719(1-2):146-160.
10. Zhu D, Caveney S, Kidder GM, Naus CC. Transfection of C6 glioma cells with connexin 43 cDNA: Analysis of expression, intercellular coupling, and cell proliferation. *Proc Natl Acad Sci U S A.* 1991; 88(5):1883-1887.
11. Saez JC, Berthoud VM, Branes MC, Martinez AD, Beyer EC. Plasma membrane channels formed by connexins: Their regulation and functions. *Physiol Rev.* 2003; 83(4):1359-1400.
12. Willecke K, Eiberger J, Degen J, et al. Structural and functional diversity of connexin genes in the mouse and human genome. *Biol Chem.* 2002; 383(5):725-737.
13. Li Z, Zhou Z, Saunders MM, Donahue HJ. Modulation of connexin43 alters expression of osteoblastic differentiation markers. *Am J Physiol Cell Physiol.* 2006; 290(4):C1248-55.
14. Stains JP, Lecanda F, Screen J, Towler DA, Civitelli R. Gap junctional communication modulates gene transcription by altering the recruitment of Sp1 and Sp3 to connexin-response elements in osteoblast promoters. *J Biol Chem.* 2003; 278(27):24377-24387.

15. Furlan F, Lecanda F, Screen J, Civitelli R. Proliferation, differentiation and apoptosis in connexin43-null osteoblasts. *Cell Commun Adhes.* 2001; 8(4-6):367-371.
16. Schiller PC, Roos BA, Howard GA. Parathyroid hormone up-regulation of connexin 43 gene expression in osteoblasts depends on cell phenotype. *J Bone Miner Res.* 1997; 12(12):2005-2013.
17. Zhang W, Green C, Stott NS. Bone morphogenetic protein-2 modulation of chondrogenic differentiation in vitro involves gap junction-mediated intercellular communication. *J Cell Physiol.* 2002; 193(2):233-243.
18. Wyatt LE, Chung CY, Carlsen B, et al. Bone morphogenetic protein-2 (BMP-2) and transforming growth factor-beta1 (TGF-beta1) alter connexin 43 phosphorylation in MC3T3-E1 cells. *BMC Cell Biol.* 2001; 2:14.
19. Stains JP, Civitelli R. Cell-cell interactions in regulating osteogenesis and osteoblast function. *Birth Defects Res C Embryo Today.* 2005; 75(1):72-80.
20. Civitelli R, Ziambaras K, Warlow PM, et al. Regulation of connexin43 expression and function by prostaglandin E2 (PGE2) and parathyroid hormone (PTH) in osteoblastic cells. *J Cell Biochem.* 1998; 68(1):8-21.
21. Pettway GJ, Schneider A, Koh AJ, et al. Anabolic actions of PTH (1-34): Use of a novel tissue engineering model to investigate temporal effects on bone. *Bone.* 2005; 36(6):959-970.

22. Schneider A, Taboas JM, McCauley LK, Krebsbach PH. Skeletal homeostasis in tissue-engineered bone. *J Orthop Res.* 2003; 21(5):859-864.
23. Carter PH, Schipani E. The roles of parathyroid hormone and calcitonin in bone remodeling: Prospects for novel therapeutics. *Endocr Metab Immune Disord Drug Targets.* 2006; 6(1):59-76.
24. Li YJ, Batra NN, You L, et al. Oscillatory fluid flow affects human marrow stromal cell proliferation and differentiation. *J Orthop Res.* 2004; 22(6):1283-1289.
25. Franceschi RT, Xiao G. Regulation of the osteoblast-specific transcription factor, Runx2: Responsiveness to multiple signal transduction pathways. *J Cell Biochem.* 2003; 88(3):446-454.
26. Schwiebert EM. Extracellular ATP-mediated propagation of Ca^{2+} waves. focus on "mechanical strain-induced Ca^{2+} waves are propagated via ATP release and purinergic receptor activation". *Am J Physiol Cell Physiol.* 2000; 279(2):C281-3.
27. Franceschi RT, Wang D, Krebsbach PH, Rutherford RB. Gene therapy for bone formation: In vitro and in vivo osteogenic activity of an adenovirus expressing BMP7. *J Cell Biochem.* 2000; 78(3):476-486.
28. Franceschi RT, Yang S, Rutherford RB, Krebsbach PH, Zhao M, Wang D. Gene therapy approaches for bone regeneration. *Cells Tissues Organs.* 2004; 176(1-3):95-108.

29. Krebsbach PH, Gu K, Franceschi RT, Rutherford RB. Gene therapy-directed osteogenesis: BMP-7-transduced human fibroblasts form bone in vivo. *Hum Gene Ther.* 2000; 11(8):1201-1210.
30. Rutherford RB, Moalli M, Franceschi RT, Wang D, Gu K, Krebsbach PH. Bone morphogenetic protein-transduced human fibroblasts convert to osteoblasts and form bone in vivo. *Tissue Eng.* 2002; 8(3):441-452.
31. Chatterjee B, Meyer RA, Loreda GA, Coleman CM, Tuan R, Lo CW. BMP regulation of the mouse connexin43 promoter in osteoblastic cells and embryos. *Cell Commun Adhes.* 2003; 10(1):37-50.
32. Griffith LG, Swartz MA. Capturing complex 3D tissue physiology in vitro. *Nat Rev Mol Cell Biol.* 2006; 7(3):211-224.
33. Huang R, Lin Y, Wang CC, et al. Connexin 43 suppresses human glioblastoma cell growth by down-regulation of monocyte chemotactic protein 1, as discovered using protein array technology. *Cancer Res.* 2002; 62(10):2806-2812.
34. Lai A, Le DN, Paznekas WA, Gifford WD, Jabs EW, Charles AC. Oculodentodigital dysplasia connexin43 mutations result in non-functional connexin hemichannels and gap junctions in C6 glioma cells. *J Cell Sci.* 2006; 119(Pt 3):532-541.
35. Holy CE, Shoichet MS, Davies JE. Engineering three-dimensional bone tissue in vitro using biodegradable scaffolds: Investigating initial cell-seeding density and culture period. *J Biomed Mater Res.* 2000; 51(3):376-382.

36. Ishaug SL, Crane GM, Miller MJ, Yasko AW, Yaszemski MJ, Mikos AG. Bone formation by three-dimensional stromal osteoblast culture in biodegradable polymer scaffolds. *J Biomed Mater Res.* 1997; 36(1):17-28.
37. Dorshkind K, Green L, Godwin A, Fletcher WH. Connexin-43-type gap junctions mediate communication between bone marrow stromal cells. *Blood.* 1993; 82(1):38-45.
38. Montecino-Rodriguez E, Leathers H, Dorshkind K. Expression of connexin 43 (Cx43) is critical for normal hematopoiesis. *Blood.* 2000; 96(3):917-924.
39. Krebsbach PH, Kuznetsov SA, Bianco P, Robey PG. Bone marrow stromal cells: Characterization and clinical application. *Crit Rev Oral Biol Med.* 1999; 10(2):165-181.
40. Rutherford RB, Nussenbaum B, Krebsbach PH. Bone morphogenetic protein 7 ex vivo gene therapy. *Drug News Perspect.* 2003; 16(1):5-10.
41. Dull T, Zufferey R, Kelly M, et al. A third-generation lentivirus vector with a conditional packaging system. *J Virol.* 1998; 72(11):8463-8471.
42. Leonova EV, Pennington KE, Krebsbach PH, Kohn DH. Substrate mineralization stimulates focal adhesion contact redistribution and cell motility of bone marrow stromal cells. *J Biomed Mater Res A.* 2006; 79(2):263-270.

43. Feldkamp LA, Goldstein SA, Parfitt AM, Jesion G, Kleerekoper M. The direct examination of three-dimensional bone architecture in vitro by computed tomography. *J Bone Miner Res.* 1989; 4(1):3-11.
44. Wallace JM, Rajachar RM, Chen XD, et al. The mechanical phenotype of biglycan-deficient mice is bone- and gender-specific. *Bone.* 2006; 39(1):106-116.
45. Lecanda F, Warlow PM, Sheikh S, Furlan F, Steinberg TH, Civitelli R. Connexin43 deficiency causes delayed ossification, craniofacial abnormalities, and osteoblast dysfunction. *J Cell Biol.* 2000; 151(4):931-944.
46. Lecanda F, Towler DA, Ziambaras K, et al. Gap junctional communication modulates gene expression in osteoblastic cells. *Mol Biol Cell.* 1998; 9(8):2249-2258.
47. Stains JP, Civitelli R. Gap junctions in skeletal development and function. *Biochim Biophys Acta.* 2005; 1719(1-2):69-81.
48. Stains JP, Civitelli R. Cell-to-cell interactions in bone. *Biochem Biophys Res Commun.* 2005; 328(3):721-727.
49. Amiel C, Bailly C, Friedlander G. Multiple hormonal control of the thick ascending limb functions. *Adv Nephrol Necker Hosp.* 1987; 16:125-136.
50. Beaman FD, Bancroft LW, Peterson JJ, Kransdorf MJ. Bone graft materials and synthetic substitutes. *Radiol Clin North Am.* 2006; 44(3):451-461.
51. Langer R, Vacanti JP. Tissue engineering. *Science.* 1993; 260(5110):920-926.

52. Valimaki VV, Aro HT. Molecular basis for action of bioactive glasses as bone graft substitute. *Scand J Surg.* 2006; 95(2):95-102.

Chapter 5

Conclusions

5.1 General Conclusions

Our experiments examined strategies to enhance the regeneration of bone, both exogenously (cell seeding and biomimetic scaffolds) and by endogenously overexpressing factors in BMSCs that would enhance bone formation (Cx43). Specifically addressed in this thesis is the role of enhanced cell-cell communication, in the form of gap junction intercellular communication (GIJC), as a tool for bone regeneration. Our results demonstrated significant increases in tissue regeneration, using both endogenous and exogenous strategies, which may have a powerful impact in the clinical setting.

As part of the experiments performed, we first validated a threshold range to utilize for analysis of tissue engineered bone ossicles (Chapter 2). Our threshold range was rigorously determined using imaging and ashing techniques to quantify tissue engineered bone in (a) Hounsfield Units (HU), (b) % of bone HU, and (c) Bone Mineral Density (mg/cc) (1000-1300, 24.2-31.5%, 25966.6- 33799.5 mg/cc, respectively). This threshold should provide some standardization and consistency for characterization of

tissue engineered bone. These threshold values were used as a guideline to compare tissue engineered bone throughout the experiments performed in this thesis.

First we addressed the question of altered initial conditions, in the form of cell seeding and surface chemistry, to increase the amount of tissue engineered bone (Chapter 3). The alternative seeding strategies developed here (filtration and micromass seeding) aimed to overcome the limitations observed with the commonly used static seeding techniques in tissue engineering. Cell density, cell-substrate adhesion and, cell-cell communication were assessed, although other factors, such as nutrient and byproduct flux, cell-cell adhesion, mechanical loading, and migration, were considered in the design of these strategies. Micromass and filtration seeding led to significant increases in GJC, osteogenic differentiation, and amount and spatial distribution of regenerated bone in-vivo. The outcomes attained by altering initial cell seeding conditions are powerful in the clinical context; namely, by altering cells initial positioning, cell-to-cell communication, and density in 3D scaffolds, higher amounts of tissue can be regenerated. Clinically, the micromass principle may have a more powerful impact in larger defects, using larger scaffolds, as different arrays of micromasses can be created with the aim to regenerate full tissue equivalents. Because the micromass is a localized strategy of highly dense clusters of cells, these can be strategically placed within the scaffold to maximize cell viability, nutrient flux, and tissue regeneration. With the aid of both mathematical modeling and experimental data, the location and size of the micromasses can be arranged to optimize outcomes in-vitro and in-vivo. Furthermore, it is likely that the optimal array of micromasses would vary as a function of scaffold geometry,

environment, cell type, and tissue. The resulting models would provide an element of flexibility that optimizes tissue regeneration under different circumstances.

Both filtration and micromass strategies are simple and inexpensive alternatives to other strategies aimed to enhance tissue formation, such as addition of inductive agents and genetic engineering. Based on the simplicity of these techniques, they should be implemented over the traditionally employed static seeding modality.

Template chemistry was also assessed as an initial and time dependant exogenous strategy to regenerate tissue. Specifically for bone, we demonstrated that a biomimetic scaffold, rich in calcium/phosphate, serves as a better template than an organic template to enhance osteogenic differentiation in-vitro and regenerate higher volumes of tissue engineered bone. However, our data shows that mineralization of the substrate does not enhance overall cell adhesion, and GJIC as hypothesized. Two main factors may have influenced these results. First, although mineralization was achieved using the simulated body fluid (SBF) procedure (Chapter 3), complete scaffold mineralization was not attained. Therefore, the current mineralization procedure may have not been optimal. Because of the low percentage of mineral, the seeding effect was the dominant factor in adhesion. This is evident in the static seeding technique, where mineralized templates exhibited significantly higher adhesion than the PLGA substrate. Thus, the mineral did have a significant effect in cell adhesion, when the novel techniques were not employed, indicating that more mineral may enhance adhesion. Efforts should be made to design a mineralization technique, perhaps through perfusion or filtration that will enable the scaffolds to mineralize at higher percentages.

A second reason for the observed effects is the time dependent release of ions from the substrate to the solution. The release of ions, such as calcium and phosphate, may have an impact on differentiation and regeneration of tissue, but may not have a significant impact in cell adhesion. Although one would expect that a higher concentration of secondary messengers, such as Ca^{++} , would lead to higher GJIC, our experiments were carried out at early times, where the dissolution effects of the substrate may have been negligible. Experiments (Shin et al) have shown that dissolution of mineral in scaffolds occurs at later times. Future experiments should examine GJIC at different times, including those in which the mineralized scaffolds show higher dissolution rates.

As an endogenous strategy, we enhanced osteogenic differentiation and in-vivo bone formation to by genetically altering BMSCs to overexpress the gap junction forming protein, Cx43. Such overexpression enhanced cell-to-cell communication, as measured by calcein-AM transfer, in a 2-dimensional monolayer and 3D cell cultures. Therefore, transduction via a lentivirus containing the Cx43 gene is an effective way to enhance communication in GJIC in areas of limited cell-to-cell communication. Coupled with the inability to communicate when BMSCs overexpressed a mutant Cx43 gene that inhibits GJIC, our results indicate that GJIC is an important and essential component to tissue regeneration, and can be augmented artificially to enhance such communication.

Because GJIC mediated by Cx43 allows the transfer of molecules as large as 1KD in size, these conduits are the main modes for transfer of ions, metabolites and, secondary messengers that affect signaling and prompt signaling cascades. As an example, osteocalcin transcription is prompted by the passage of secondary messengers through

gap junctions that enable phosphorylation of the Sp1 transcription factor. When GJIC is high, phosphorylation of Sp1 is significantly greater than when cells exhibit low GJIC. Many of these messengers are a function of the local external environment in which the cells are present. For tissue engineering purposes, this is an important component, as the local environments of cells in the periphery (exposed to nutrients) and those entrapped in the core of the constructs may be significantly different. Enabling higher cell-to-cell communication may help transfer important secondary messengers in bone formation, such as calcium, ATP and inositol triphosphate. Such communication may overcome the limitations exhibited by some cells in less than optimal environments, to differentiate and regenerate tissue.

As a tissue engineering strategy, enhanced GJIC can also be used in tandem with another agent, such as BMP 7, to increase the overall effect of the agent and enhance tissue formation and uniformity of distribution. When BMP 7 binds to type I receptors in the cell membrane, it enables a cascade of secondary messengers to be released inside the cell. These messengers trigger transcription of proteins that induce differentiation and can be transferred to neighboring cells through the conduits formed by the docking of Cx43 enabled gap junctions. Augmenting the communication enables the secondary messengers to reach cells that may have not been exposed to the stimuli. This dynamic allows transcription mechanisms to develop in cells that prompt differentiation, which leads to tissue formation. Therefore, BMP 7 and gap junctions generated by Cx43 work synergistically when BMP 7 prompts secondary messengers, such as calcium and other transcription factors, that can be distributed through gap junctions.

The overexpression of Cx43 (with or without BMP 7) also enhanced the distribution of regenerated tissue, suggesting that cell-to-cell communication is important for effective tissue regeneration in the core of 3D bone ossicles. Our in-vitro data comparing the osteogenic differentiation of cells in the surface and core regions of a 3D construct supports this conclusion; when Cx43 was overexpressed, cell communication and osteogenic differentiation were enhanced in the core regions, relative to BMSC control groups. Furthermore, we showed that GJIC plays a greater role in 3D compared to a 2D monolayer. Communication between BMSCs is limited to a greater extent in 3D cultures. However, when BMSCs overexpress Cx43 both 3D and 2D cultures have similar transfer efficiencies. Because homeostasis is such an important component of tissue formation, we speculate that enhancing GJIC enables the population of cells seeded in the 3D construct to have a higher level of coordination, enabling more spatially distributed tissue regeneration. Because of the ubiquitous nature of Cx43, our strategy could be applied to different tissues, with the aim of solidifying such overexpression as a powerful mechanism to enable higher cell-to-cell communication during differentiation and tissue formation. Also, these findings are not limited to tissue engineering, as they can also be applied to targeted gene therapy, such as cancer therapy, and development of 3D culture model systems that are highly coordinated.

The findings from this thesis propose important and novel strategies for the regeneration of 3D tissue engineered bone that can have an immediate impact in the clinical setting. We have presented three exogenous strategies (micromass seeding, filtration seeding, mineralized template) and an endogenous one (overexpression of Cx43) that significantly enhance cell differentiation and bone regeneration. In both

exogenous and endogenous strategies, it was shown that increased GJIC enhanced differentiation, bone regeneration, and distribution throughout the engineered tissue.

5.2 Future work

In addition to the combination of endogenous and exogenous strategies to regenerate larger volumes of tissue, two main directions should follow the results presented in this thesis. First, it is important to examine the effects of other exogenous parameters, such as nutrient flux and migration, in tissue regeneration. These parameters were taken into consideration when designing the seeding strategies and their specific and isolated roles in bone formation should be understood. Secondly, investigate both the mechanistic aspect of GJIC and the potential applications that expand outside the realm of tissue engineering, such as targeted delivery and cancer therapy.

Micromass and filtration seeding were proposed (Chapter 2) because the potential to take advantage of several factors believed to play a role in tissue formation. Of these factors, the effects of osteogenic differentiation and bone formation due to migration and effect of nutrient flux should be examined next. The ability for nutrients to flow in and byproducts out may be a dominant factor with respect to cell viability while cell migration may dictate osteogenic patterns and distribution of bone.

Migration may play an important role by setting a gradient of differentiation that is that enables differentiation to occur at different locations and times. Micromass seeding was aimed to produce such a gradient of differentiation as cells were seeded in the core of the scaffolds, where they were presumed to migrate outward. Time dependent and distribution studies need to be performed to examine (1) differentiation and (2) cell

motility in the scaffold. To control motility, the scaffold pore sizes may be altered. The framework of the 3D experiments (Chapter 4, 5) may work to analyze the effect of motility and differentiation.

Micromass seeding was also designed with the aim to permit more nutrient and byproduct flux for the cells seeded in the scaffold. An apparatus was designed and built (Appendix 1) that controls several parameters, including flux and gas exchange, for in-vitro experimentation of 3D tissue engineered structures. By quantifying the concentration of oxygen, and the distribution of such concentration throughout a 3D structure, the alternative seeding techniques (filtration and micromass) can be compared.

Although high flux in-vitro systems have been studied extensively (Chapter 4), studying the effects of increased nutrient flux in-vivo has been elusive, particularly because of the difficulties present with interfacing a flux generating system, that creates such flux in-vivo. Using advances in micro-fluidics, a system can be designed and built to create a nutrient flux that is exogenous to the animal model. The proposed system would incorporate small, degradable channels that pass through the 3D scaffolds. Once transplanted, a small outlet would be set outside the body, to allow continuous or non-continuous flow to enter via a pump or injection. The micro-fluidic tubes would be permeable to the nutrients as to allow for delivery throughout the construct in-vivo. To test the validity of this system, in-vitro studies would be necessary, to assess nutrient delivery to all regions, and in-vitro osteogenic differentiation. As nutrient flux is a generally favorable condition for all tissues, such an approach can yield positive results through out the tissue engineering realm.

GJIC is a highly studied phenomenon that plays a role in most tissues and may have far-reaching implications in fields other than tissue engineering, such as cancer prevention, cancer treatment, targeted delivery to communication incompetent cells, and as a main component to induce homeostasis. Therefore, mechanistic studies to understand the roles of GJIC in various aspects of biology are necessary. In bone, studies have shown that the lack of GJIC in cells inhibits the phosphorylation of Sp1 transcription factor, which promotes the transcription of osteocalcin. The effects of such phosphorylation on cells with higher GJIC need to be elucidated. Also, based on the results presented in this thesis (Chapter 4, 5), higher GJIC enhances ALP. Thus the mechanistic role of GJIC in the transcription of ALP, and other bone differentiation indicators, need to be studied.

Also, mechanistic studies need to be performed to understand the potential feedback/control mechanism of Cx43 to control the regeneration of tissue. One proposal to ignite this process may be to label the cells seeded in the constructs with green fluorescent protein (GFP) to observe what their fate is. This way, the interference of outside cells may be quantified by determining what cells are embedded in mineral.

The studies with connexin 43 can be extended to targeted delivery therapy with important implications. The loss of gap junction mediated cell to cell communication not only leads to compromised development in many tissues and organs, but also facilitates tumorigenesis and autonomous cell behavior in cancerous cells. Enabling delivery of connexin 43 to cancerous cells may help eliminate the autonomous behavior that characterizes them, which is caused by a lack of intercellular communication. Furthermore, low GJIC is an early sign of potentially cancerous cells. Based on this data,

a novel assay based on Cx43 expression could be generated to provide patients with high cancer susceptibility an opportunity to detect a problematic site, and treat it at the early stages.

Although transduction with a lentivirus provided to be an effective means of enhancing GJIC, identification, examination and production of a pharmacological agent that enhances the expression of Cx43 in cells may yield a powerful tool to tackle health related problems that are caused by compromised cell-to-cell communication. Of the potential health hazards that are may be caused by low GJIC, two are at the top of the list of illnesses that claim lives in the United States; namely, heart disease and cancer. As with any drug, the specificity, safety and, efficacy would have to be assessed in animal models and human trails, before it is employed.

Combined with the work performed in this thesis, experiments elucidating the mechanistic role, pharmacological intervention, and eventual application of connexin 43 to human stem cells will strengthen the understanding and application of GJIC in tissue engineering and may serve as a future strategy for targeted cancer therapy.

Appendices

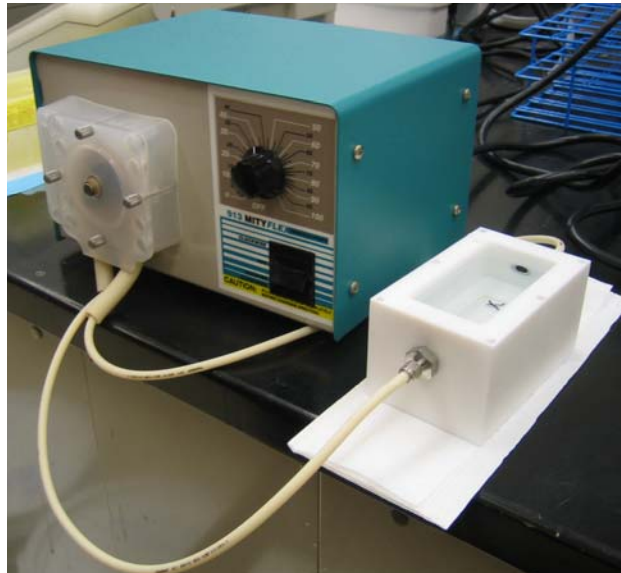
A1. FlowCulture Perfusion System Design and Specifications



PerfuSys

FloCulture Perfusion System

User Manual



By: Ricardo Rossello and 450 Group

INTRODUCTION




The PerfuSys FloCulture Perfusion System is a perfusion system specially designed for bone cell cultures. The perfusion system consists of a chamber, pump, and tubing and is designed to provide a laminar flow of media across a cell plate at different, user controlled flow rates. To ensure laminar flow, low flow rates must be used. Media circulates through perfusion system continuously to facilitate transport of nutrients and waste without the need to constantly change the media. Once the perfusion system is set up and turned on, it can run continuously for up to 24 hours.

The PerfuSys FloCulture Perfusion System is an excellent tool for users who want to test cell growth and survival under different test conditions, while being confident that all other variables remain constant. The perfusion system is easy to operate, and it provides reliable results.

.

NOTES ON SAFETY

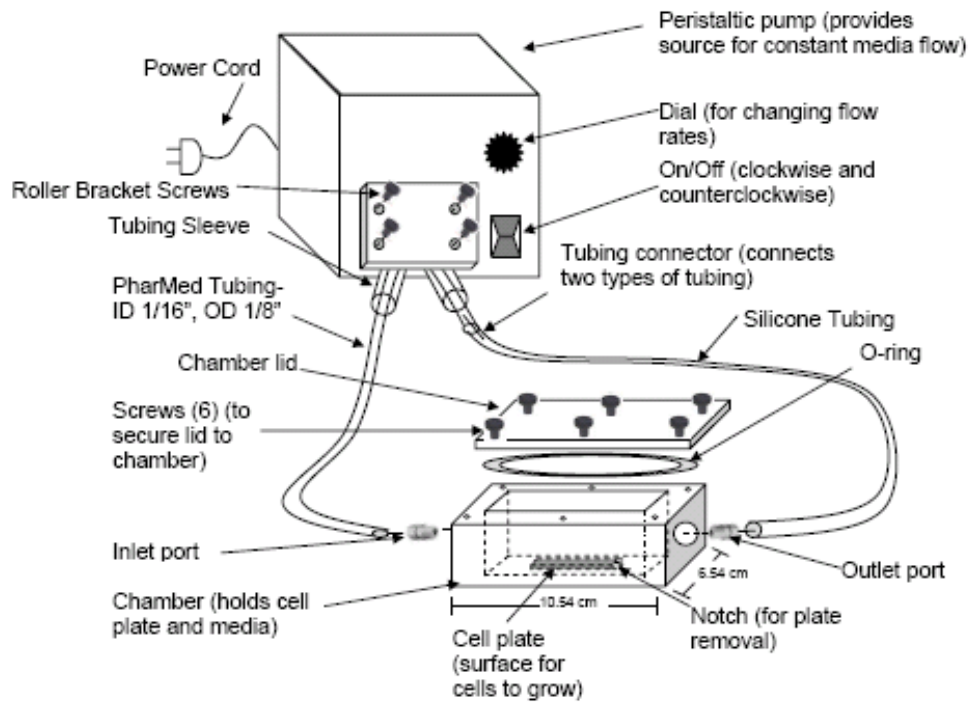
The warning signs and icons shown and explained on this page are intended to assist you in using the product correctly and safely to prevent harm to you, others, and the system.

- The  icon indicates something that is mandatory.
- The  caution icon indicates matters in which bodily harm or material damage to the product or local environment could occur as a result of incorrect handling.
- The  icon indicates extra information.

CAUTION:

- AVOID DIRECT CONTACT WITH THE CELLS AND MEDIA. Cells can carry diseases that are harmful to humans.
- Dispose of materials correctly and sterilize equipment thoroughly between each experiment to prevent the spread of disease.
- Use materials that are biocompatible and non-toxic when replacing parts that come in contact with the cells or media.
- Follow sterilization protocols in this user manual
- Avoid electrocution when dealing with pump plug and electrical socket.

Figure 1. LAYOUT DIAGRAM



QUICK REFERENCE GUIDE

1. Prepare the cells by seeding the cells on a sterile cell plate, submerging the cell plate in a container of media, and placing the container in the incubator for 48 hours to allow the cells to adhere to the plate and begin growing.
2. Sterilize all the components of the perfusion system (chamber, tubing, pump, and reservoir, if applicable), except the cell plate.
 - a. Autoclave the bottom part of the chamber (Teflon part), all tubing (PharMed® and Silicone), the o-ring, and the 6 thumb screws.
 - b. Use a 70% ethanol solution for the pump and top of chamber.
 - i. Pump- Spray with ethanol before assembling system
 - ii. Top of chamber- Submerge in 70% ethanol for 1 minute, remove and let dry under chemical hood.
3. Assemble perfusion system under chemical hood.
 - a. PharMed® tubing runs through the pump and connects to the chamber inlet and silicone tubing.
 - b. Silicone tubing connects to the outlet of the chamber and the PharMed® tubing.
4. Insert the plate and sponge (if desired) securely into the chamber. This may be done by hand (with sterile gloves on) or using sterile forceps (spray both gloves and forceps with 70% ethanol before use).
5. Prime the perfusion system with media:
 - a. Fill chamber with media (pour from media bottle or use a 25 ml pipette).
 - b. Turn pump on until bubbles stop coming out of tubing.
 - c. Turn pump off.
6. Secure the lid onto the chamber with thumb screws and check for leaks.
7. Move the perfusion system into the incubator.
8. Make sure the incubator is set to proper temperature and carbon dioxide levels.
9. Plug the pump into a socket in the incubator.
10. Set the peristaltic pump to desired flow rate level (1-4 ml/min) and turn it on.
11. Check again that there are no leaks.
12. Close the incubator and allow the system to run for the desired period of time.
13. Turn off the peristaltic pump and move the perfusion system to the chemical hood.
14. Take out a media sample and the cell plate to use for further testing.
15. Disassemble and clean the perfusion system. Sterilize all components before doing another experiment.

CARE AND MAINTENANCE

A. STORING PERFUSION SYSTEM

1. After all components have been sterilized (Detailed How-To's – Experimentation Preparation, C, p 8), ensure that all components are dry and free of foreign material.
 2. Store in a dry place until needed for next experiment. Leave the chamber open to prevent excessive bacterial growth while in storage.
- ❗ Sterilize the perfusion system immediately before use, particularly when system has been stored.

B. PHARMED® TUBING REPLACEMENT

1. If tubing is worn, cracked or leaking, cut a new piece of 1/16" ID PharMed® tubing to desired length, typically 1.5 ft.
2. Sterilize new piece of tubing. (Detailed How-To's – Experimentation Preparation, C, p 8).

C. SILICONE TUBING REPLACEMENT

1. When the silicone tubing deteriorates, replace it with new 1/16" ID silicone tubing.
2. Cut new silicone tubing to the desired length, typically 4 ft.
3. Sterilize the new silicone tubing. (Detailed How-To's – Experimentation Preparation, C, p 8).

D. TUBING DISPOSAL (Silicone and PharMed®)

1. After each experiment, inspect tubing for signs of wear and degradation.
2. If cracks, holes, or worn areas are present, dispose of tubing properly.
3. Remove tubing from system while wearing gloves.
4. Place tubing in autoclave for 30 minutes at 30 PSI (270° F).
5. Once tubing is autoclaved, place in red biohazard bin for waste disposal.

E. PERFUSION SYSTEM DISPOSAL – STERILIZE FIRST

- ❗ Dispose of the perfusion system only once it is no longer in use.
1. Disassemble perfusion system by removing tubing from pump as directed above.
 2. Place bottom half of chamber in autoclave along with tubing, tubing connector, o-ring, and thumb screws. Autoclave components for 30 minutes at 30 PSI (270° F).
 3. Place autoclaved components in red biohazard bin for waste disposal.
 4. Soak chamber lid in 70% ethanol for a 1 minute, and then dispose of in red biohazard bin.
 5. Clean pump with a dry cloth and wipe down with a 70% ethanol solution. If it is still in working order, store for future experiments.

DETAILED HOW-TO'S – EXPERIMENTATION PREPARATION

A. HOW TO DETERMINE TUBING LENGTH

1. The PharMed® tubing should be cut so there is an adequate amount of tubing to pass through the pump, leaving extra for connections on either end. The standard length is 1.5 ft.
2. The silicone tubing must be long enough to allow for sufficient perfusion of carbon dioxide between the media and incubator. The necessary length depends on the amount of media being used and the flow rate. Use trial and error to determine the length necessary for your experiments. The standard length is 4 ft.
ⓘ Note: If the media becomes too acidic during the experiment, there is not enough gas exchange and the length of the silicone tubing should be extended. Acidic conditions are indicated by the media turning orange and then yellow or by a pH reading below 7.1.

B. HOW TO CALIBRATE PUMP

- ⓘ Calibration does not need be repeated for each experiment once it has been performed for a given tubing diameter. The calibration only needs to be done when the diameter of the tubing is changed. As a regulatory measure, it is recommended that calibration be performed every 6 months to confirm the precision of the flow rates from the pump, even if the tubing diameter has not been changed.
1. Set up the pump (Detailed How-To's – Experimentation Procedure, G, p. 13).
2. Make sure the power switch is in the "off" position.
3. Take a beaker or other container with at least 100 mL of volume and fill it up with water.
4. Put both the inlet and the outlet tubing into the beaker and turn the pump on.
5. Prime the system such that the tubing volume is fully occupied by water.
ⓘ When the system is not primed, water bubbles will be seen leaving from the outlet tubing. The cessation of bubbles from the outlet tubing, therefore, is a good indication that the system is adequately primed.
6. Turn the pump off temporarily.
7. Take the outlet tubing out of the water beaker and place it over a graduated cylinder. Do not allow water to drip into the graduated cylinder until the flow is on again.
ⓘ Note that during this time, no water should flow out of the tubing due to a vacuum formed in the tubing.
8. Turn the dial on the pump to the lowest setting (0).
9. Turn the pump on and let the water collect in the graduated cylinder for a timed period of 5 minutes.
10. At the end of the 5 minute period, turn the pump off, and observe how much water was expelled by the pump. Record the volume.
ⓘ One convenient feature of using a graduated cylinder as the collecting container is that it already has markings to determine volume.
11. Divide the volume observed by 5 minutes to get the flow rate at that setting in mL/min.

12. Repeat steps 8-10 at the different pump settings to calibrate and quantify the flow rates at those settings.
13. Once calibrated, either add labels directly onto the face of the pump around the dial with the appropriate flow rates, or record in a notebook the flow rates that correspond to each of the settings on the dial.

Figure 1. ATTACHING TUBING TO THE PUMP

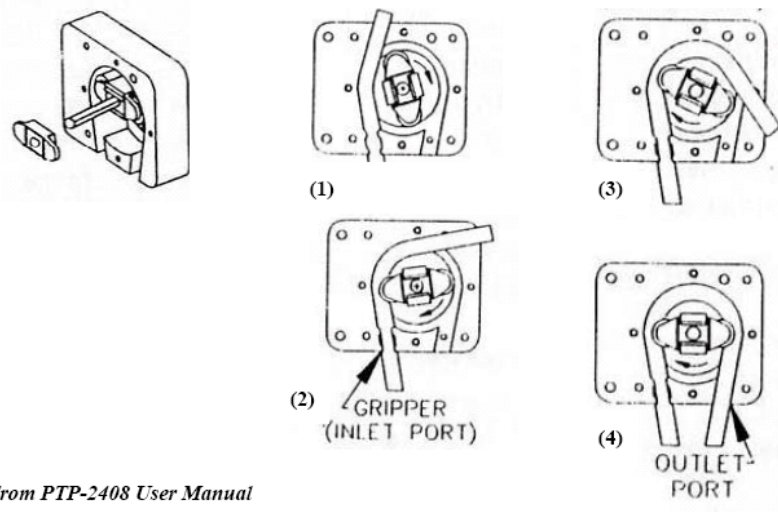


Image From PTP-2408 User Manual

C. STERILIZATION PROTOCOLS FOR PERFUSION SYSTEM COMPONENTS

- 1) Chamber
 - a) Teflon base with inlet/outlet ports, thumb screws, o-ring, and tubing connector:
 - i) Autoclave-Steam for 30 minutes at 30 PSI (270° F)
 - ii) The Teflon and inlet/outlet ports remain connected during autoclave cycle. There is no need to disconnect the inlet/outlet ports from the Teflon.
 - b) Acrylic lid:
 - i) Under sterile hood soak in 70% ethanol for 1 minute and remove.
 - ii) Let lid dry under the sterile hood for 20 minutes.
 - iii) If further sterilization is desired, treat with UV for 5 minutes.
- 2) Silicone and PharMed® tubing and tubing sleeve for pump: Autoclave-Steam for 30 minutes at 30 PSI (270° F).
- 3) Peristaltic Pump: Thoroughly spray all pump surfaces with 70% ethanol before assembling system under sterile hood.
- 4) Cell plates:
 - a) Under sterile hood soak in 70% ethanol for 1 minute and remove.
 - b) Let the plates dry under the sterile hood.
 - c) If further sterilization is desired, treat with UV for 5 minutes.

DETAILED HOW-TO'S – EXPERIMENTATION PROCEDURE

A. GENERAL ASEPTIC TECHNIQUE FOR CELL CULTURE

1. First wipe work area and hands with 70% ethanol.
2. To prevent contamination, never uncover containers such as sterile flasks, bottles, and Petri dishes until they are to be used. Replace cover immediately. Never leave containers open to the environment.
3. Unwrap sterile pipettes ONLY at the time of use. Sterile pipettes do not have to be flamed. ▲ Pipetting your cells with a hot pipette will kill them.
4. When removing the cap from any container do not place the cap on any surface. Keep cap interior facing downward. This will prevent contamination by precipitate. If possible, tilt the container so that any falling microorganisms fall onto the lip, rather than directly into the interior of the container.
5. Be careful not to talk, sing, or whistle when you are performing these sterile procedures to minimize contamination.
6. To avoid cross contamination, use a single pipette per container, especially when pipetting media.
7. Techniques should be performed as rapidly as possible to minimize contamination. DO ALL WORK IN STERILE HOOD.

B. HOW TO SEED CELLS

1. Suspend the cells to be seeded, in desired growth media.
2. Filter the solution using a Steriflip to ensure solution is sterile.
3. Place the cell plate (side with the x marked on it should be face down) in a Petri Dish large enough to hold the plate. The side without the “x” is coated to promote cell adhesion.
4. Add solution containing media and cells. The media should cover the plate.
5. Place the Petri Dish (containing the cell plate) into the incubator for 48 hours in order to let the cells adhere to the plate and begin proliferation.
6. Cells are seeded on cell plate and now ready for testing in the perfusion system.

C. STERILIZATION PROCEDURES FOR ASSEMBLY OF PERFUSION SYSTEM

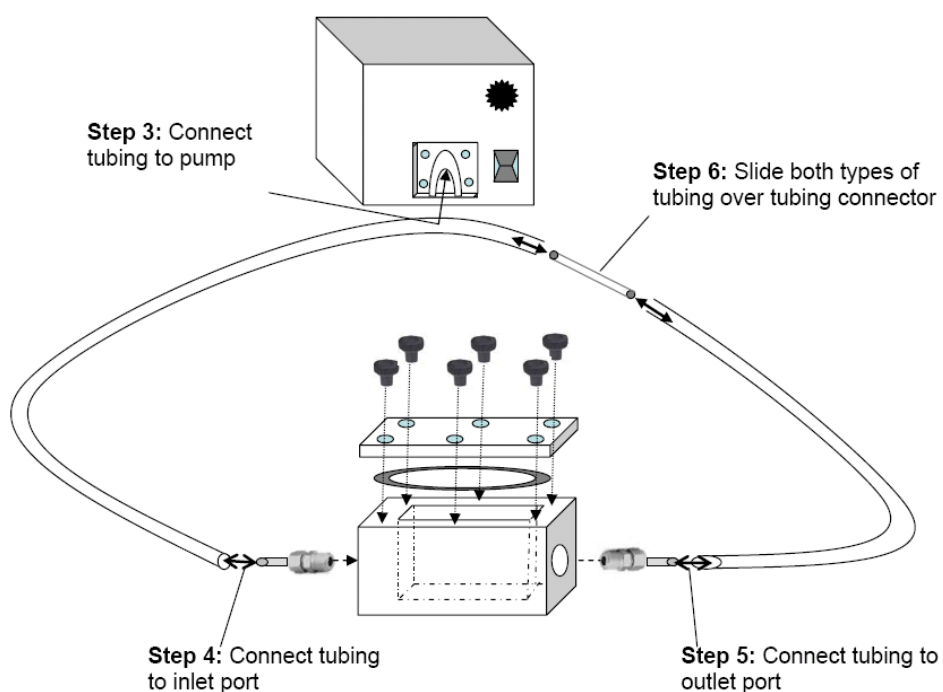
1. Follow standard aseptic technique for cell culture while assembling the perfusion system.
2. Clean every component of the perfusion system according to perfusion system sterilization protocol below.
3. Before placing in sterile hood, spray all objects (including hands) thoroughly with 70% ethanol.
4. Assemble entire perfusion system under the sterile hood.
5. Minimize the amount of time transferring the perfusion system from the sterile hood to the incubator to reduce contamination.

D. HOW TO SET UP SYSTEM

1. When the cultured cells are ready, sterilize all components of the system except the cell plate (Detailed How-To's – Experimentation Preparation, C, p 8).
2. Place all components under the sterile hood immediately after being sterilized.

3. Feed the PharMed® tubing through the pump (Detailed How-To's – Experimentation Procedure, G, p 13).
4. Connect the PharMed® tubing to the inlet of the chamber by sliding the tubing over the metal inlet port so that the direction of flow is from the pump into the inlet.
- ④ Note: The inlet is the side of the chamber that is farthest from the notch.
5. Connect the silicone tubing to the outlet of the chamber by sliding the tubing over the metal outlet port
6. Connect the free ends of the PharMed® and silicone tubing to each other by sliding them each halfway over the metal tubing connector until they touch.
- ④ For all tubing connections, plastic pull-ties can be used to secure the tubing on the connectors for a tighter seal if desired or if leakage occurs.

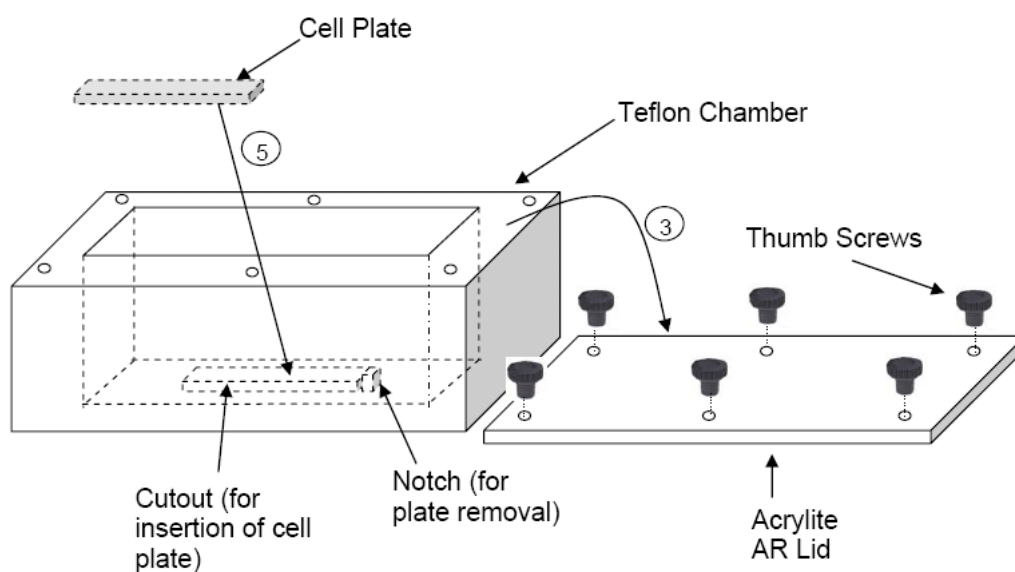
Figure 3. ASSEMBLY DIAGRAM



E. HOW TO INSERT CELL PLATE INTO CHAMBER

1. The assembled perfusion system should be clean, sterile, and under the sterile hood.
2. Bring the cell plate from the incubator to the sterile hood.
3. Remove lid of chamber by unscrewing all six thumb screws and lifting it off.
4. Using sterile forceps or gloved hands, slide one of the short ends of the cell plate into the indentation at the bottom of the chamber.
 - ❗ Every time you leave the sterile hood, you should re-sterilize your gloved hands with ethanol before re-entering the sterile hood.
5. Press the plate firmly into the indentation. The plate should now be immovable, and the top of the plate should be flush with the bottom of the chamber.
 - ❗ Touch the plate only around the edges and as little as possible.

Figure 4. INSERTION OF CELL PLATE



F. HOW TO CUT AND INSERT SPONGE

1. Determine the size of the sponge that is needed for testing.
2. Open the sterile sponge packaging under the sterile hood.
3. Using sterile scissors or a scalpel cut the sponge to the desired dimensions.
 - ❗ Note: The inner dimensions of the chamber are 4 cm wide, by 8 cm long, by 4 cm high.
4. Under the sterile hood, place the cut sponge directly over the cell plate before adding media to the chamber.
 - ❗ The larger the sponge is, the less likely it is to move when the pump is turned on.

G. HOW TO SET UP PUMP

1. Place the pump in the work area.
2. Plug pump into a 120V AC GFI outlet (50-60 cycles).
 - ⚠ The peristaltic pump requires electricity. Without a working power source, the pump is not functional.
 - ⚠ Use extreme caution while dealing with electricity. Avoid contact with the plug while it is inside the electric socket, and make sure the area near the power source is dry.
3. Unscrew the four screws that hold the plastic cap on the face of the pump (See Figure 5).
4. Select sterilized 1/16" diameter PharMed® tubing, and slide the sterilized tubing sleeve provided with the pump over the 1/16" diameter tubing.
 - ⚠ The 1/16" diameter tubing is too slender for the peristaltic pump to effectively push fluid through it without the tubing sleeve. Only tubing that is covered by the sleeve should be in the pump for the 1/16" tubing size.
5. Adjust the dial on the pump to the lowest possible setting (0).
6. Turn the pump on by using switch on the face of the pump.
 - 🕒 Note: There are two settings on the pump: clockwise and counterclockwise. The clockwise setting will push media/fluid out of the bottom right portion of the pump-tubing interface. The situation is reversed for the counterclockwise setting. Choose one of the two settings to run the experiment in (See Figure 1).
7. To get the tubing into the pump, follow the rotary device on the face of the peristaltic pump, gently easing the thick tubing into the empty spaces as the rotor keeps moving. Continue easing tubing into the groove until the tubing is secured around the rotary device (See Figure 2).
 - ⚠ Exercise caution when pushing in the tubing because your fingers can easily be caught between the rollers and the plastic base. This can lead to injury. Use the slowest setting to minimize the possibility of harm.

Figure 5 BASIC PUMP ASSEMBLY

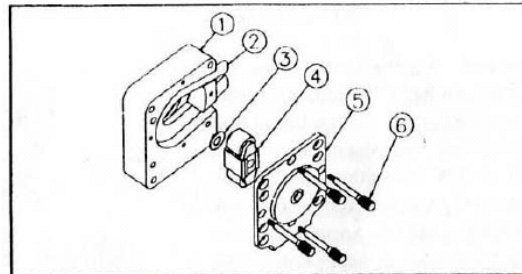


Illustration of the pump assembly.

- 1 - Pump Housing
- 2 - Tube
- 3 - Washer
- 4 - Roller Bracket Assembly
- 5 - Pump Cover w/bearing
- 6 - Thumb Screws

After the thick segment of the tubing is in place, turn pump off and check to make sure there is enough PharMed® tubing extending from the pump to connect the inlet of the chamber and the silicone tubing.

8. If there is not enough exposed tubing on one side, repeat steps 5-8 until sufficient tubing is exposed on both sides.
9. Place the plastic cap mentioned in step 3 over the pump-tubing interface. Secure the plastic cap tightly onto the metallic pump using the four screws provided. The pump is now ready for use.
 - The screws serve not only to hold the plastic cap over the tubing, but also to secure the entire plastic pump-tubing interface tightly against the immovable metallic outer covering of the pump.

H. HOW TO SET PUMP FOR DESIRED FLOW RATE

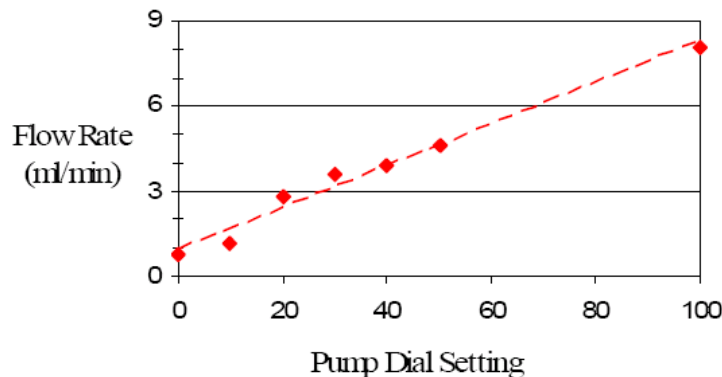
Below is a table with the pump dial settings from 0 to 50 and their corresponding flow rates for 1/16" PharMed® tubing. The maximum flow rate that can be achieved occurs when the dial is turned to the 100 setting and is 8.1 mL/min.

Table 1. PUMP CALIBRATION



Pump Dial Setting	Flow Rate (ml/min)
0	0.78
10	1.2
20	2.85
30	3.6
40	3.95
50	4.6
100	8.1

If your experiment calls for a flow rate within the range of the 1/16" diameter tubing that is not among the flow rates listed in the table above read off the required setting from the figure below.

Figure 6. PUMP CALIBRATION CURVE



I. HOW TO PRIME THE PERFUSION SYSTEM WITH MEDIA

1.  Connect the tubing to the chamber before putting media into the system.
1. Pipette media into the corners of the chamber (avoid dumping it directly onto the cells).
2.  Fill the chamber with media in such a way as to minimize bubble formation in the chamber.
2. Continue filling chamber until media is 5 mm below the top of the chamber.
3. With the lid still off, turn the pump on and watch the inlet of the chamber. Once bubbles have stopped coming out of the inlet, turn the pump off. Check that there are no bubbles in the system. If there are, remove them immediately (Troubleshooting, p 19).
4. Pipette more media into the chamber until the media is 5 mm below the top of the chamber.

J. HOW TO INSERT O-RING INTO LID AND SECURE LID TO CHAMBER




1. Line up o-ring along groove in chamber lid, see below.
 2. Press o-ring into lid.
 3. If o-ring pops out of groove, hold the o-ring into groove while sliding the lid onto the top of the chamber.
 4. Screw the lid onto the chamber, tightening all the screws evenly, see Figure 8. Screws should be tightened in the following order: (1) A corner screw, (2) screw in opposite corner from first screw, (3) another corner screw, (4) the final corner screw, (5) one side screw, and (6) the final screw. The screws should be tightened by going through the sequence of screws 3 times. The first time through tighten each screw until there is an increase in resistance. The second time through tighten each screw until there is significant resistance. When there is significant resistance the lid should be held tightly on to the chamber. The third time through simply check that each screw is tight and tighten any that are loose.
-  Make sure that the o-ring is positioned in its groove correctly to form a tight seal with the top of the chamber
-  Do not tighten one screw completely before tightening the others at all. This can lead to more rapid deterioration of the interior threading.
-  DO NOT OVERTIGHTEN SCREWS.

Figure 7. BOTTOM VIEW OF CHAMBER LID

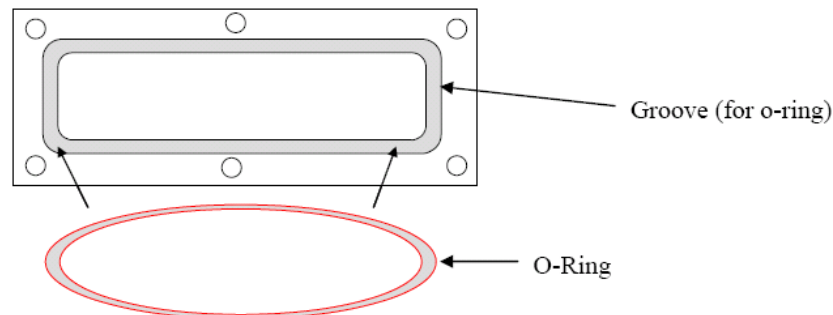
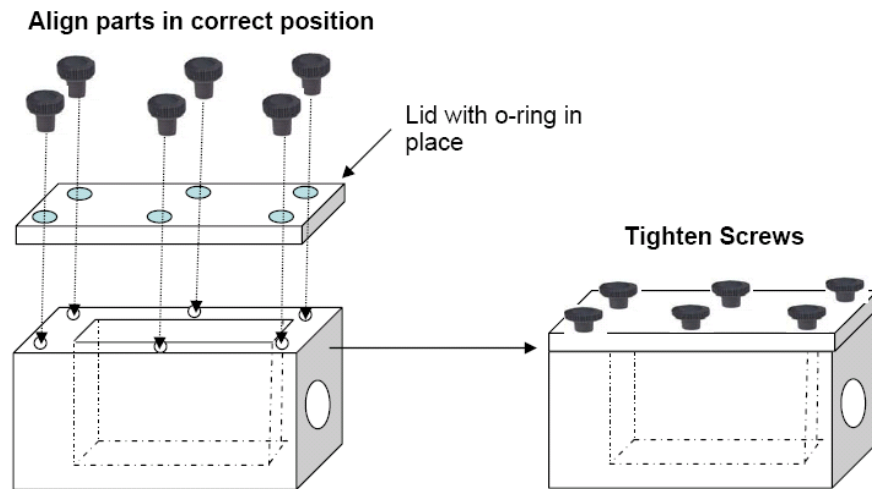


Figure 8. LID ATTACHMENT



K. HOW TO CHECK FOR LEAKS

1. Dry the outside of the system with a paper towel. Look for visible signs of leaking, especially at connections of tubing with other components and around the lid.
2. Wipe all connections with a dry paper towel to see if any liquid is present on the outside of the chamber or at tubing connections.
 - ❗ If the towel gets wet, that component is leaking, and the leak should be fixed immediately (see Troubleshooting section for how to fix leaks).

L. HOW TO RUN SYSTEM

1. Place the perfusion system in the incubator.
2. Set incubator to 37 C and 5% CO₂.
3. Plug pump into GFI electrical outlet inside incubator.
4. Ensure pump is set to desired flow rate and turn it on using power switch on the front of the pump.
5. Check for leaks as above.
6. Close incubator and allow to run for desired period of time (up to 24 hours).
7. After experiment is completed, turn pump off, unplug pump, and remove perfusion system to sterile hood.

DETAILED HOW-TO'S – POST-EXPERIMENT PROCEDURES

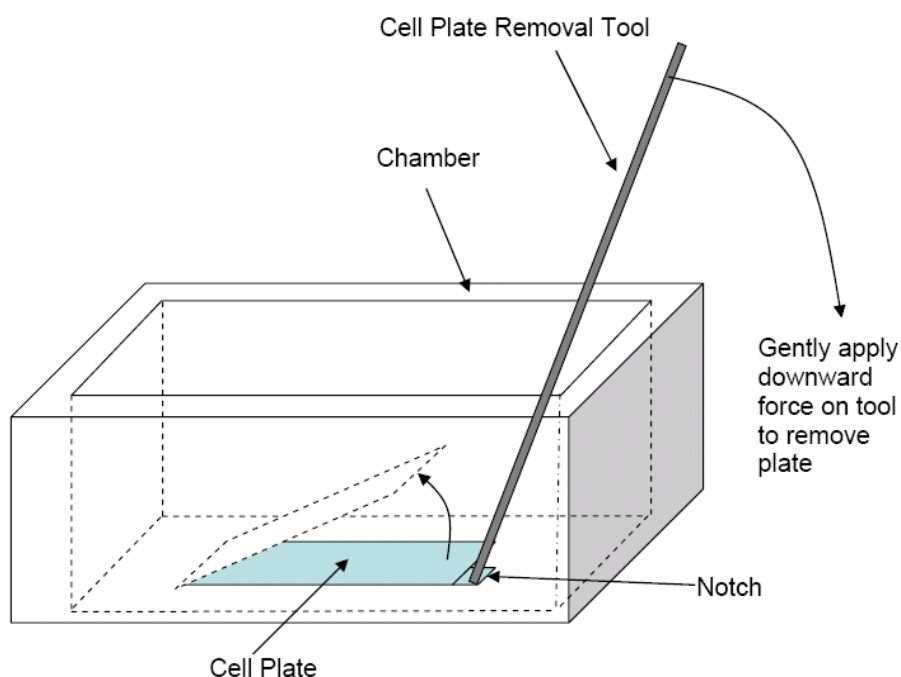
A. HOW TO REMOVE THE MEDIA AND CELL PLATE

⚠ All perfusion system internal surfaces and tubing may have been in contact with media. Treat all surfaces as potential biohazards. Any spillage should be sprayed thoroughly with 70% ethanol and wiped with a paper towel. All used paper towel should be disposed of in a red biohazard container.

1. Remove lid from chamber. Unscrew each screw slightly and then unscrew each one completely. Place lid on paper towel under sterile hood and spray down with 70% ethanol.
2. To take a sample of the media from the chamber for testing, use a large pipette to transfer the used media into a clean, sterile, glass container.
3. Aspirate the rest of the media from the chamber into a sealable, disposable, autoclavable container.
4. To remove the cell plate, position a sterile, thin-tipped rigid tool such as forceps in the notch at an angle away from the cell plate. Use this as a lever to gently pry the end of the cell plate out of the indentation in the bottom of the chamber. See Figure 9 below.

⚠ Be gentle so that the plate does not pop completely out of the indentation, because this could adversely affect the cells if the plate flips over.

Figure 9. PLATE REMOVAL



5. Once the end of the cell plate is elevated from the bottom of the chamber, use sterile forceps or your gloved fingers on the edge of the plate to carefully lift it out of the chamber and into a Petri dish or other sterile surface under the sterile hood.
⚠️ AVOID contact with the surface of the cell plates as this could impact results of any cell plate tests done.
6. Remove the silicone tubing from the outlet port of the chamber and place it in a small container of 30 ml PBS.
⚠️ A small amount of media may escape when moving tubing. Treat with caution and follow the above protocols to clean it up.
7. Turn pump on and set dial to maximum setting (100). Run pump for 2 minutes. Turn off pump.
⚠️ Make sure that the open end of the silicone tubing is completely submerged in the PBS solution throughout the 2 minutes.
8. Re-aspirate the chamber to remove all the media into the same container as before.
9. To dispose of the media see Disassemble System below.

B. DISASSEMBLE SYSTEM

1. Disconnect silicone tubing from tubing connector. Hold tubing vertically above used media container and allow fluid to drain from tubing for 2 minutes. Perturb the tubing gently to ensure tubing drains fully.
⚠️ Be careful that the end of the tubing remains above the media container.
2. Disconnect the PharMed® tubing from the tubing connector and inlet port. Place paper towel under each end of the tubing to absorb fluid flowing out of the tubing.
3. Unscrew four screws and remove plastic cap from front of pump (Figure 5).
4. Turn pump on to slowest setting in counterclockwise direction. Gently pull tubing out of pump in a counterclockwise fashion. Turn pump off.
5. Remove PharMed® tubing from tubing sleeve by pulling it out.
6. Hold PharMed® tubing vertically above used media container and allow fluid to drain from tubing for 2 minutes. Perturb the tubing gently to ensure tubing drains fully.
⚠️ Be careful that the end of the tubing remains above the media container.
7. Seal used media container. Place in autoclave and remove top (leave top in autoclave). Run autoclave for 30 minutes at 30 PSI (270 F). Once cooled, pour media down drain.
8. Spray all surfaces of pump, chamber, chamber lid, screws, tubing connector, o-ring, and PharMed® and silicone tubing with 70% ethanol. Leave components in sterile hood for 20 minutes or until dry.
9. Sterilize all components (Detailed How-To's – Experimentation Preparation, C, p 8).

ADDITIONAL FEATURES

The perfusion system can be modified to increase the scope of experiments that it is useful for:

1. **HIGHER FLOW RATES:** The chamber has been designed and validated to have laminar flow at pump speeds of 1-4 ml/min. Faster pump speeds and/or larger tubing can also be used to get higher flow rates. In order to employ larger tubing, new tubing connectors of desired diameter must be substituted for the current 1/16" diameter tubing connectors. The connectors can be screwed in, and Teflon tape can be used to secure the connectors if necessary. Note: It is not guaranteed that at flow rates faster than 1-4 ml/min, the flow profile will be laminar. Also, the tubing connectors should not be changed often, because this can lead to deterioration of the Teflon threading.
2. **RESERVOIR:** The perfusion system has been designed for easy incorporation of a reservoir. The reservoir should have two openings that the inlet and outlet tubing can pass through. The openings must be sealed to the outer diameter of the tubing to ensure that the system is closed and there are no leaks. The addition of a reservoir will allow the user to take pH measurements of the media, provided that another opening in the reservoir accommodates a pH meter.
3. **LID SCREWS:** The threads of the screw holes used to secure the lid on the chamber may deteriorate over time. If this occurs, holes can be drilled through the lid and the top of the chamber walls at new locations around the top of the chamber to extend the life of the product.
4. **ADDITIONAL CELL PLATES:** The Chemistry Instrument Shop has the pattern for the cell plates, so more cell plates can be cut quickly, as needed. The cell plates were originally cut out of a Corning® CellBIND® Polystyrene CellSTACK® chamber.

TROUBLESHOOTING

Problem	Cause	Correction
No flow/Pump not working	No power to pump	Plug in pump power cord Check to make sure that the outlet has electricity Turn off pump and connect tubing correctly Turn off pump, clean and sterilize tubing, re-connect Turn off pump and connect all components securely. Use plastic pull-ties to secure tubing if necessary. Press o-ring completely into groove, slide lid onto top of chamber walls, tighten all screws Check all components for deterioration. Replace or fix cracked parts or tubing that has cuts or holes in it. Use thin tool to remove bubbles and/or re-prime system See above corrections for leaks Try again with a different tool or wait for chamber to cool down and try again Disconnect system components and sterilize then reconnect system Place under hood immediately. Clean any spills. Continue experiment as normal unless notable contamination has occurred.
No flow/Pump not working	No power to pump	
No flow	Tubing not connected properly	
No flow	Tubing clogged	
Leak	Components not connected properly	
Leak	Lid is loose	
Leak	Component failure	
Bubbles	Did not prime system correctly	
Bubbles	Leak in system	
Cell plate stuck in chamber	Too tight or sticky	
Components become disconnected when moving from hood to incubator		
Components become disconnected when moving from incubator to hood		

⚠ If the sterility of the system is ever seriously jeopardized as a result of a leak or component disconnection, the experiment must be started over with new cells, fresh media, and clean, sterile components.

CAUTIONARY NOTES

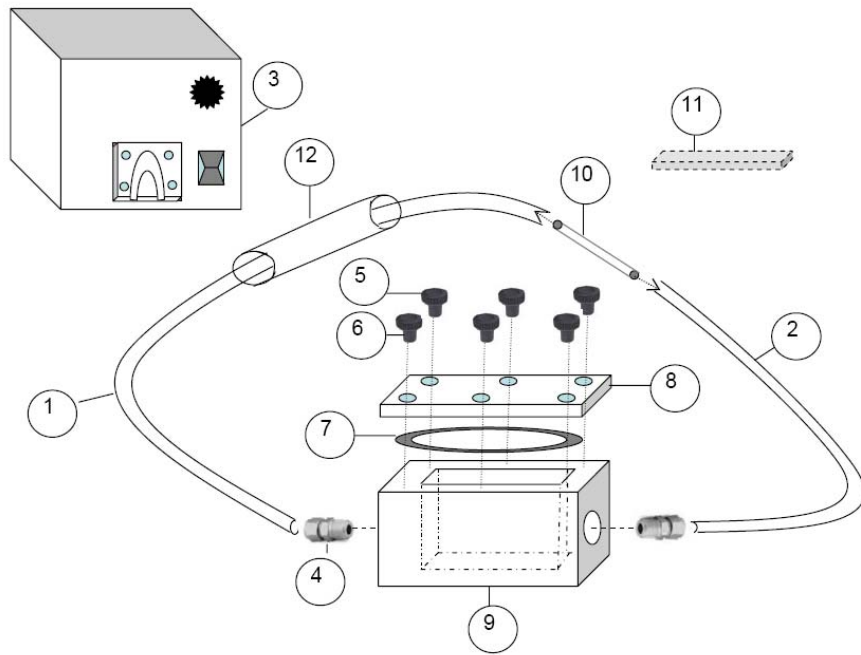
1. Do not drop the chamber or pump.
2. Be gentle with the chamber to avoid damaging the connections with the metal tubing connectors. Never hold the chamber by the metal tubing connectors.
3. Avoid unscrewing the metal tubing connectors, because you could damage the threading.
● Note: These end pieces may be unscrewed occasionally if tubing of a different diameter is desired. Teflon tape can be used to seal them. (See Additional Features.)
4. If there is any physical damage to the chamber, take it to the machine shop for repair.
5. Do not autoclave the chamber for too long or at higher pressures, because you could damage the interface between the Teflon and the metal.
6. Always dry all components thoroughly before storage to prevent corrosion and bacterial growth.
7. Do not over-tighten screws for top of chamber.
8. Do not completely tighten one screw at a time. Tighten all evenly by tightening them all small amounts alternately until all are tight.
9. DO NOT AUTOCLAVE THE TOP OF THE CHAMBER
10. Do not autoclave the pump.
11. Do not disassemble the pump.

DETAILED SPECIFICATIONS

Flow range (with 1/16" tubing):	0 to 8.1 ml/min
Accuracy at settings 0-50:	Flow: $\pm 7\%$
Power source:	AC adapter
Chamber dimensions (base with lid):	Outer: 10.54 cm (l) x 6.54 cm (w) x 5.5 cm (h) (length is ??? cm with tubing connectors)
	Inner: 8 cm (l) x 4 cm (w) x 4 cm (h)
Flow duration:	Up to 24 hours
PharMed® tubing life in pump:	1000+ hours
Perfusion system storage temperature:	-100° F to 180° F

PARTS

Item	Part #	Quantity	Name	Material	Source
1	PHT-062A-10	1 (10 ft roll)	Inlet tubing	PharMed® Tubing	Small Parts Inc.
2	SCT-063-25	1 (10 ft roll)	Outlet tubing	Silicone Tube	Small Parts Inc.
3	PTP-2408	1	Pump	Peristaltic Pump	Small Parts Inc.
4	SS-100-1-4	2	Tubing Connector	Stainless Steel	Swagelock
5	94052A125	6	Instant Thumb Screws		McMaster-Carr
6	92196A146	6	Socket Head Screws	Stainless Steel	McMaster-Carr
7	ORS-151	1	O-Ring	Silicone	Small Parts
8	8560K241	1 (11 3/4 Sq. In. of 3/8")	Top	Acrylic Sheet	McMaster-Carr
9	8546K24	1 (4 1/2" length of 3/8")	Base and Sides of Chamber	Teflon	McMaster-Carr
10		1	Tubing Connector	Stainless Steel	McMaster-Carr
11	3330	1	Material for Cell Plates	Polystyrene	Small Parts Inc.



CONTACT INFO

For general questions about the FloCulture Perfusion System:

Email: rossello@umich.edu

To order additional cell plates or have the chamber repaired:

Kim Firestone, Instrument Maker II
The University of Michigan Chemistry Instrument Shop
Room A509 Chemistry Building
930 North University Avenue
Ann Arbor, MI 48109-1055
Phone: (734) 764-7363
Fax: (734) 615-4314
Email: kff@umich.edu

A2. ALP activity assay (24 well plate)

Ricardo Rossello and David H. Kohn

Solutions

- a. Hank's balanced solution (or EBSS+ solution)
- b. Harvest buffer
 - 10 mM Tris-HCl, pH=7.4
 - 0.2% Igepal (CA-630)
 - Add PMSF to the final concentration 2 mM freshly {make 200mM PMSF (0,3484g/10ml EtOH→ aliquot to 1ml each) and add 1/100 of the total volume}
- c. Assay buffer
 - 100 mM glycine (3.785g/500ml)
 - 1 mM MgCl₂, 47.61mg/500ml
 - pH=10.5
- d. PNPP: 50 mM of p-nitrophenylphosphate
- e. Stop solution: 0.1N NaOH

Procedure

1. Wash cells twice with 1ml of Hank's solution
2. Harvest cells in 400ul (2 times x 200ul) of the harvest buffer into 1.5ml eppendorf tube on ice
3. [optional step] Keep the tube at -80°C (or -20°C) for storage
4. Homogenize at low power (7-8 level, 3 times x 10sec) (sonicator in Dr. Francheski's lab)
 - Keep the tube on ice before and after the homogenization
 - Keep the tube on a beaker (ice + ethanol) during the homogenization so that the sample is not overheated by the sonicator tip
5. Centrifuge the homogenized sample at 12,500 rpm for 10 min (Set the centrifuge at 4°C in advance)
6. Mix the following components in a new eppendorf tube placed in 37°C water bath
 - 250ul assay buffer
 - 140ul harvest buffer
 - 100ul PnPP
 - 10ul sample (set the timer from this moment to measure exactly 15 min); for example, put the sample into the tube every 30 seconds.
7. Put 500ul 0.1N NaOH (stop solution); for example, put this stop solution every

- 30 seconds so that every tube are on reaction for exact 15 min
8. Read them at A405nm in the spectrophotometer (Dr. Taichiman(?)'s lab, #)

DNA quantitation- refer to the picogreen DNA quantitation protocol

Calculation

$$E_{405}=18500$$

$$\text{Units/ml}=(A_{405})/(18.5)(\text{minutes})(\text{ml})$$

A3. Cell Counting with Hemocytometer

Ricardo Rossello and David H. Kohn

I. Equipment and Supplies

Chemicals: 70% Ethanol (bottle for instruments & spray bottle)
Ice
PBS (1X)
Hanks Balanced Salt Solution (HBBS, Gibco/BRL #14170-120)
Fetal bovine serum (Gibco/BRL # 16000-044)
Alfa-MEM (Gibco/BRL Cat. #12571-063 –alfa-MEM, 1X)

Media

Note: All media preparation and other cell culture work must be performed in a laminar flow hood. Use a Steril 500ml Nalgene filter to prepare the media.

For 500 ml
50ml Fetal calf serum
5ml Penicillin Streptomycin
Balance alfa-MEM

Consumables: Gloves
Plastic Vials
Flasks (Nalge Nunc Int #136196 – polystyrene sterilized filter cap flask, angled neck, 50 ml, 25 cm(2) culture area)
Kim-wipes
Paper towels
Nalgene Filter
Plastic bags

Equipment Laminar-flow hood + suction system (tube/large liquid waste flask)
Test tube rack (for 1.5ml tubes)
Microscope
Filtration Device
Centrifuge

II. Procedures:

1. Trypsinize cells (use *Trypsinizing Cells protocol*)
 - a. Check flask after initial trypsinization and retrieval of cells to observe the quantity of non trypsinized cells.
 - b. If significant, repeat trip protocol.
 - c. Trypsinize several times in order to retrieve an optimal amount of cells.

2. Prepare A Pellet from Cell Suspension

Note: This is done several times to retrieve fats when culturing cells.

 - a. Place the Cell suspension 15 ml falcon tubes and centrifuge.
 - i. Centrifuge at about 1000 RPM for about 3 mins.
 - b. Retrieve the supernatant and decant.
 - c. Re suspend with media again.
 - d. Centrifuge again (mostly for when passaging, otherwise, centrifuging once is enough).

3. Cover the Hemacytometer with Slide (see fig 1)

4. Prepare a Cell suspension of known volume.
 - a. Re suspend the pellet in a known volume (e.g. 1ml of solution). Let sit for 3mins.
 - i. Usually you want to count such that you have about 100 cells in each of the compartments (fig 2). Thus, determine the volume based on the expected number of cells you think you will have. (e.g. if you think you will have 7million cells, then use about 7ml volume). Note that for a number significantly more than 100, you should re-suspend accordingly, because the measurement is less accurate
 - b. Take 10 μ L of the suspension and pipette it gently into one of the sides (fig 1) of the Hemacytometer and 10 more for the other slide.

5. Count the cells that in compartments A, B, C, and D.
 - a. Take an average of these counts
 - b. The number you get in a, multiply it by 10⁴ cells
 - c. Finally, multiply that number by your fixed volume, and you will have the total number of cells in that suspension.

$$\text{Number of Cells} = \left[\frac{A+B+C+D}{4} \right] [10^4 \text{ cells/ml}] [\text{fixed volume}]$$

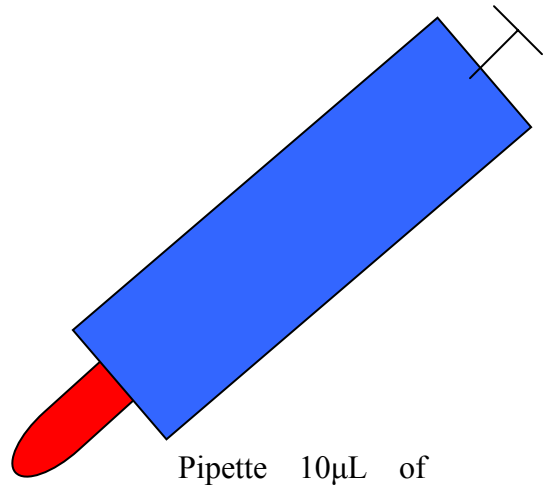


Figure 1: Hemacytometer:

Pipette 10 μ L of

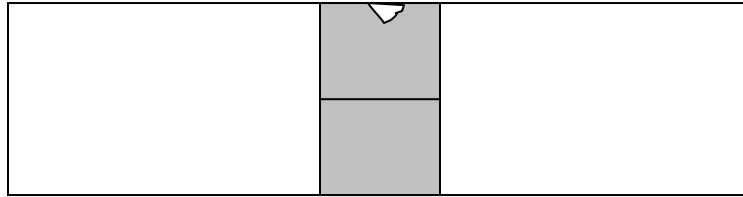
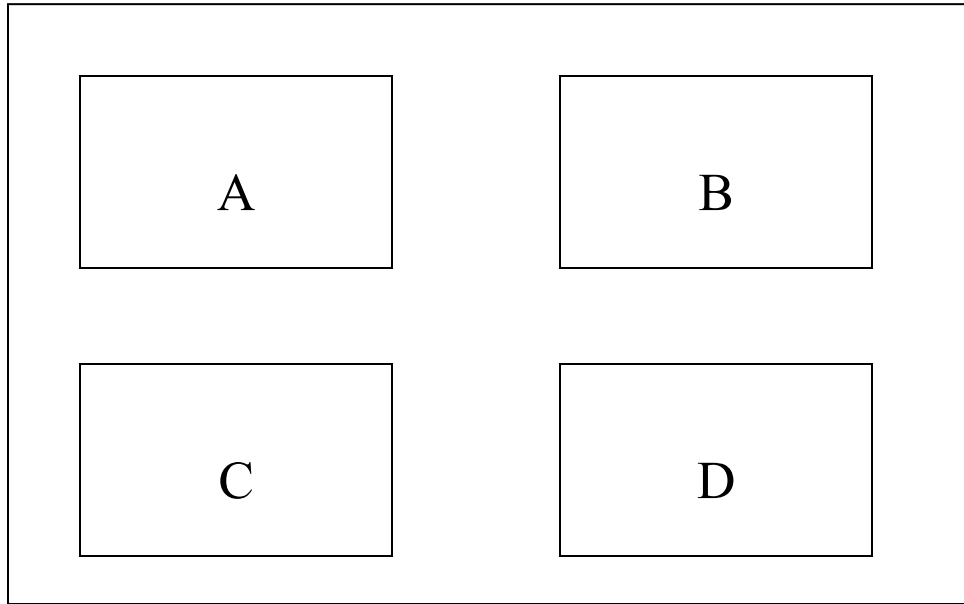


Figure 2: Counting Chambers: Count the number of cells in each of the chambers under the microscope and take the average of them.



A4. Cell Proliferation by Flow Cytometry (BrdU and PI)

Ricardo Rossello and UM FLOW CYTOMETRY CORE

This method, modified from Hoy CA, et.al, is applied to adherent cell cultures. It may also work with suspension cultures, with modifications germane to their culture conditions.

Notes:

- An ideal sample is $1-2 \times 10^6$ cells. Keep all samples to about the same number of cells to avoid artifacts associated with cell concentration changes.
- Flow cytometry setup controls needed:
 - 1) Cells stained with PI alone.
 - 2) Cells with no BrdU pulse, and only the antibodies added.
- Amount of BrdU added may vary according to cell type, and proliferative potential.
- BrdU is light sensitive and should be added in the dark.
- Cells pulsed with BrdU may be photosensitive -- incubations should be in the dark as well.

Reagents (Product code)

BrdU (5-bromo-deoxyuridine) -- Sigma (B-5002)

RNAse A (from bovine pancreas) -- Boehringer Mannheim (109-169)

Tween 20 -- Fisher Biotech (BP337-500)

Triton X-100 -- Sigma (X-100)

Propidium Iodide (PI) -- Sigma (P-4170)

Ca⁺⁺, Mg⁺⁺-free Delbecco's PBS

HPLC-grade H₂O

Fetal calf Serum (FCS)

Internal standard (IS, trout erythrocyte nuclei) – BioSure (1008)

Antibodies

Purified Mouse-anti-BrdU - Pharmingen (33281A)

Goat-anti-Mouse IgG (Whole molecule) FITC conjugate - Sigma (F0257)

Solutions

0.5 mg/ml RNAse A in PBS

PTS -- PBS with 0.5 % Tween 20 and 5 % FCS

HCl-Triton -- 0.1 N HCl containing 0.7 % Triton X-100

1. At desired time point(s), incubate cells with 30 μ M BrdU for 15 min.
2. Remove BrdU media. Rinse 1x with PBS.
3. Detach cells -- as appropriate; trypsin, EDTA, etc. – and resuspend in 10 ml media.
4. Permeabilize cells:

Determine cell count. Aliquot desired number of cells per test sample to 15 ml conical tubes. Pellet at 1200 rpm for 5 min at 4 °C. Decant supernatant, wash with 3 ml PBS, and re-pellet. Resuspend pellet in 0.3 ml PBS, agitate gently, then add 0.7ml ice-cold 100 % EtOH slowly. Mix gently with a 1 ml glass transfer pipette. The cell concentration following permeabilization should be approximately 10⁶ cells/sample. Samples can be stored in EtOH for up to 2 weeks at 4 °C.

5. Add IS if desired, at a concentration of 10⁵ IS per 10⁶ cells. Mix gently with a 1 ml glass transfer pipette. Pellet at 1100 rpm for 8 min at 4 °C. Decant supernatant, wash with 5 ml PBS, re-pellet and decant supernatant.
6. Add 1 ml PBS containing 0.5 mg/ml RNase A. Agitate tube gently. Incubate at 37 °C for 30 min. Add 5 ml PBS, pellet at 1100 rpm, 8 min at 4 °C. Decant supernatant.
7. Agitate pellet, then resuspend with 1 ml of HCl-Triton solution. Vortex gently. Incubate on ice for 10 min. Add 5 ml PBS, pellet at 1100 rpm for 8 min at 4 °C. Decant supernatant and blot gently to dry.
8. Add 1 ml sterile HPLC water, vortex gently. Incubate at 97 °C for 15 min. Note: be sure to cap tubes loosely to allow for expansion, and keep lid on water bath to control heat range.
9. Immediately chill in ice-water bath for 15 min. Add 5 ml PBS containing 0.5 % Tween 20. Pellet at 1100 rpm, 8 min at 4 °C. Decant supernatant.
10. Add 100 µl PBT. Agitate gently with transfer pipette. Transfer sample to a 1.5 ml microcentrifuge tube.
11. Add 100 µl of a 1:100 dilution of anti-BrdU Ab. Incubate at RT for 30 min. Add 1.2 ml PBT. Pellet at 3200 rpm for 2 min in a microcentrifuge (Eppendorf Centrifuge 5415 C). Decant supernatant. Note: Speed and time are IMPORTANT -- at this point, the pellet is very loose and it may be necessary to re-pellet.
12. Add 150 µl of a 1:20 dilution of FITC-conjugate Ab. Incubate at RT for 30 min. Add 1.2 ml PBT. Pellet at 3200 rpm for 2 min in a microcentrifuge.
13. Resuspend pellet in 0.5 ml PI stock solution. Transfer sample to a 0.5 ml snap-top microcentrifuge tube. Cover samples with foil.
14. Leave samples at RT for 1 hr before taking them to the Flow Lab.

A5. Designing a Filtration Device for Scaffolds

Ricardo Rossello

A filtration device has proven to increase the cell retention in porous PLGA and Mineralized PLGA scaffolds significantly [Appendix 1]. The basic principle is to have cell suspension filter through tightly packed scaffolds, in order to (1) create a gradient so that cells can pack the scaffold, and (2) those cells that filter through will have other

opportunities to attach as the suspension cycles. The basic components of the apparatus (figure 1) are:

1. Peristaltic Pump
2. Tubes
3. Chamber

There are other components that may become essential based on the experiment, such as a reservoir of media. Although these three components are simple in essence, they need to be tailored to the particular experiment. I will discuss the design criterion needed to adjust the apparatus for any particular experiment.

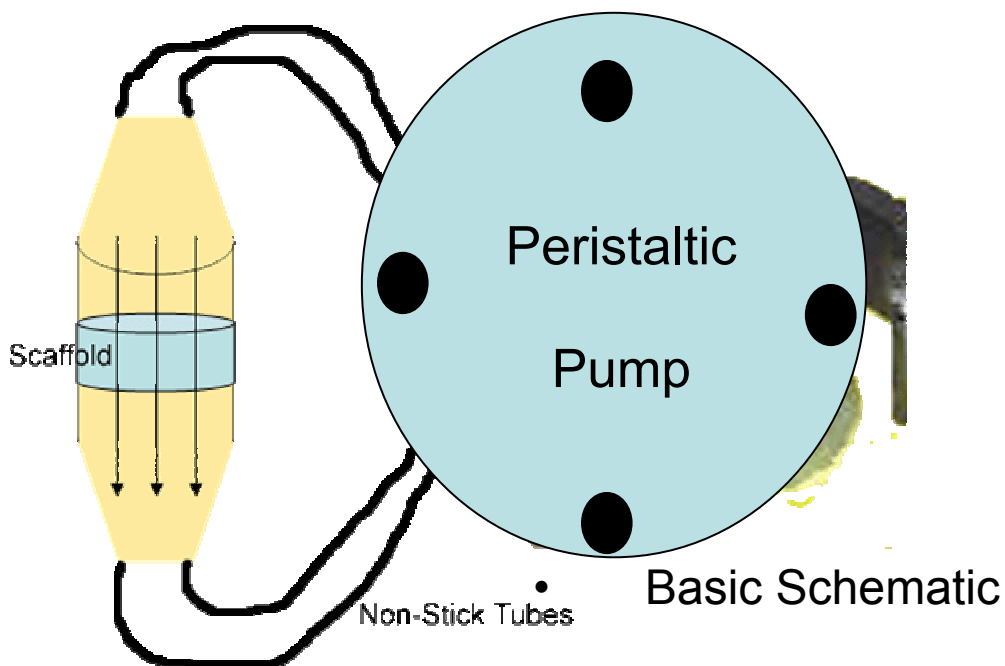


Figure 1: Basic Schematic of a filtration device to seed cells into Scaffolds.

Factors of Importance

Design Parameters

When designing the filtration experiments the first order of business is determining the dimensions of the scaffold (Diameter, Thickness, mm³). This is very important because based on these all other parameters have to be determined. Scaffold Diameter will drive

the diameter of both the chamber and tubes. Scaffold thickness will determine how many scaffolds you can use to get an even cell profile.

Other important parameters are the flow rate, inner diameter and length of the tubes. These have to be determined based on the flow profile (laminar vs. turbulent; RE see next section), and desired stress component. Fluid dynamic equations that should be used to determine these parameters are in Appendix 2.

Fluid Dynamics

Tests have been conducted to determine which type of flow causes the best cell proliferation, and of turbulent flow, laminar flow, and no flow, laminar flow causes the greatest amount of cellular growth. [1] Turbulent flow causes stagnant points and dramatic shear stress variations, which may kill cells or tear them from the plate's surface. Laminar flow is a steady flow in which a velocity gradient is present that extends from the fastest velocity at the center of the flow to zero flow at the wall or stationary object. Laminar flow occurs when viscous forces dominate in the flow. This is determined by the Reynolds number which is a non-dimensional number takes into account the parameters of the flow. If the Reynolds number is less than 2300, the flow is laminar. If the Reynolds number is greater than 2300, the flow is not laminar.

When fluid flow undergoes a change in **diameter** there is a region in which turbulent flow can occur for a limited distance. This turbulent region is called the *entrance region*. This entrance region can be calculated from the Reynolds number and the diameter of the new region of flow. This distance begins at the point where the radius of the cross sectional area of flow is no longer changing [See Appendix 2 for equations],

Contamination

Physiological conditions are not the only factors that affect cell growth. Contamination from bacteria can easily occur in cell culture systems if special care is not taken to keep the system sterile. Providing an environment that cells find ideal to live and reproduce in means that other organisms, such as bacteria, find this environment favorable too. Just one component being contaminated can lead to bacterium infecting the system and ruining an entire experiment by killing other cells or creating byproducts that can alter experimental results. Bacteria multiply and grow very quickly, which is why it is extremely important to make sure that every component in the system is completely sterile before and during the experiment.

Tubing

PharMed® tubing and silicone tubing were used in our perfusion system. Silicone tubing was used to connect the outlet of the chamber to the inlet of the reservoir and was selected because it is an industry standard for cell culture tubing. Silicone tubing is

permeable to gas, which allows CO₂ exchange in the incubator. This allows the pH of the media to be controlled. PharMed® tubing was used to connect the reservoir outlet to the entrance of the chamber. The reason for using two different types of tubing in our system design is durability. **When using Silicone tubing for peristaltic pumps, it has a 75 hour operating life before failure, which means it would have to be changed often** (based on the 6hour optimal time period, every 12 runs or so, Appendix 1). On the other hand, PharMed® tubing’s operating life before failure is over 1000 hours, so it lasts a long time in the pump. However, PharMed® does not meet an acceptable gas permeability requirement, so the Silicone tubing is needed for part of the system to allow for the necessary gas exchange. Figure 9 shows the gas permeability coefficient of the two types of tubing for various gases. Tube specs and info in appendix 3.

Permeability Coefficient Comparison

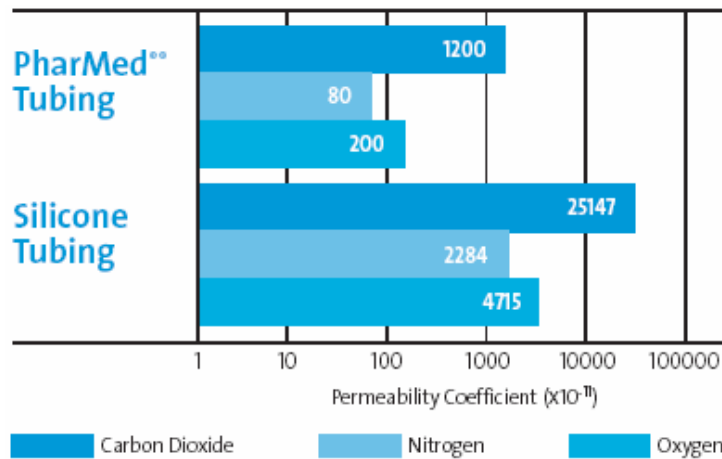


Figure 9: The permeability of carbon dioxide is over 25 times larger in Silicone tubing than in PharMed® tubing.

Pump

The peristaltic pump is the research standard for cell culture perfusion systems. The main reason for this is that there is no contact between the media and the pump. This eliminates the pump from being a possible contaminant to the cells being cultured. The peristaltic pump also provides a constant flow at variable flow rates. **Our lab purchased the PTP-2408 (drawer labeled peristaltic pump in 2228) from Small Parts, Inc** (please note that based on your requirements, you may need a different peristaltic pump) . It has a pump speed of 1.5-26 RPM and allows for flow rates from 0.3 to 90 ml/min based on the inner diameter of the tubing used.

Chamber Design

The design of the chamber is the primary concern in designing the system. The chamber must be designed such that there is laminar flow through the scaffolds. Shear stress and uniformity of flow are variables to take into account which can affect a biological outcome. The chamber must also be biocompatible and sterilizable. There is no specific upper constraint on size except that it fit in the incubator, but the larger the chamber, the more media will be required and the larger the scaffold may have to be (this should not be a concern for our scaffolds are small).

For scaffolds, the chamber will be a cylindrical non-stick glass tube that will be sterilizable [these glass vials are sold on fisher, pending the size]. Typically this tube is the same one used for casting the scaffolds. A chamber can also be made from Teflon, if a particular size is desired. The tradeoff is the observational capabilities of glass, versus the ability to have a machined chamber with the specific size that is desired. Other options are acceptable so long as they follow the basic criterion that the chamber needed be biocompatible, sterilizable, and non-adhesive for cells.

Inlets and outlets to the chamber can be machined if such a difference in cross sectional areas is desired. However, for most cases, matching the inner diameter of the tubes to the outer diameter of the chamber and placing a rubber stopper over it will work. Figure 2 shows the flowchart schematic.

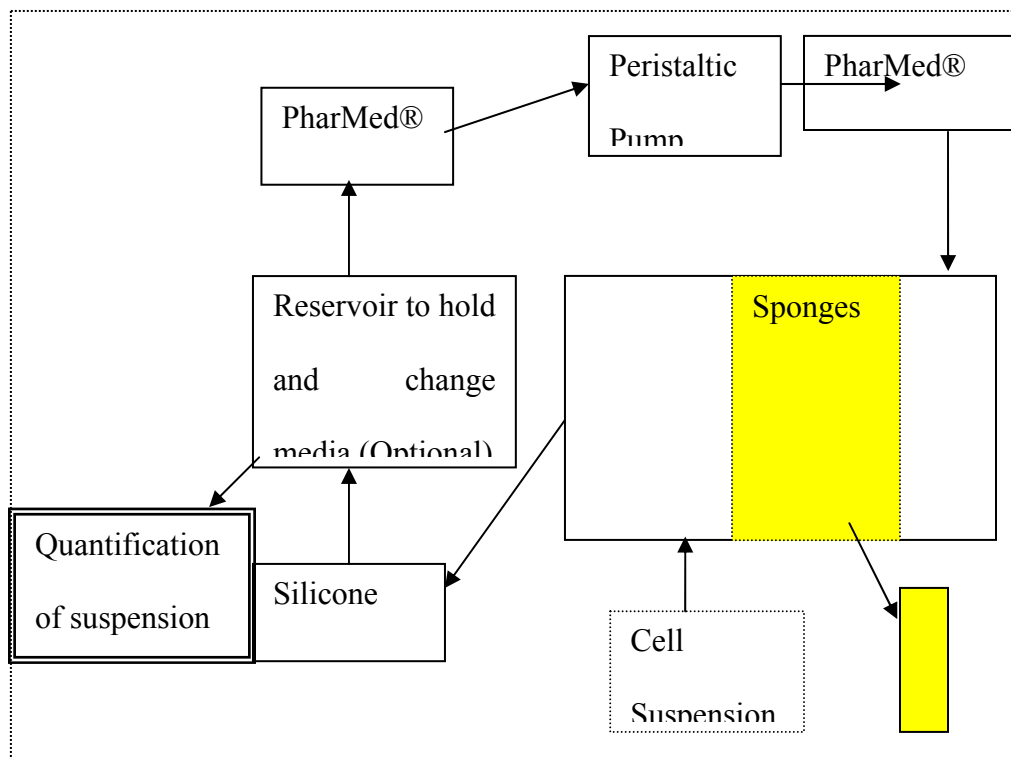


Figure 2: Flowchart

Assembly of System and Priming

After sterilizing all of the components, the user will have to assemble the perfusion system. The perfusion system should be assembled under a hood to prevent any contamination during assembly. The basic setup, however, is as follows. The pump is connected to the chamber entrance and reservoir by PharMed® tubing. Silicone tubing is used to connect the exit of the chamber to the reservoir.

Filling the perfusion system with cell suspension, securing the inlet and outlet stoppers, and checking for leaks are the next steps. Working under the chemical hood, prime suspension into the system (and reservoir if necessary) until the chamber, reservoir, and tubing are full, and without air bubbles. Priming can be done in a variety of ways, pending on the size of the tubes and such. I poured as much of the suspension as possible, and then filled the remaining spaces with a syringe. After checking for leaks and ensuring there are none, you can then carefully move the perfusion system into the incubator. The incubator has a rubber stopper in the back end, which will be necessary to remove in order to connect the AC outlet.

Running Experiment

Once in the incubator, you need to prepare the system for the experiment. Secure the chamber in the incubator to ensure that it will not move during experiment and connect the AC outlet. After the chamber is secured, once again check for leaks and make sure everything is connected properly. Check that the incubator is set to proper temperature and carbon dioxide levels. Then set the peristaltic pump to desired flow rate level (1-4ml/min).

After making sure everything is set up properly, the user is ready to run the experiment. First, turn on the peristaltic pump and look to make sure media is flowing through the system. Next, check once again that there are no leaks. Finally, close the incubator and allow the system to run for the desired period of time.

Once the desired experimental run time is complete the user can open the incubator and turn off the peristaltic pump. Next, move the perfusion system from the incubator to the chemical hood. The user can then take out the plate and media from the reservoir and save them for further testing.

Finally, the last step is to disassemble and sterilize the system again. Empty the remaining media-suspension from the system into a jar with bleach. Decant the bleach-suspension solution into a sink approved for biological disposal (Culture room). Then the system can be taken apart and sterilized with appropriate sterilization protocols (pending on what materials used, autoclave or ethanol are cleansing).

Preliminary filtration data

Adhered Cell Count (Ricardo Rosselló)

Filtration seeding had a significantly higher percentage of cells adhered, than the dynamic or static seeding (figure 4). Filtration seems to have reached carrying capacity at the 6 hour period (92.32 ± 6.12), while the other two methods show a steady increase in attached cells. Mineralized scaffolds showed no significant difference to the PLGA only scaffolds. However, as time increased, the p-values decreased. For the filtered seeded scaffolds the p-values decreased from $p=0.781$ in the first hour, to $p=0.13.2$ in the 24th hour.

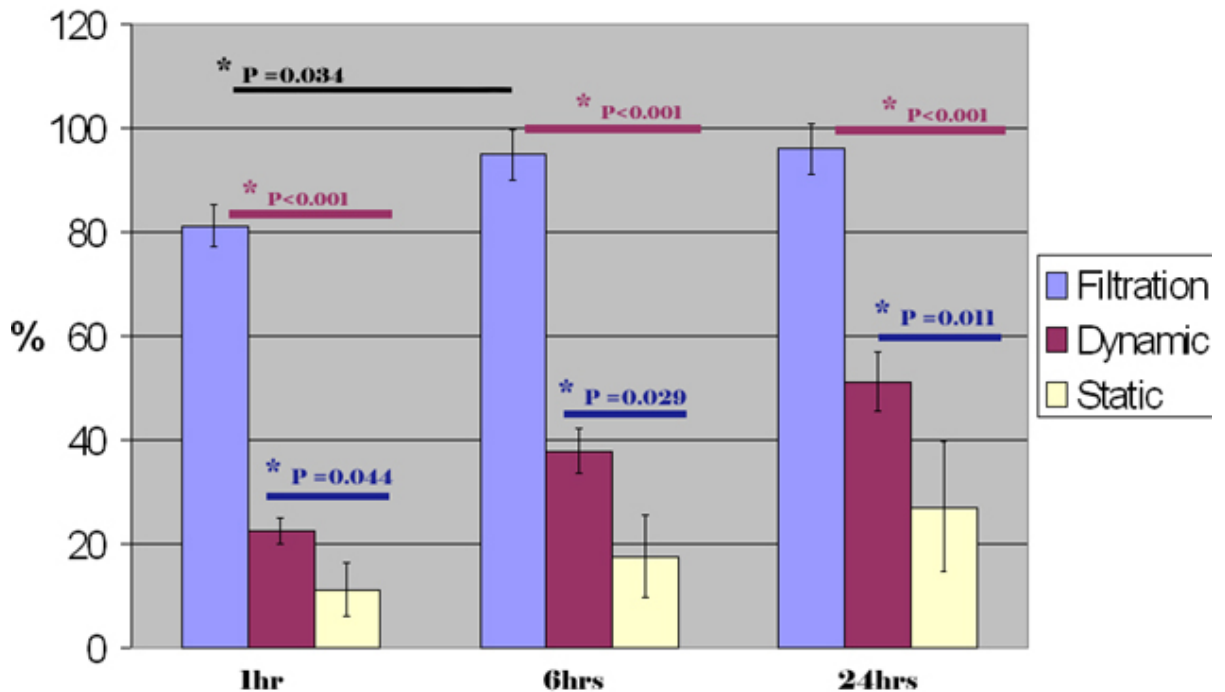


Figure 4: The number of cells was accounted for after each time period, and for each method. The scaffolds were washed to remove the free cells trapped in the construct. The remaining cells were trypsinized and accounted for. There is a significant difference ($p < 0.001$) at all time points between seeding techniques. There is also a significant difference between the 1 hour and 6 hour mark in the filtration process ($p = 0.034$). Another interesting result to note is that there is

a much smaller variation is observed at all points in the filtration process than in the highly variable static seeding.

Flow Calculations

The following formulas were used for deriving the flow dynamics within the chamber.

The effective diameter for an arbitrary shape is D_e :

$$D_e = \frac{4WH}{2W + 2H}$$

The velocity of the fluid is:

$$V = \frac{Q}{WH}$$

The Reynolds Number is given by:

$$\Re = \frac{D_e V \rho}{\mu}$$

The entrance length is:

$$L_e = 0.06 D_e \Re$$

The pressure differential is give by:

$$P = \frac{12 V \mu L}{D^2}$$

The shear stress at the wall is given by:

$$\tau_w = \frac{P D}{4 L}$$

A6. Protocol for Extracting Bone Marrow Stromal Cells from Rat Femur and Tibiae

Ricardo Rossello and David H. Kohn

I. Equipment and Supplies

Chemicals: 70% Ethanol (bottle for instruments & spray bottle)
PBS (1X)
Hanks Balanced Salt Solution (HBBS, Gibco/BRL #14170-120)

Media

Note: All media preparation and other cell culture work must be performed in a laminar flow hood. Use a Steril 500ml Nalgene filter to prepare the media.

For 500 ml
50ml Fetal calf serum
5ml Penicillin Streptomycin
Balance alpha-MEM

Consumables: Gloves

Glass (Pasteur) pipettes + canister (sterile)
Pipette tips
Petri Dishes
3.0 ml Syringe
1.5 ml tubes
Flasks (Nalge Nunc Int #136196 – polystyrene sterilized filter cap flask, angled neck, 50 ml, 25 cm(2) culture area)
Kim-wipes
Nalgene Filter
Sharpie marker

Equipment

Laminar-flow hood
Tweezers, forceps (sterile + keep in EtOH under hood)
Microscope
Markers
Vortexer
Hemocytometer

General Procedural Notes

- Rinse gloves w/EtOH every time one re-enters hood
- Clean the hood with EtOH before and after the procedure.
- Autoclave dissection instruments before hand

- All culture vessels, test tubes, pipet tip boxes, stocks of sterile eppendorfs, etc. should be opened only in the laminar flow hood.

II. Procedure

1. Set up
 - a. Place the petri-dish containing the bones inside the hood.
 - b. Set up 3 additional petri dishes
 - i. Media
 - ii. Bone remains
 - iii. BMSC
 - c. Place about 15 ml of media to the media petri dish. Use extreme caution when using the syringe; only touch the part necessary for suction.
2. Retrieval of BMSC
 - a. With forceps, use a clipper to break the outer extremities of the bones
 - i. A cut should be done at or close to where the bone marrow can be seen.
 - b. Retrieve 3ml of media with the syringe. Use the syringe to flush out the bone marrow out of the bone, and into the BMSC plate.
 - c. Use the same media decanted from the bone, to further flush marrow cells. This time flush the cells through the other side of the bone. Do this procedure about 4 times.
 - d. Perform a-c for all of the bones
 - e. See if there is any marrow left in the small peaces of the bone, so that you could retrieve that too.
3. Re-suspend the marrow cells
 - a. Use the syringe to re-suspend the BMSC
4. Observation and storage
 - a. Mark the date and strain of rat used
 - b. Count the cells with a Hemacytometer (see *Cell Counting with Hemacytometer Protocol*)
 - c. Place cells in a CO2 incubator
5. Further observation
 - a. Observe and monitor the cells every two days.
 - b. Change media every 2-3 days.
 - c. Passage the cell, as specified in the tripsinizing and sub culturing cells protocol, in 7-10 days.

A7. Filtration Seeding of Scaffolds

Ricardo Rossello and David H. Kohn

I. Equipment and Supplies

Chemicals: 70% Ethanol (bottle for instruments & spray bottle)
Ice
PBS (1X)
Hanks Balanced Salt Solution (HBBS, Gibco/BRL #14170-120)
Fetal bovine serum (Gibco/BRL # 16000-044)
Alfa-MEM (Gibco/BRL Cat. #12571-063 –alfa-MEM, 1X)

Media

Note: *All media preparation and other cell culture work must be performed in a laminar flow hood. Use a Steril 500ml Nalgene filter to prepare the media.*

For 500 ml

50ml Fetal calf serum

5ml Penicillin Streptomycin

Balance alfa-MEM

Consumables: Gloves

24 well vials

Plastic Vials

Flasks (Nalge Nunc Int #136196 – polystyrene sterilized filter cap flask, angled neck, 50 ml, 25 cm(2) culture area

Kim-wipes

Paper towels

Nalgene Filter

Plastic bags

Equipment Laminar-flow hood + suction system (tube/large liquid waste flask)

Tweezers, forceps (sterile + keep in EtOH under hood)

Test tube rack

Microscope

Incubator (CO₂)

Filtration Device

General Procedural Notes

Autoclave Filtration Materials before usage.

II. Procedure

Cell Suspension

Trypsinize cells (see *Trypsinizing Cells*)

Observe flasks after trypsinization, if there appears to be a large number of cells on the flask after trypsinization, repeat the procedure again.

Pipette media into the flask to stop trypsinizing effects. Use this media a few times to wash of some cells, by tilting the flask to the side (fig 2) and repidately washing.

Device Setup (fig 1)

Connect tubes to the pump.

Place wetted scaffold (see *Wetting of Scaffolds*) on to the sterilized crystal tube. Utilize the sterilized tweezers to place it.

Insert cell suspension into to the tubes. Make sure it is saturated with the desired cell suspension density (see *Cell Count Protocol*).

Close filtration loop

3. Place Filtration Device into CO2 Tank

Connect the Device to the adaptor (at the far end of the incubator)

Turn on the pump.

NOTE: For Maximum Cell Count – Switch off direction of flow periodically , to maximize seeding and adhesion.

Retrieve scaffolds from the apparatus

Take the tubes out of the apparatus.

Carefully detach the tubes in the hood, over a Petri dish.

Utilize tweezers to take scaffold out.

Place scaffold in Petri dish or 24 well plates. To ensure hydration of the scaffold, wet the scaffold by pipetting a small amount of media to the scaffold. **Make sure the scaffold stays hydrated.** For example: for a 4mm diameter and 1 mm thick scaffold, pipette about 12 μ L of media.

Place plate in CO2 Incubator until ready for use in vitro or in vivo.

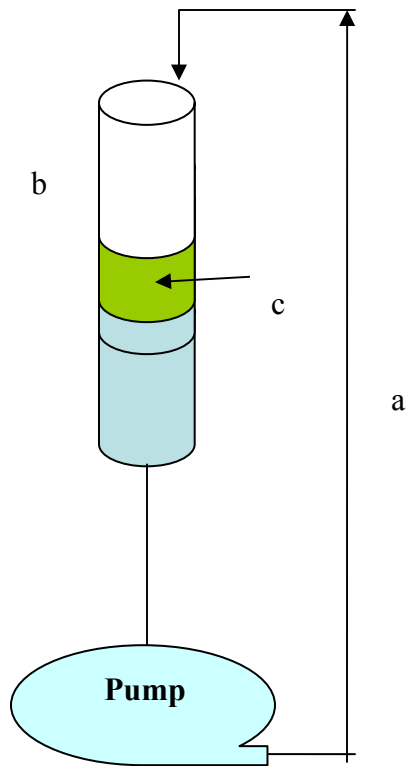
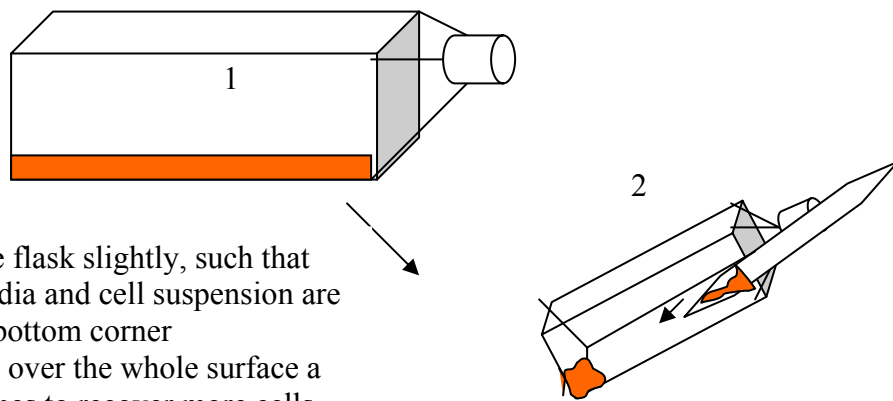


Fig 1: Filtration apparatus:

- a) the arrows signify the tubes that where the flow occurs
- b) This is the crystal tube where the scaffold is placed
- c) Scaffold
- d) Variable pump system
 - a. Contains velocity control and directional control

Fig 2: Pipetting media over trypsinised cells.



1. Tilt the flask slightly, such that the media and cell suspension are in the bottom corner
2. Pipette over the whole surface a few times to recover more cells

A8. Subcutaneous Transplantation of Gelform-BMSCs into Mice

[Purpose] Gelform is the usual hemostatic sponge in dental clinic, which consists of absorbable gelatin. To have the in vivo study of MSCs, we cast Gelform blocks as carriers for tissue engineering cell-scaffold implantation.

Chemicals: Ketamine
Xylazine
Saline

Consumables: Sterile Gelfoam sponge. 12 sq cm× 7 mm
Sterile gauze
Serum-free alpha-MEM serum
6-well culture plate

Equipment: Laminar Flow Hood
Surgical scissors, blade (15#) and scalpel

[Procedure]

1. Under sterile environment, place the Gelform sponge onto a 100mm Petri-Dish. Slice the sponge horizontally in half with the scalpel (3.5 mm height each). Use scissors to cut the Gelform into 3.5 mm cubes, place the Gelform cubes onto a pre-wet gauze (by alpha-MEM), press with dry gauze to drive off the air bubbles. Then dry Gelform with another dry gauze.
2. Cells were harvested and counted, then aliquoted into ependorf tubes at 2-3 million/ml/tube. Centrifuge and aspirate the supernatant, reserve 30-50 μ l medium and suspend cell pellet by pipetting.
3. Place one sponge/tube and incorporate cells suspension into it by gently dipping sponge to the bottom of the tube. Co-culture the cell-sponge at 37°C in an incubator for 30 minutes.
4. Take tubes and surgical instruments to Room 6203 (SCID room). Anesthetize mice (figure 1) with intraperitoneal ketamine cocktail.

Ketamine cocktail:

0.3 ml Ketamine

0.2 ml Xylazine

0.5 ml Saline

Dosage: 50- 100 μ l /mouse

5. Make two small vertical incisions (1 cm-long) on the back along the spine. One incision at hindlimbs level and the second one at forelimbs level.
6. Make bilateral subcutaneous pouches by dissecting the skin with blunt scissors. Place one sponge in each "quadrant" of the animal's back. Total: 4 sponges/animal.
7. Suture the incision to close wounds (figure 2).
8. Monitor mice recovery until the next day.
9. Removal the suture 2 weeks post-operation (if not absorbable)



Figure 1: Inject mice by grabbing the skin over the cervix and Holding the tail (and leg if necessary with one of our loose fingers)



Figure 2: Suture the incision

A9. Cell Seeding by Micromass

Ricardo Rossello and David H. Kohn

I. Equipment and Supplies

Chemicals: 70% Ethanol (bottle for instruments & spray bottle)
Ice
PBS (1X)
Hanks Balanced Salt Solution (HBBS, Gibco/BRL #14170-120)
Fetal bovine serum (Gibco/BRL # 16000-044)
Alfa-MEM (Gibco/BRL Cat. #12571-063 –alfa-MEM, 1X)

Media

Note: *All media preparation and other cell culture work must be performed in a laminar flow hood. Use a Steril 500ml Nalgene filter to prepare the media.*

For 500 ml
50ml Fetal calf serum
5ml Penicillin Streptomycin
Balance alfa-MEM

Consumables: Gloves

Plastic Vials

Flasks (Nalge Nunc Int #136196 – polystyrene sterilized filter cap flask, angled neck, 50 ml, 25 cm²) culture area

Kim-wipes
Paper towels
Nalgene Filter
Plastic bags

Equipment Laminar-flow hood + suction system (tube/large liquid waste flask)
Test tube rack (for 1.5ml tubes)
Tweezers, forceps (sterile + keep in EtOH under hood)
Microscope
Filtration Device
Centrifuge

II. Procedures:

Trypsinize cells (use *Trypsinizing Cells protocol*)
Check flask after initial trypsinization and retrieval of cells to observe the quantity of non trypsinized cells.

If significant, repeat trip protocol.

Trypsinize several times in order to retrieve an optimal amount of cells.

Prepare A Pellet from Cell Suspension

Note: This is done several times to retrieve fats when culturing cells.

Place the Cell suspension 15 ml falcon tubes and centrifuge.

Centrifuge at about 1000 RPM for about 3 mins.

Retrieve the supernatant and decant.

Count the cells using the Hemocytometer (see *Cell Counting with Hemocytometer Protocol*).

Resuspend the cell pellet, and aliquot an, on 1.5ml tubes, the amount desired for the making of the macro-mass of cells you are going to seed. For example. If you have a cell count of 1 Million Cells, and you want to make micro masses of 0.2 million cells, aliquot 1/5 of the cell suspension to 5 tubes, and centrifuge them.

After centrifuge, extract the supernatant (as much as you can), and leave the pellet. In order to do this carefully, retrieve the final micro liters of supernatant with a micropipette.

Place 1.5ml tubes containing the pellet into the CO₂ Incubator for 30mins-1hr.

Micropipette these micro masses into the scaffolds (which are on a 24 well plate or Petri Dish), by placing the dense glob on the geometrically desired position. Slightly hydrate with some media. Place the seeded scaffolds into the incubator for another hour. Retrieve the plate and hydrate the scaffolds (more than before). Place Scaffolds in incubator until ready for use.

A10. Protocol for Flow Cytometry Activated Cell Separation (FACS)

Ricardo Rossello and UM FLOW CYTOMETRY CORE

Device:

BD Biosciences FACSCalibur

Materials:

Sterile 10-cm tissue culture dishes

6,12,24 well plates

cell strainers (Falcon 2235)

Falcon Tubes

Cell culture medium

Trypsin/EDTA

PBS

Calcein-AM stock Solution (Sigma)

Vybrant DiI stock solution (Molecular probes)

Gap Junction Competent Cell Line (e.g. BMSCs)

1. All solutions need to be stored in 4⁰C.

Pre-loading solution:

1. Add 1 μ L of Calcein stock solution to 1mL medium mix.

2. Add 1 μ L of DiI stock solution and mix again.

3. Vary mixes accordingly to specifications

4. Make 1.5-2mL of solution for each 6cm plate of cells to be labeled.

A11. Immunohistochemistry stain on Connexin43-treated cranial defect sections

Ricardo Rossello, Zhuo Wang, and David H. Kohn

Day 1:

1. Deparaffinized slides.
Xylene 10 min×2
2. Rehydration
100% EtOH 2×1 min
95% EtOH 1 min
75% EtOH 1 min
3. PBS 10 min wash
4. H₂O₂ 5 ml (Stock 30% 20 ml + 180 ml dd H₂O ----> 3% final concentration)
5. PBS 10 min wash

Use a decloaker chamber, set up 2 mins (first switch over 20 min, then turn back), merge the slides in Antigen-retrieval reagent (1×(Biocare Medical), diluted with PBS)

6. PBS 10 min wash
7. Block the slide with sniper for 5 min, room temperature
8. Primary Ab incubation (diluted 1:1000 in Da Vinci Green antibody diluent (Biocare Medical)), load 100 µl on each slide
9. Place the slides on a wet chamber overnight at 4° C.

Day 2:

10. Drain with PBS 10 min
11. 2nd Ab incubation (Biotinylated Coat-anti-Rabbit IgG (BioCare Medical) 10-15 min, room temperature)
12. PBS 10 min wash
13. Incubate for 15 minutes with streptavidin-HRP (Biocare Medical)
14. PBS 5 min wash
15. DAB reaction (Zymed; South San Francisco, CA, 12.5µl + 1 ml buffer all, 75 µl on each slide) for 30 seconds.
16. PBS wash 5 min
17. Stain with hemotoxylin for 30 seconds, then rinse with tapping water immediately
18. Dehydrate (reverse the first 3 steps), mount and coverslip.

A12. Westernblot Protocol and Preocedures

Ricardo Rossello and David H. Kohn

- 1) Load 20 to 25 microgram of whole cell lysate per lane in an SDS-PAGE mini gel.
- 2) Run at 20 mA per gel untill the dye front is close to the bottom.
- 3) Transfer the proteins to a nitrocellulose membrane (S&S NCTM) at 250 mA in transfer buffer for 1-4 h, depending on the size of the target protein.
- 4) Incubate the blot with blocking buffer (5% non-fat dry milk in TBS) overnight at 4oC or 2 h at room temperature (RT).
- 5) Incubate the blot with primary antibody (diluted 1:250 to 1:1000 in blocking buffer) for 1 h in blocking buffer at RT.
- 6) Wash the blot 3 x 10 min in washing buffer (TBS containing 0.1% Tween 20) with shaking.
- 7) Incubate blot with anti-rabbit IgG-HRP conjugate (Sigma) (diluted 1:10,000 - 1:2,000 in blocking buffer) for 1 h in blocking buffer at RT.
- 8) Wash 3 x 10 min in washing buffer with shaking.
- 9) Drain washing buffer, add ECL solution (Amersham) and develop for 1 min.
- 10) Expose to X-ray film for 1 to 30 min.

A13. Infection Protocol for Adherent Cell Types

Ricardo Rossello, Thomas Langinan, Eddy Kizana, and David Kohn

This protocol may be used for the infection of adherent cell lines. The use of qualified retroviral supernatant in custom infections is absolute. To qualify the viability of retroviral supernatant, use either the Titer Assay for Retrovirus protocol or the 'Qualification of FIV-GFP Supernatant Infection Efficiency SOP'.

Materials

- 1 6-well Tissue Culture Plate at 5.0×10^5 cells per well and appropriate media
- 1 Disposable 9in Glass Pasteur Pipette
- 3.75ml Qualified 10x retroviral supernatant
- 2.5 μ l 4 μ g/ml 0.22 μ m Filter Sterilized Polybrene dissolved in Milli-Q
- 2.5 μ l 4mg/ml 0.22 μ m Filter Sterilized Protamine Sulfate dissolved in Milli-Q
- 1 5ml Pipette
- 1 30ul Pipette tip

Equipment

- 1 Pipette Aid
- 1 20 μ l Pipette-Manu
- Tissue Culture Hood
- 37C Incubator w/ 5% CO₂
- 32C Incubator w/ 5% CO₂
- Eppendorf 5810R Centrifuge w/ multi-well plate swinging bucket

Procedure

Prepare Cells For Infection.

- Split target cells into a 6-well tissue culture plate at 2.5×10^5 and incubate overnight at 37C w/5.0% CO₂. This will provide ~50% confluent cells the following day.

Infection.

- Observe cells under microscope to verify that they look healthy and are at the right confluence.
- In a Tissue Culture Hood, aspirate cellular media from the first row of wells and aliquot 1.25ml viral supernatant as described below.
- Once the viral supernatant is applied to the cells, aliquot the localization molecule into the wells as described below and gently rock the plate for even distribution of molecule. The final concentration of each localization molecule is 8µg/ml.

Table 1. Aliquot the retroviral supernatant into the corresponding wells as described. The media plus localization molecule wells serve as controls to monitor any cell death.

1.25ml 10x Sup 2.5µl 4mg/ml Polybrene	1.25ml 10x Sup 2.5µl 4mg/ml Protamine Sulfate	1.25ml 10x Sup
1.25ml Media 2.5µl 4mg/ml Polybrene	1.25ml Media 2.5µl 4mg/ml Protamine Sulfate	Neg Control

- Spin-inoculate the cells by placing the plate in a multi-well plate swinging bucket rotor and place in Eppendorf 5810R Centrifuge. Spin the plate at 2500rpm for 90m at 30C.
- Incubate the cells at 32C with 5%CO₂ for 24-48h.
- Replace viral supernatant with appropriate cell media and return cells to incubator.
- Analyze trans-gene expression >72 hours post infection. In some instances, trans-gene expression may take up to 7 days post Infection.

Extra Notes

- The splitting of the cells, preparation of infection conditions, infection of target cells, and changing the media must be done using sterile technique in a biological safety cabinet to prevent contamination.
- At any step during the infection, antibiotics may be added to the media or supernatant if contamination is present.
- The starting number of cells may be varied to account for total cell availability. Successful transductions have been carried with as little as 2.0×10^5 cells per well. This does however translate into fewer total cells successfully transduced.
- The cell death control wells may be disregarded in favor of more wells of cells to be transduced once the effects of the localization molecules have been noted.
- The duration the viral supernatant is on the cells can go from overnight to 2 days. We have seen that a longer exposure can produce higher transduction efficiency, although this is proportional to increasing cell death, as VSVG and the localization molecules can be toxic. We usually let the 911 cells go overnight.
- Multiple infections may be preformed on the same cells to increase the transduction efficiency. To do this allow the primary infection to stay on the cells overnight, replace the supernatant with media and allow the cells to recover for 24h and then infect again overnight. This cycle may be repeated 3-4 times.

A14. Repair of craniotomy defects with genetically modified cells

Ricardo Rossello, Zhuo Wang, and David Kohn

All experiments were performed in accordance with the University Committee on Use and Care of Animals (UCUCA). Animals were housed in a light- and temperature-controlled environment and given food and water ad libitum.

Animals

4- to 5-week-old female SCID mice (N:NIH-bg-nu-xid; Charles River Laboratories, Raleigh, NC, USA)

Chemicals: Ketamine
Xylazine
Saline

Consumables: Sterile Gelfoam sponge. 12 sq cm× 7 mm
Sterile gauze
Serum-free alpha-MEM serum
6-well culture plate

Equipment: Laminar Flow Hood
Surgical scissors, blade (15#) and scalpel
4-0 Chromic Gut suture

Procedure

1. Under sterile environment, place the Gelform sponge onto a 100mm Petri-Dish. Slice the sponge horizontally in half with the scalpel (3.5 mm height each). Use scissors to cut the Gelform into 3.5 mm cubes, place the Gelform cubes onto a pre-wet gauze (by alpha-MEM), press with dry gauze to drive off the air bubbles. Then dry Gelform with another dry gauze.
2. Cells were harvested and counted, then aliquote into ependorf tubes at 2-3 million/ml/tube. Centrifuge and aspirate the supernatant, reserve 30-50 µl medium and suspend cell pellet by pipetting.
3. Place one sponge/tube and incorporate cells suspension into it by gently dipping sponge to the bottom of the tube. Co-culture the cell-sponge at 37°C in an incubator for 30 minutes.
4. Take tubes and surgical instruments to Room 6203 (SCID room). Anesthetize mice (figure 1) with intraperitoneal ketamine cocktail.

Ketamine cocktail:
0.3 ml Ketamine

0.2 ml Xylacine
0.5 ml Saline
Dosage: 50- 100 μ l /mouse

5. A linear scalp incision was made from the nasal bone to the occiput and full-thickness flaps were elevated.
6. The periosteum overlying the calvarial bone was completely resected. A trephine was used to create a 5-mm craniotomy defect centered on the sagittal sinus and the wounds were copiously irrigated with Hanks' balanced salt solution (HBSS) while drilling.
7. The calvarial disk was removed carefully in order to avoid injury to the underlying dura or brain.
8. After careful hemostasis, gelatin sponges previously loaded with cells were placed into the defects. The sponges filled the entire defect and attached the bone edges around the entire periphery.
9. The incisions were closed with 4-0 Chromic Gut suture (Ethicon/Johnson & Johnson, Sommerville, NJ) and the mice recovered for anesthesia on a heating pad.



Figure 1: Inject mice by grabbing the skin over the cervix and Holding the tail (and leg if necessary with one of our loose fingers

A15. Transduction of BMSCs with LV-Cx43-GFP

Ricardo Rossello, Zhuo Wang, and David Kohn

For the protocol prior to culturing, 25 ml of fresh whole bone marrow cells in a 50 ml tube will be transduced with 25 ml of the produced lentiviral particles in suspension in a rotation incubator at a MOI of 50 in Media. Transduction will be carried out for 5 h at room temperature in the presence of 100 M deoxynucleoside triphosphates (Amersham Pharmacia Biotech Inc., USA) and protamine sulfate (8 µg/ml), or at 37°C in the presence of 8 µg/ml polybrene (Sigma, USA). After transduction, cells will be washed twice by centrifugation at 100 g for 12 min, followed by re-suspension of the cells in 1xPBS. After 12 days of culture, the TRC3 cell product, including adherent and non-adherent cells, will be evaluated for GFP expression by fluorescence microscopy. Quantification of the proportion of GFP cells will also be performed after a week of transduction. Non-transduced BMSC will be used as negative control for GFP expression.

For transduction during culture, BM MNC will be plated at a density of 22.5×10^6 cells per T75 flask. The lentiviral vector with a titer of 10^8 cells/ml will be used to perform a transduction at day 3-4 of culture when individual colony-forming units are initiated which are at a high proliferative status susceptible to viral transduction. In addition, transduction will be carried out in the presence of 8 µg/ml of protamine sulfate that can enhance the transduction efficiency. 5 ml of filtered virus-containing media will be mixed with 5 ml of fresh LTBMCM and 8 µg/ml protamine sulfate will be added to the cell cultures for approximately 16 h (infection phase), followed by replacing this media with fresh media for 6-8 h (recovery phase). The cells will be exposed to three cycles of virus infection. After 1, 2, 4, 8, 12 days of incubation, BMSCs cells will be examined under fluorescent microscopy, and will be trypsinized for FACS analysis.

Controls will include non-transduced cells, cells subjected to transfection medium without viruses, and cells transduced with the vector minus GFP.

I. Equipment and Supplies

Chemicals: 70% Ethanol (bottle for instruments & spray bottle)
Ice
PBS (1X)
Hanks Balanced Salt Solution (HBBS, Gibco/BRL #14170-120)
Fetal bovine serum (Gibco/BRL # 16000-044)
Alfa-MEM (Gibco/BRL Cat. #12571-063 –alfa-MEM, 1X)
LV-Cx43-GFP titers [frozen at 10x; Titer 10^6 cells/ml]
Protamine [8µg/ml]

Media

Note: All media preparation and other cell culture work must be performed in a laminar flow hood. Use a Steril 500ml Nalgene filter to prepare the media.

For 500 ml
50ml Fetal calf serum

5ml Penicillin Streptomycin
Balance alfa-MEM

Consumables: Gloves

24 well vials

Plastic Vials

Flasks (Nalge Nunc Int #136196 – polystyrene sterilized filter cap flask, angled neck, 50 ml, 25 cm(2) culture area)

Kim-wipes

Paper towels

Nalgene Filter

Plastic bags

Equipment Laminar-flow hood + suction system (tube/large liquid waste flask)

Tweezers, forceps (sterile + keep in EtOH under hood)

Test tube rack (for 1.5ml tubes)

Microscope

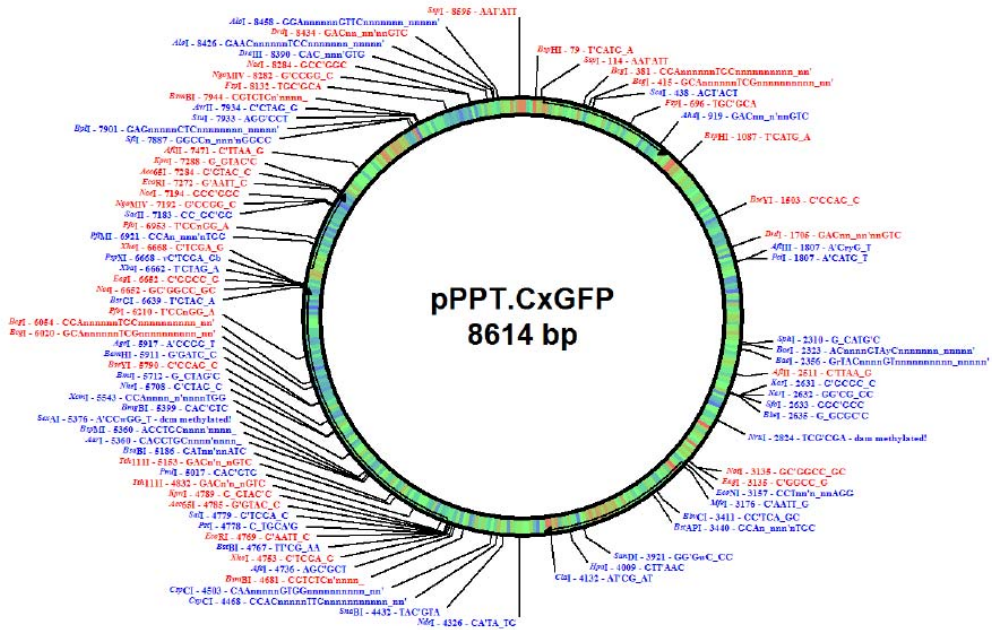
Incubator (CO₂)

1. Culture cells as indicated in tissue culture protocol
2. Achieve 30-50% confluency before infection with virus
3. Unfreeze the LV titer in a water bath; heat media to 37C in the same water bath
4. Calculate the Titer necessary for your infection [based on Multiplicity of Infection (MOI)– Check MOI protocol].
5. Remove all the media from the flask or well plate, and place 10⁷⁻⁸ titer into flask or plate. Immediately after, pipette 8ug/ml protamine into the flask. 1ml for each 8ml of media-virus suspension used.
6. Incubate for 16 hours for infection to occur.
7. After this time period, remove Media and wash with HBBS two times.
8. Pipette fresh cell media –as described above – to flasks for 6-8 hours.
9. Repeat step 7
- 10 Repeat steps 8, only let media for 3-4 days.

Trouble shooting: When cells are not thriving – increasing the FBS to 15-20% is a helpful alternative.

A16. LVCx43GFP Plot

Provided by Inder Verma and Eddy Kizana



A17. Calvarial Defect Model: Enhanced GJIC regenerates more bone in a critical sized defect

Tissue engineering can be defined as the process by which a functional 3D tissue is generated using cells, scaffolds and devices that enable cell growth, organization, and differentiation.{{253 Griffith,L.G. 2006;60 Vacanti,J.P. 1999; 61 Langer,R. 1993; }}. Successful and complete regeneration of tissues can be achieved for certain types of tissue that are either thin in nature (skin), or avascularized{{263 Freed,L.E. 2002;264 MacNeil,S. 2007; }}. Regeneration of bone has been more challenging, since the thick nature of the tissue inhibits necessary transport of nutrients and cues for bone formation through out the 3D construct{{36 Laurencin,C. 2006; }}.

Our group has shown that overexpressing the gap junction protein Cx43 in bone marrow stromal cells, increases intercellular communication and differentiation in 3D cultures over cells expressing normal levels of Cx43. In addition, we have shown that the effects of a known bone osteoinductive agent, BMP7, are augmented when Cx43 is overexpressed. We have also shown that Cx43 overexpression leads to greater distribution and more bone regeneration in an ectopic model (Chapter 4). Our current study investigates the effects of GJIC in a more clinically relevant model by examining the healing of a critical sized defect in the calvaria of nude mice.

Materials and Methods

Bone marrow stromal cell (BMSCs) isolation and culture

Five-week old C57BL/6 mice were used to isolate bone marrow cells from the femoral, tibial and humeral cavities (six bones per animal) as previously described^{11, 55}. Briefly, the bone marrow was mixed with minimum essential medium (α -MEM; Gibco Laboratories, Grand Island, NY) containing 10% fetal bovine serum (FBS) (Gibco) and antibiotics (100 μ g/ml penicillin G and 100 IU/ml streptomycin) at 37°C in 5% CO₂/95% air). Cells were pelleted by centrifugation at 1000 rpm for 5 min at 4°C, resuspended in 10 ml α -MEM and plated at a density of 30,000 nucleated cells/cm², and cultured under the same conditions. The culture medium was replaced three times per week and at near confluence (90%) the adherent cells were washed with phosphate- buffered saline solution and enzymatically detached by means of a 0.25% trypsin-EDTA solution (Sigma, St. Louis, MO). Cells were re-plated at a density of 30,000 cells/cm² and a subsequent passage performed 7-10 days after, when cells achieved near confluence.

Viral Vector Production

Vectors encoding Cx43 and BMP-7 were produced by the University of Michigan Vector Core employing standard transient transfection methods to produce replication incompetent viral vectors. The development and production of adenovector encoding BMP7 under the transcriptional control the human CMV promoter has been previously described⁵⁰ Similarly the development and production of the lentiviral vector encoding Cx43GFP has also been previously described³⁵. The latter vector system was based on the human immunodeficiency virus Type 1 (HIV-1) and the four plasmids (Rossello et al)

required for vector production were kindly supplied by Professor Inder Verma from the Salk Institute, San Diego USA. Empty vectors or vectors encoding GFP were also produced for lentivirus (LVGFP, LVMT) and adenovirus (ADCMVMT), as a control group for the experiments (Rossello et al).

Transduction of BMSCs

BMSCs were plated at a density of 2.25 million cells per T75 flask after second passage. For Cx43-GFP, GFP, and MT transductions, lentiviral vector with a titer of 10^6 transducing units/ml was used on day 3-4 of culture. Transduction was carried out in the presence of 8 $\mu\text{g/ml}$ of protamine sulfate to enhance the transduction efficiency. Five ml of filtered vector-containing media was added to the cell cultures for approximately 16 h (transduction phase), followed by replacing this media with fresh media for 6-8 h (recovery phase). The cells were exposed to three cycles of transduction. After 12 days of incubation, transduced BMSCs cells were examined under fluorescent microscopy to determine transduction efficiency through GFP fluorescence. Transductions with ADCMVBMP7 and ADCMVMT were done as previously stated. Briefly, for in-vitro transduction of BMSCs, adenovirus at the desired titer to achieve a multiplicity of infection of 200 PFU was added to cells in serum-free α -MEM. After 4 h, FBS was added to a final concentration of 2% and medium was kept on cells for an additional 24 h.

Calvarial defect surgeries

All surgeries were performed in accordance with the University Committee on Use and Care of Animals (UCUCA). Animals were housed in a light- and temperature-controlled environment and given food and water ad libitum. A sample size of 4 scaffolds per condition was determined based on the results of the previous subcutaneous experiments. 5-week-old female SCID mice (N:NIH-bg-nu-xid; Charles River Laboratories, Raleigh, NC, USA) were used for each experiment. Animals were anesthetized with intraperitoneal injections of ketamine–xylazine (50 and 5 $\mu\text{g/g}$, respectively) in saline. A linear scalp incision was made from the nasal bone to the occiput and full-thickness flaps were elevated. The periosteum overlying the calvarial bone was resected. A trephine was used to create a 5-mm craniotomy defect centered on the sagittal sinus. The wounds will be irrigated with Hanks' balanced salt solution (HBSS) while drilling. The calvarial disk will be removed carefully in order to avoid injury to the underlying dura or brain. After careful hemostasis, gelfoam scaffolds (D=5mm, t=0.3mm) previously loaded with cells will be placed into the defects (500,000 cells). The scaffolds filled the entire defect and attached to the bone edges around the entire periphery. The incisions were closed using 4-0 Chromic Gut suture (Ethicon/Johnson & Johnson, Sommerville, NJ) and the mice were let to recover from the anesthesia on a heating pad (Kent Scientific). After 4, 8, and, 12 weeks, animals were sacrificed and the calvaria was removed for micro CT and histological analysis.

Micro-CT 3D image acquisition and analysis

Ossicles were scanned on a high resolution cone beam micro-CT system (Enhanced Vision Systems (now GE Healthcare Preclinical Imaging), London, Ontario, Canada) while immersed in distilled H₂O. The x-ray source voltage and current were 80 kVp and 80μA, respectively. To reduce the potential for beam hardening artifact, the x-rays were passed through a 0.2mm Al filter immediately upon exiting the source and the specimens were immersed in dH₂O during the scanning process. Projection images were acquired over 198 degrees using 2x2 binning and an exposure time of 1100 ms, and four frames were averaged for each projection to improve the signal to noise ratio. The projection data was then corrected and reconstructed using the Feldkamp cone-beam algorithm to create three-dimensional images with an isotropic voxel size of 18μm. The scanner was calibrated once daily using a phantom that contained air, water and hydroxyapatite.

Bone volume fractions were determined by using a MatLab program designed to integrate all grayscale voxels above a particular threshold. To determine the overall volume of the ossicles, the program determined the perimeter of each 2D μCT slice by tracing the outer edge. The program then integrated all the perimeters to determine the 3D surface area, and the number of voxels inside the surface defined the total volume. High density voxels outside of the 3D surface and unattached to the ossicle were discarded, while voxels inside were evaluated at the specified thresholds to determine the BVF, which was calculated as the number of voxels above the threshold relative to the total number of voxels. A threshold of 1100 was used to quantify the BVF⁶⁴. Rendered images of the whole calvaria were taken at this threshold to show the regeneration of bone on the defect form both an aerial and a sagittal perspective.

Histology and morphological analyses

Ossicles were removed from the site of the defect in the calvaria. The ossicles were rinsed in water and then decalcified in 10% formic acid for 5 days. After decalcification, the tissues were embedded in paraffin. 5 μ m sections were made and placed on 10 slides with 3 sections per slide. The tissue was deparaffinized hydrated, and the first, fifth, and tenth slides were stained with H & E. Image Pro Plus 4.0 was used to take pictures of the histological sections in order to observe the overall bone formation, cortical thickness, and trabecular-like bone formation.

Results

Cells overexpressing Connexin 43 exhibit increased cell to cell communication and differentiation in core regions of the scaffold. Regeneration of bone was also significantly altered both in volume fraction and apparent pattern of osteogenesis. Regenerated bone was significantly affected based on GJIC (figure 3). When cells were transduced to overexpress the mutant Cx43 Δ 7, bone regeneration (fig 3a-c, BVF; 4 week: 6.1 \pm 1.1, 8 week: 4.8 \pm 0.9, 12 week: 5.2 \pm 1.3) was significantly less compared to all groups ($p < 0.001$, against all groups). Furthermore, there was no significant difference in regenerated bone between the different time points in cells overexpressing the mutant connexin. Cells overexpressing Cx43 (BVF; 4 week: 21.8 \pm 6.1, 8 week: 53.9 \pm 13.2, 12 week: 46 \pm 9.5), however, regenerated larger tissue equivalents of bone

than BMSCs alone ((BVF; 4 week: 21.8+/-6.1, 8 week: 53.9+/-13.2, 12 week: 46+/-9.5) at all time points (p(4 weeks) =0.012, p(8 weeks)<0.001, p(12 weeks)<0.001).

Cells overexpressing BMP7 also exhibited larger volume fractions of regenerated bone when GJIC was enhanced (figure 3p). The cotransduced group regenerated significantly more bone than groups with BMP7 alone in the critical sized defect region. However, when cells overexpressed BMP7 only, large volumes of bone were regenerated outside the region of the defect (figure 3j-l), that are not observed in cotransduced cells (3m-o).

Further qualitative depiction of regenerated bone was obtained through histological analysis (figure 4) in the interface between the calvaria and the tissue engineered bone. Cx43 Δ 7 overexpressing group exhibits no bone regeneration, with undifferentiated cells still entrapped in the gelatin scaffold (figure 4a). BMSC-regenerated bone is non-continuous, although some bone is regenerated, containing entrapped cells and some marrow (fig 4b). When Cx43 is overexpressed, the bone tissue is continuous, with entrapped cells, no marrow cavity is present and, it is contained within the region of the defect (fig 4c). The presence of BMP7 in BMSCs enabled regeneration of bone with full marrow cavity, encapsulated with a thin layer of bone containing entrapped cells (fig 4d). Some trabecular bone is observed and the regeneration of bone extends further outside the region of the defect. Interestingly, such large amounts of regenerated bone outside the defect region are not observed when cotransduced cells are used (fig 4e).

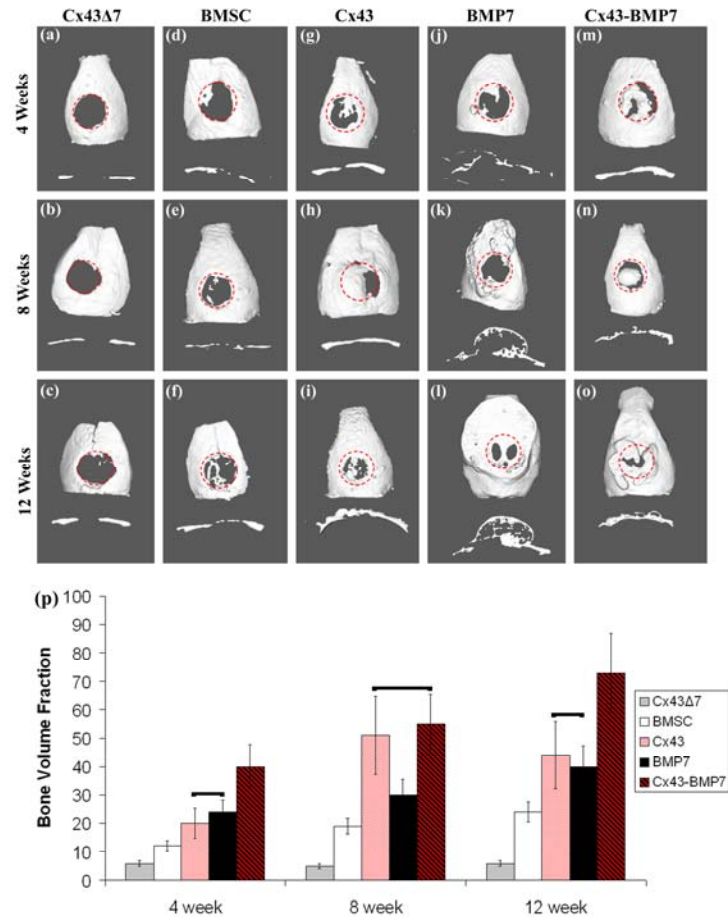


Figure 1: Increased GJIC increases bone volume fraction of critical sized mouse calvarial defects. Rendered images of aerial (top) and sagittal (bottom) views defect sizes (a-o) show the level of GJIC enhanced or inhibited the bone volume fraction. Cx43 overexpression exhibits larger distribution of bone healing, relative to the BMSCs group at all time points. The same is observed when these groups are also treated with BMP7, where the co transfected group produced large coverage over the defect site at all time points. Deletion mutants (Cx43Δ7) exhibited little bone healing in the defect site. To quantify these observations, the BVF is determined (b). Groups overexpressing Cx43 exhibited significant increases in BVF over their control groups. In this case of the co-transformation, the healing of the defect is maximized over all other groups in the 4th and 12th week (b). Deletion mutants were characterized by low BVF from the onset, with no significant change in the growth of bone at later time periods.

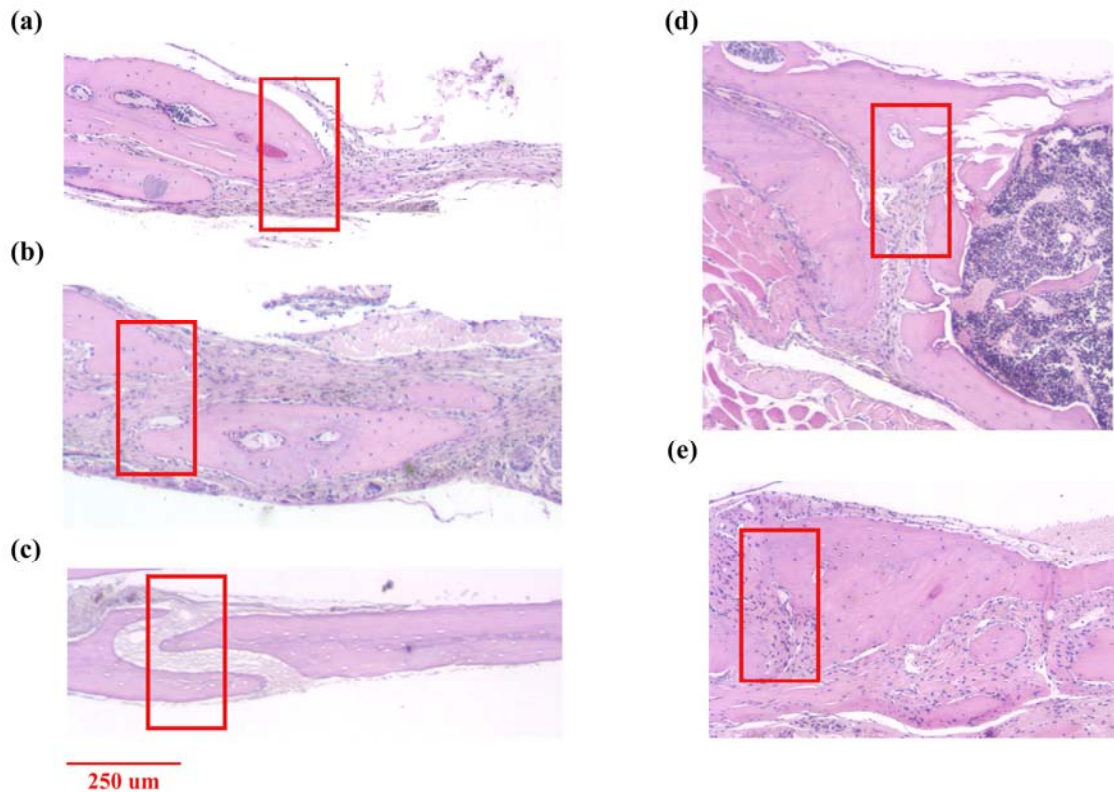


Figure 2: Histological sections of 12 week transplants showing the interface between calvaria and new bone formation. Cx43 Δ 7 ossicles are characterized by little or no bone formation in the interface between the ossicle and calvaria (a). Overexpression of Cx43 (b) produces more of a continuous cortical-like bone formation throughout the defect, compared to that generated by BMSCs (c). Expression of BMP7 increased healing with the periphery (d, e), and the effect of Cx43 with BMP7 was to produce bone regenerates that were more specific to the defect size (e), compared to a larger bone ossicle with complete bone marrow cavities produced by the BMP7 only ossicles. Red boxes indicate the interface site between ossicle and calvaria.